

# Emission-line stars discovered in the UKST $H\alpha$ survey of the Large Magellanic Cloud; Part 1: Hot stars

Warren A. Reid<sup>1,2\*</sup> and Quentin A. Parker<sup>1,2,3\*†</sup>

<sup>1</sup>*Department of Physics, Macquarie University, Sydney, NSW 2109, Australia*

<sup>2</sup>*Macquarie University Research Centre in Astronomy, Astrophysics & Astrophotonics, Macquarie University, Sydney, NSW 2109, Australia*

<sup>3</sup>*Australian Astronomical Observatory, PO Box 296, Epping, NSW 1710 Australia*

Accepted 2012 June 7. Received 2012 June 5; in original form 2012 February 1

## ABSTRACT

We present new, accurate positions, spectral classifications, radial and rotational velocities,  $H\alpha$  fluxes, equivalent widths and B,V,I,R magnitudes for 579 hot emission-line stars (classes B0 - F9) in the Large Magellanic Cloud (LMC) which include 469 new discoveries. Candidate emission line stars were discovered using a deep, high resolution  $H\alpha$  map of the central 25 deg<sup>2</sup> of the LMC obtained by median stacking a dozen 2 hour  $H\alpha$  exposures taken with the UK Schmidt Telescope (UKST). Spectroscopic follow-up observations on the Anglo-Australian Telescope (AAT), the UKST, the Very Large Telescope (VLT), the South African Astronomical Observatory (SAAO) 1.9m and the 2.3m telescope at Siding Spring Observatory have established the identity of these faint sources down to magnitude  $R_{\text{equiv}} \sim 23$  for  $H\alpha$  ( $4.5 \times 10^{-17}$  ergs cm<sup>-2</sup> s<sup>-1</sup> Å<sup>-1</sup>).

Confirmed emission-line stars have been assigned an underlying spectral classification through cross-correlation against 131 absorption line template spectra covering the range O1 to F8. We confirm 111 previously identified emission line stars and 64 previously known variable stars with spectral types hotter than F8. The majority of hot stars identified (518 stars or 89%) are class B. Of all the hot emission-line stars in classes B-F, 130 or 22% are type B[e], characterised by the presence of forbidden emission lines such as [S II], [N II] and [O II]. We report on the physical location of these stars with reference to possible contamination from ambient H II emission. Only 13 of the emission-line stars require additional high resolution spectroscopic observations in order to assign a spectroscopic classification. They have nonetheless been added to the catalogue.

Along with flux calibration of the  $H\alpha$  emission we provide the first  $H\alpha$  luminosity function for selected sub-samples after correction for any possible nebula or ambient contamination. We find a moderate correlation between the intensity of  $H\alpha$  emission and the V magnitude of the central star based on SuperCOSMOS magnitudes and the Optical Gravitational Lensing Experiment (OGLE-II) photometry where possible. Cool stars from classes G-S, with and without strong  $H\alpha$  emission, will be the focus of part 2 in this series.

**Key words:** stars: emission-line, Be - stars: rotation - Magellanic Clouds - surveys - stars: kinematics and dynamics - line: profiles.

## 1 INTRODUCTION

The Large Magellanic Cloud (LMC) is a unique laboratory in which to study the peculiar characteristics of massive and luminous emission-line stars. At a known distance of  $\sim 50$  kpc (see Reid & Parker 2010 and references therein) to all

LMC members, modest inclination angle to the line of sight ( $\sim 21$ deg) and with relatively low interstellar extinction ( $R_V = 3.41 \pm 0.06$ ; Gordon et al. 2003), apparent brightness is a good indicator of absolute luminosity to within a few tenths of a magnitude.

We take advantage of these benefits as we identify and begin basic analysis of emission-line stars in the LMC. The most prominent observational feature of the emission-line stellar group is the presence of the  $H\alpha$  line. The presence of

\* E-mail: warren.reid@mq.edu.au; war@aa0.gov.au (WR);

† E-mail: quentin.parker@mq.edu.au (QAP)

this emission feature has been widely used as an identifier in the many previous searches for emission-line stars in the LMC (eg. Feast et al. 1960; Henize 1956; Lindsay 1963,1974; Bohannan & Epps 1974; Grebel 1997; Keller et al. 1999; Grebel & Chu 2000; Keller et al 2000; Olsen et al. 2001). None of these surveys went particularly deep. More recently, the OGLE II database has prevailed as the main tool used to uncover emission-line star candidates (Sabogal et al. 2005).

The UKST  $H\alpha$  survey of the central  $25\text{deg}^2$  of the LMC has changed this situation. It was adjunct to the successful Southern Galactic Plane  $H\alpha$  survey (Parker et al. 2005) and has revealed large numbers of various emission objects. In addition to revealing 460 new planetary nebulae within the survey region which were confirmed spectroscopically (Reid & Parker, 2006a,b), spectroscopic followup and careful analysis has revealed 579 hot emission-line stars with spectral classes B-F out of a total sample of 1,062 emission-line stars of all spectral types uncovered. Only 111 of these were previously known or identified while 469 are newly discovered. The majority are Be, B[e], Bpe and HAeBe stars but two are Luminous Blue Variable (LBV) candidates. Identifying these objects will assist our understanding of the main sequence evolution of massive stars. We have also identified 6 new and 33 previously known Wolf-Rayet stars, which are not included in this number but will be the special focus of a follow-up paper.

Be stars are known to be variables which undergo active and quiescent stages (Telting 2000; Bjorkman et al. 2002). A single epoch survey could miss many of these stars if they were undergoing a quiescent stage. This problem has already been demonstrated by several follow-up investigations (Hummel et al. 1999; Keller et al. 1999; Wisniewski and Bjorkman 2006) which were unable to identify all of the previously identified Be stars in the Magellanic Clouds and in the Galaxy. In addition, these same follow-up studies revealed previously unidentified Be stars. Our  $H\alpha$  survey, utilising 12  $H\alpha$  exposures taken over a three year period has largely alleviated such problems and revealed a large number of emission-line stars in the survey region to a magnitude of  $R_{\text{equiv}} \sim 22$  for  $H\alpha$ .

In order to study the Balmer emission we have measured the Equivalent Width (EW) and Full Width Half Maximum (FWHM) of the  $H\alpha$  emission-lines. In addition, we include  $H\alpha$  fluxes from medium resolution spectroscopy of 575 (99.3%) of the detected emission-line stars within the survey area. Our follow-up spectroscopy was conducted from November 2004 to February 2005 on a variety of telescopes, allowing us to re-observe several known variable stars and detect minor changes in spectral characteristics. All but 2 candidate emission-line stars found in the  $H\alpha$  survey had some degree of  $H\alpha$  emission detectable in their spectrum at the time of observation. After describing flux calibration (section 5), we explain the method used to assign a spectral classification and luminosity class to each star using cross-correlation against well-established templates (section 6). Section 7 describes our method for deriving the rotational velocities and section 8 outlines a simple method for correcting or at least estimating nebula contribution in the spectrum. Section 9 details our routine for assigning accurate positions to each star.

In section 10 we describe the method used for measuring the radial velocity of each star. Velocities accurate to  $\sim 4$  km

$\text{s}^{-1}$  have been found for 572 emission-line stars using both the weighted emission-line and cross-correlation techniques on our higher dispersion spectroscopic data. These velocities can be used to search for kinematical substructures in the LMC disk, create a 3D kinematic map of the LMC for comparison with the HI disk, assist studies of age-metallicity dispersion and distribution, potentially find stellar associations and streams, and compare medium to old age populations such as planetary nebulae within the LMC (Reid & Parker 2006b).

In section 11 we show the projected distribution of emission-line stars and late-type stars across the survey field of the LMC. In section 12 we measure the intensity of the  $H\alpha$  emission considering ambient sky and any nebula contamination in order to create the first luminosity function for these stars in the LMC. Then, in section 13 we assess the emission by comparing BVI photometry from SuperCOSMOS and OGLE-II data where available. We discuss the stellar photometry, its reliability and problems associated with variability. In section 14 we briefly discuss the variability already found in many of the candidate emission-line stars. The full catalogue of emission-line stars is described in section 15 and presented in the appendix. Individual spectra and  $H\alpha$  images will be available (2nd half 2012) on a dedicated web page hosted by the Astronomy Department at Macquarie University.

## 2 BACKGROUND TO HOT EMISSION-LINE STARS

The origin of emission-lines in hot stars such as Be stars is not well understood. Such emission-line stars are found near the main sequence of luminosity classes V to III exhibiting Balmer emission (Jaschek et al. 1981, Frew & Parker 2010). Various mechanisms have been proposed to explain how gaseous circumstellar disks may form around Be stars (see Porter & Rivinius, 2003 for a review). Struve (1931) was the first to speculate that Be stars exhibit rapid rotation. Recent theoretical studies suggest that classical Be stars may be rotating close to their critical velocity (Townsend et al. 2004) and exhibiting a strange form of variability (Kaler 1997). Other models of circumstellar disk formation include the wind-compressed model (Bjorkman & Cassinelli 1993), pulsations arising from the stellar photosphere (Rivinius et al. 2001) and the magnetically torqued and wind compressed disk model (Cassinelli et al. 2002). While variables such as Cepheids and Miras are known to pulsate radially, many stars also pulsate non-radially, producing subtle magnitude variations and changing the shape of absorption lines. It has been suggested that these oscillations, common on the O and B main sequence, may be powerful enough to drive the winds which produce the Be phenomenon (Kaler 1997).

In the case of pre main sequence (PMS) T Tauri stars, the origin of the emission lines is understood in terms of the magnetospheric accretion model, where the emission lines originate from magnetospheric accretion columns (Uchida & Shibata 1985; Königl 1991; Hartmann et al. 1994; Muzerolle et al. 1998, 2001). With the detection of magnetic fields in a few Herbig AeBe stars (Hubrig et al. 2004; Wade et al. 2005), the magnetospheric accretion model was successfully

applied to these objects (Muzerolle et al. 2004). However, the mechanism for triggering the accretion is still not known.

B[e] stars have all the characteristics of Be stars but they additionally include forbidden emission lines in their spectra. Although lines such as [O III] $\lambda$ 5007 are suggestive of planetary nebulae (PNe), the presence of Fe emission and He absorption in the strong blue continuum clearly separate B[e] stars from PNe.

The evolutionary sequence of these stars is still not well known. Nor is the non-spherically symmetric circumstellar environment which is responsible for the B[e] phenomenon. Strong variability often reported from these objects has been explained by outbursts and shell phases (Hutsemekers 1985; Andrillat & Houziaux 1991).

Related stars such as Herbig Ae/Be (HAeBe) stars, first discussed by Herbig (1960) are found above the main sequence on the HR diagram and are believed to be making their way toward it along radiative tracks as first postulated by Henyey et al (1955). Along with T Tauri stars, they share the characteristic of being associated with a nebula and infra-red emission indicating the presence of circumstellar dust (Hillenbrand et al. 1992; Lada & Adams, 1992). What immediately separates them from T Tauri stars is their larger mass of between  $2M_{\odot}$  and  $10M_{\odot}$ . In order to separate HAeBe stars from B[e] supergiants, Waters and Waelkens (1998) included the condition that HAeBe stars should be of luminosity classes V to III.

As well as the Balmer lines, other optical emission-lines often observed in HAeBe emission-line stars include He I ( $\lambda$ 5876Å and  $\lambda$ 6678Å), O I ( $\lambda$ 7774Å and  $\lambda$ 8446Å) and the Ca II triplet ( $\lambda$ 8498Å,  $\lambda$ 8542Å and  $\lambda$ 8662Å) (Herbig 1960; Hamann 1994; Böhm & Catala 1994; Böhm & Hirth 1997; Corcoran & Ray 1998; Viera et al. 2003; Acke et al. 2005). We do not attempt to separate HAeBe stars from B[e] stars since many HAeBe and B[e] stars are spectroscopically indistinguishable.

### 3 OPTICAL OBSERVATIONS

#### 3.1 The H $\alpha$ survey

Over a period of three years, from 1997, a series of repeated narrow-band H $\alpha$  and matching broad-band short red (SR) exposures of the central LMC field were taken in order to produce a deep H $\alpha$  and SR image with a 1 magnitude depth gain over a single image frame. The twelve highest quality and well-matched UK Schmidt Telescope 2-hour H $\alpha$  exposures and six 15-minute equivalent SR-band exposures were selected. From these exposures, deep, homogeneous, narrow-band H $\alpha$  and matching broad-band SR maps of the entire central 25 deg<sup>2</sup> region of the LMC were constructed.

The full aperture H $\alpha$  filter used for this survey was effectively the world's largest monolithic interference filter to be used in astronomy (Parker & Bland-Hawthorn 1998). The choice of central wavelength ( $\lambda$ 6590Å) and bandpass (70 Å FWHM) work effectively in the UKST's fast f/2.48 converging beam meaning the H $\alpha$  line remains within the filter band-pass for velocities up to 400 km s<sup>-1</sup>. Peak filter transmission is >85%. The fields for the survey were exposed on non-standard, overlapping 4-degree centres due to the circular aperture of the H $\alpha$  filter. These overlapped fields enabled

full contiguous coverage of the entire LMC/SMC region in H $\alpha$  despite the circular aperture.

The successful implementation of high resolution, panchromatic Tech-Pan film on the UKST, coupled with its peak sensitivity at H $\alpha$ , was a prime motivation for the survey. Tech-pan film was an ideal wide-field photographic detector for use with an H $\alpha$  filter. The resulting images produced were unequalled in terms of their combined resolution, sensitivity and LMC coverage. Further details of the properties of Tech-Pan can be found in Parker & Malin (1999).

The SuperCOSMOS plate-measuring machine at the Royal Observatory Edinburgh (Hambly et al. 2001) was used to scan, co-add and pixel match these selected exposures creating 10 $\mu$ m (0.67 arcsec) pixel data which extends 1.35 (H $\alpha$ ) and 1 (SR) magnitude deeper than individual exposures, achieving the full canonical Poissonian depth gain, e.g. Bland-Hawthorn, Shoppell & Malin (1993). This gives a depth  $\sim$ 21.5 for the SR images and  $R_{\text{equiv}} \sim$ 22 for H $\alpha$  ( $4.5 \times 10^{-17}$  ergs cm<sup>-2</sup> s<sup>-1</sup> Å<sup>-1</sup>) which is at least 1 magnitude deeper than the best wide-field narrow-band LMC images previously available. An accurate world co-ordinate system was applied to yield sub-arcsec astrometry (see section 9), essential for success of the spectroscopic follow-up observations.

#### 3.2 Emission-line star discovery technique and criteria

The deep UKST H $\alpha$  survey of the LMC was originally undertaken in order to uncover multiple compact emission sources. Our successful search for extremely faint PNe (Reid & Parker 2006a,b) is proof of its worth. It soon became clear, however, that the depth and resolution of the maps allowed us to also search for low luminosity stellar sources which exhibit detectable emission-lines. Since our aim was to uncover faint sources, we largely ignored extremely bright stars, whether or not they exhibited H $\alpha$  emission. Many of the better known, bright emission-line stars in the LMC will therefore not appear in this work. What we have included in our survey is a large sample of emission-line star candidates that comply with the expected luminosity of brightest LMC PNe ( $M_B$  13 - 24).

Candidate emission-line stars were found using an adaptation of a technique available within KARMA, first reported in Reid & Parker (2005). The SR images were assigned a false red colour and merged with the H $\alpha$  narrow-band images assigned a blue colour. Careful selection of software parameters allowed the intensity of the matched H $\alpha$  and SR .fits images to be perfectly balanced allowing only peculiarities of one or other pass-band to be observed and measured. Using this technique, normal continuum stars appear uniformly pinkish in colour. Emission objects such as H II regions and PNe are strongly coloured blue. The broader point spread function (PSF) of the H $\alpha$  line in emission-line stars creates a faint blue aura around the star, allowing them to be easily detected. Figures 1 to 5 show a small 30  $\times$  30 arcsec area of the stacked SR and H $\alpha$  maps featuring Be stars, RPs255, RPs256, RPs285, RPs286 and RPs338<sup>1</sup> respectively

<sup>1</sup> RPs refers to Reid Parker star

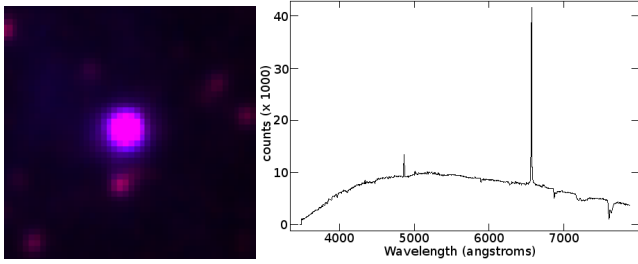


**Figure 1.**  $H\alpha/R$   $30 \times 30$  arcsec image and 2dF low resolution spectrum of RPs255 also known as BE474 (Bohannon & Epps, 1974) and as L333 (Lindsay, 1963).  $M_{H\alpha}=16.37$ . Compact  $H\alpha$  emission 9.6 arcsec dia is largely due to PSF. North is upwards.

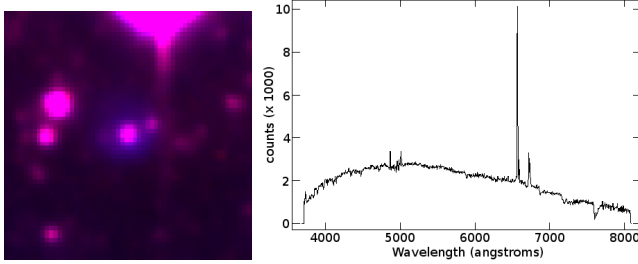


**Figure 2.** Same as above for newly discovered emission-line star RPs256.  $M_{H\alpha}=19.34$ . Forbidden lines lead to B[e] classification.

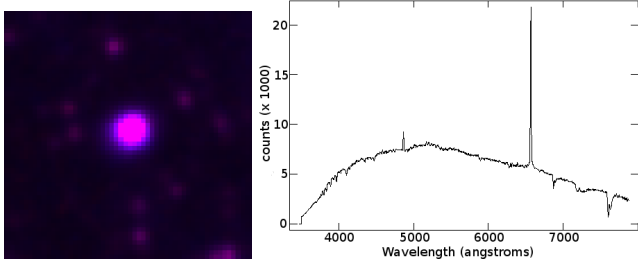


**Figure 3.** Same as above for RPs285 also known as BE411 (Bohannon & Epps, 1974).  $M_{H\alpha}=16.92$ .

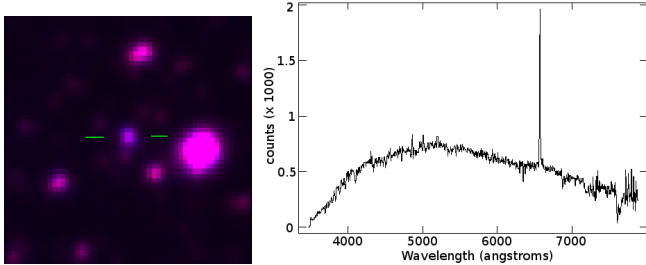


**Figure 4.** Same as above for RPs286 also known as BE426 (Bohannon & Epps, 1974).  $M_{H\alpha}=19.37$ . Only 2.4 arcsec dia on the image including minor PSF contribution.

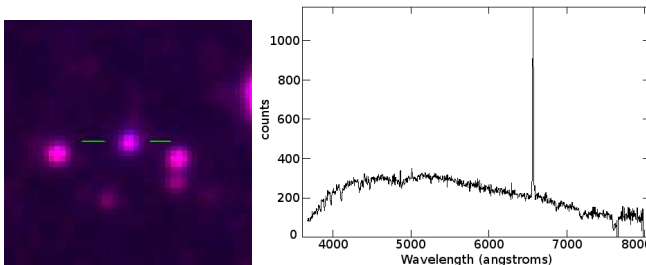


**Figure 5.** Same as above for newly discovered emission-line star RPs338.  $M_{H\alpha}=20.19$ . Only 2.8 arcsec dia. on image.

at the centre together with their confirmatory 2dF spectrum. Spectroscopic confirmation shows us that the wider and more diffuse halo seen surrounding examples such as RPs256 (Figure 2) strongly indicates the presence of forbidden lines in the spectrum, leading to its classification as a B[e] star.

Even with a narrow band  $H\alpha$  filter, the presence of faint Balmer lines in LMC emission-line stars can be very difficult to detect. Although it can be quite easy to miss such faint sources, the colouring and merging of the maps makes detection straightforward, preventing objects above a certain EW threshold from being overlooked and allowing the full depth gain of the maps to be utilized.

#### 4 SPECTROSCOPIC CONFIRMATION OF CANDIDATE EMISSION-LINE STARS

Having used the stacked  $H\alpha$  and SR maps to catalogue over 2,000 emission sources, a large follow-up spectroscopic programme was undertaken in order to identify and classify each source. The most effective and efficient way to follow-up such a large number of objects was to use wide-field multi-object spectroscopic (MOS) systems such as 2dF on the Anglo-Australian Telescope (AAT), 6dF on the UK Schmidt Telescope (UKST) and FLAMES on the Very Large Telescope (VLT). Bright, extended emission objects were selected to be observed individually using long-slit spectroscopic systems on the South African Astronomical Observatory (SAAO) 1.9m telescope and the Mount Stromlo and Siding Spring Observatory (MSSSO) 2.3m telescope.

In Table 1 we summarise details regarding the spectroscopic follow-up observations. The field names are observation identifications or object names in the case of the 2.3m observations. Each of these multi-fibre observations have different central coordinates. The first three 2dF fields, with prefix ST..., are service time runs. Classical observations using 2dF on the AAT provided 15 pointings of 1 degree radius labeled A to O. FLAMES observations on the VLT provided 9 field pointings with an 11 arcminute radius. The FLAMES observations were centred on several of the densest areas on the LMC main bar. The three fields observed with 6dF on the UKST were repeated, subsequently with a different set of stars and extended objects, maximising use of the wide 6 arcsec fibres.

##### 4.1 2dF observations

A five night observing run on the AAT using 2dF (Lewis et al. 2002) was undertaken in December 2004 to spectroscopically confirm LMC emission candidates. The identification of peculiarities associated with  $H\alpha$  excess in various object types (see Reid & Parker 2006a for more details) indicated that we could expect our candidates to be a mixture of PNe, compact H II regions, and emission-line stars such as Be, Ae, WRs, T Tauri, M giants, carbon stars and a number of symbiotics. 2dF was an ideal choice of instrument for the spectroscopic follow-up of large numbers of candidate emission objects due to its unique ability to simultaneously observe 400 targets (including objects, fiducial stars and sky positions) with 2 arcsec fibres over a wide 2 degree diameter

**Table 1.** Observing logs for LMC Emission-line object follow-up. In some instances the same object has been observed multiple times at different resolutions and in overlapping fields.

Field Name	Telesc.	Date	Grating Dispenser	Dispersion Å/pixel	Central λ (Å)	Coverage λ (Å)	T <sub>exp</sub> s	N <sub>exp</sub>	N <sub>obj</sub>
2dF-ST1	AAT	26 Nov-03	300B	4.299	5841	3650 - 7960	1500	2	131
2dF-ST2	AAT	26 Nov-03	300B	4.299	5841	3650 - 7960	1500	2	80
2dF-ST3	AAT	15 March-03	300B	4.299	5852	3660 - 7970	1800	2	81
a1550,061-213	1.9m	09-13 Nov-04	300	5	5800	3850 - 7738	800	2	11
a1550,214-324	1.9m	11-15 Nov-04	1200	1	6563	6000 - 7120	1000	2	10
FLAMES 1-9	VLT	5-7 Dec-04	LR2	0.339	4272	3960 - 4567	1000	3	420
FLAMES 1-9	VLT	5-7 Dec-04	LR3	0.339	4797	4500 - 5077	1000	3	420
FLAMES 1-9	VLT	5-7 Dec-04	LR6	0.339	6822	6438 - 7172	1000	3	420
2dF A-O	AAT	13-16 Dec-04	300B	4.3	5852	3660 - 7970	1200	3	3603
2dF-1200R A-O	AAT	17-18 Dec-04	1200R	1.105	6793	6220 - 7340	1200	2	3303
RPs	2.3m	07-18 Jan-05	600R+B	2.2	4600	3600 - 5570	900	2	56
RPs	2.3m	07-18 Jan-05	600R+B	2.2	6563	5515 - 7520	900	2	56
6dF 1-3	UKST	3-5 Feb-05	425R	0.62	6750	5318 - 7576	600	3	573
6dF 1-3	UKST	3-5 Feb-05	580V	0.62	4750	3948 - 5600	600	3	573

field area. The large corrector lens incorporates an atmospheric dispersion compensator, which is essential for wide wavelength coverage using small diameter fibres.

The observations provided  $\sim 4,000$  spectra. Individual exposure times were mostly 1200s using the 300B grating with a central wavelength of  $5852\text{\AA}$  and wavelength range  $3600\text{-}8000\text{\AA}$  at a dispersion of  $4.30\text{\AA}/\text{pixel}$ . These low-resolution observations, at  $9.0\text{\AA}$  FWHM, were the primary means of object identification and were used in cross-correlation to provide spectral classifications. All fields were then re-observed using the higher resolution 1200R grating to gain our radial velocities with wavelength range  $6220\text{-}7340\text{\AA}$ .

#### 4.2 ESO VLT FLAMES observations

Our data includes additional spectroscopic observations in dense regions of the LMC main bar, undertaken using the multi-object fibre spectroscopic system, FLAMES (Pasquini 2002) on the VLT UT2 over three nights in December 2004. The OzPoz positioner on FLAMES was used to position the 130 available fibres with an accuracy of better than 0.1 arcsec. Gratings LR2 and LR3 allowed us to cover the most important optical diagnostic lines for emission-line stars in the blue including [O III]  $\lambda 4363$ , He II  $\lambda 4686$ , H $\beta$  and [O III]  $\lambda 4959$  &  $\lambda 5007$  in emission and absorption lines such as He I  $\lambda 4471$ ,  $\lambda 4387$ ,  $\lambda 4144$ ,  $\lambda 4121$ ,  $\lambda 4026$ ,  $\lambda 4009$  and  $\lambda 3820$ . Grating LR6 covered the H $\alpha$ , [N II]  $\lambda 6548$  and  $\lambda 6583$  lines as well as the [S II]  $\lambda 6716$  &  $\lambda 6731$  lines. Using these low resolution gratings allowed us to both identify and classify objects and observe micro-structures such as self-absorption within the Balmer emission lines. The observed FLAMES 25 arcmin diameter fields, containing a total of 420 objects, overlapped with 2dF fields, providing a continuous coverage of the main bar region.

#### 4.3 6dF observations

A 3 night observing run was also undertaken on the 3-5th February 2005 using the 6dF 150 fibre MOS system on the

UKST. Each of these observations covered an impressive 6 degree diameter field on the sky and allowed us to observe candidates that were missed in 2dF observations due to crowding. The separate 580V and 425R gratings provided continuous coverage across the optical range from  $3700\text{\AA}$  to  $7550\text{\AA}$  for 573 objects observed. A proportion close to 50% were re-observations of objects previously covered using 2dF, providing additional object confirmation. The wider 6 arcsec fibres on 6dF, compared to the 2 arcsec fibres on 2dF, meant that we had to re-examine the location of each object in order to avoid observing close stellar sources with that instrument. On the other hand, the 6 arcsec fibre meant that it was an excellent choice of instrument for extended sources such as large PNe with post AGB halos and compact H II regions.

#### 4.4 Long-slit observations

Long-slit spectra were obtained using the 1.9m telescope at the South African Astronomical Observatory in November 2004 and 2.3m telescope at Mount Stromlo and Siding Spring Observatory (MSSSO) in January 2005. Both of these observing runs not only provided spectra for object confirmation and classification but assisted our flux calibration for fibre-based observations. Individually, the 1.9m telescope provided both low dispersion spectra for object identification and higher resolution spectra for radial velocities. Light fed to the double-beam spectrograph on the MSSSO 2.3m telescope was split by a dichroic and sent to red and blue optimised detectors. The resulting medium resolution red and blue spectra also provided spectroscopic confirmation of individual objects that were missed during multispec-observations due to overcrowding on field plates.

#### 4.5 Reduction of spectra

The 2dF data were reduced using the sophisticated 2dFDR reduction software provided by the Australian Astronomical Observatory (AAO) specifically for the reduction of 2dF

multi-fibre spectra. The software performed the standard reduction procedures of bias and dark subtraction, flat fielding, sky subtraction, tram-line mapping to the fibre locations on the CCD, fibre extraction, arc line identification, wavelength calibration and fibre throughput calibration as well as providing a user interface with several options, specific to 2dF multi-fibre reductions. Specific bias frames are not required as the software simply makes use of the under-scan/overscan bias strips on each CCD exposure.

The FIT method of fibre extraction was used as it simultaneously fits Gaussians to the spectrum being extracted and to the two either side of it, allowing the amount of overlap at each point along the spectrum to be evaluated. This method also minimises contamination between fibres and was applied to all the reductions.

To perform the sky subtraction, the data was first corrected for the relative fibre throughput, based on a throughput map derived from about 15 dedicated sky fibres which were carefully selected across the 2dF field to avoid stars and ambient emission. The relative intensities of the skylines in the object data frame were used to determine the relative fibre throughput. This method saves time, as no off-set sky observations were required.

Cosmic rays were rejected either automatically during the process of combining two or more observations on the same field setup. This method was used because under certain circumstances the spatial profile is sometimes sensitive to the spectral structure of the data and it can mistake a strong emission-line for a cosmic ray.

Raw data from 6dF on the UKST was reduced using a tailored 6dF variant of the same (2dFDR) data reduction software. A specific input file informs the software that 6dF data is to be reduced. Like 2dF, a separate file relating to the specific grating must be used. Again, cosmic rays were rejected automatically during the process of combining two or more observations of the same field.

VLT FLAMES data were reduced using the pipeline system provided by ESO through the ‘GASGANO’ Java-based data file organiser developed and maintained by ESO. This graphic interface identifies the input file types, produces a master bias, flat, and dark frame, then reduces and combines the science frames.

The 2.3m and 1.9m telescope spectra were reduced using the standard long-slit IRAF tasks IMRED, SPECRED and CCDRED and FIGARO’s task BCLEAN. Cosmic rays were rejected when combining frames. One-dimensional spectra were created and the background sky was subtracted. Final flux calibration used the standard stars LTT7987, LTT9239, LTT2415 and LTT9491.

## 5 FLUX CALIBRATION OF THE 2DF FIBRE SPECTRA

The large proportion of objects observed with 2dF means that a reliable flux calibration of the LMC stellar emission-lines was required in order to compare stellar spectra from different 2dF fields, to make meaningful comparisons between fibre spectroscopy and long-slit observations of individual objects, and to create a luminosity function.

Altogether, 18 overlapping 2dF fields, 9 FLAMES fields and 6 6DF multi-object fields were observed in order to cover

the entire central 25deg<sup>2</sup> survey region of the LMC. To calibrate the resulting data counts, we used PNe with low continuum levels and well determined fluxes gained from HST observations (see Reid & Parker 2006a, 2006b). These objects were deliberately included and observed on each field plate for use as flux calibrators for each individual field.

The process involved matching each spectral line on each field plate from each CCD camera to raw PN fluxes gained from HST exposures. The individual H $\beta$  and H $\alpha$  2dF line intensities for known PNe observed on each CCD and each field plate exposure were plotted against HST-gained published fluxes for the same lines (see Figure 2 in Reid & Parker, 2010).

The agreement of flux-calibrated PNe from each spectrograph/field plate combination was considered robust enough (within 0.2 dex) to allow calibration to all the H $\beta$  and H $\alpha$  emission-lines for other emission objects observed in the same field. In each case, a line of best fit was derived and the underlying linear equation extracted. This equation became the calibrator for each emission-line in each object where the CCD and individual 2dF field plate exposure was the same. Full details including a discussion on the reliability of the method are presented in Reid & Parker (2010).

## 6 SPECTRAL CLASSIFICATION

Spectral classification of all the emission-line stars was undertaken to assist in various studies such as the distribution of emission by stellar population, the estimation of central star temperatures, creation of H-R diagrams and improving our understanding of Balmer emission in stars of varying temperatures. We touch on some of these issues later in this paper.

### 6.1 Method of classification

To assign a spectral classification, it is necessary to measure the strengths and widths of various absorption features which depict specific stellar temperatures and surface gravities, independent of any associated emission characteristics. To assist this process we used standard stellar spectra supplemented by 10 LMC emission-line stars from our sample with recognised spectral classifications as templates. The spectral standards were based on observations available from Jacoby et al (1984), Turnshek et al (1985), Silva and Cornell (1992), Pickles (1998) and Le Borgne et al. (2003).

The classification of emission-line stars is complex and often problematic due to their variability and atmospheric activity. The strength and profile of the Balmer lines in emission only lend moderate assistance to classification, although the equivalent width of H $\gamma$  can be a good indicator of spectral type and luminosity in main sequence stars (Underhill & Doazan 1982). In the spectra of young stars such as T Tauri stars, photospheric absorption lines can be filled in or disguised by UV radiation from accretion hotspots (Hartigan et al. 1995; Gullbring et al. 1998), making classification difficult. Further complication arises from active Post Main Sequence (PMS) stars where most spectral lines are in emission (Cohen & Kuhl, 1979; Hernández et al., 2004). These

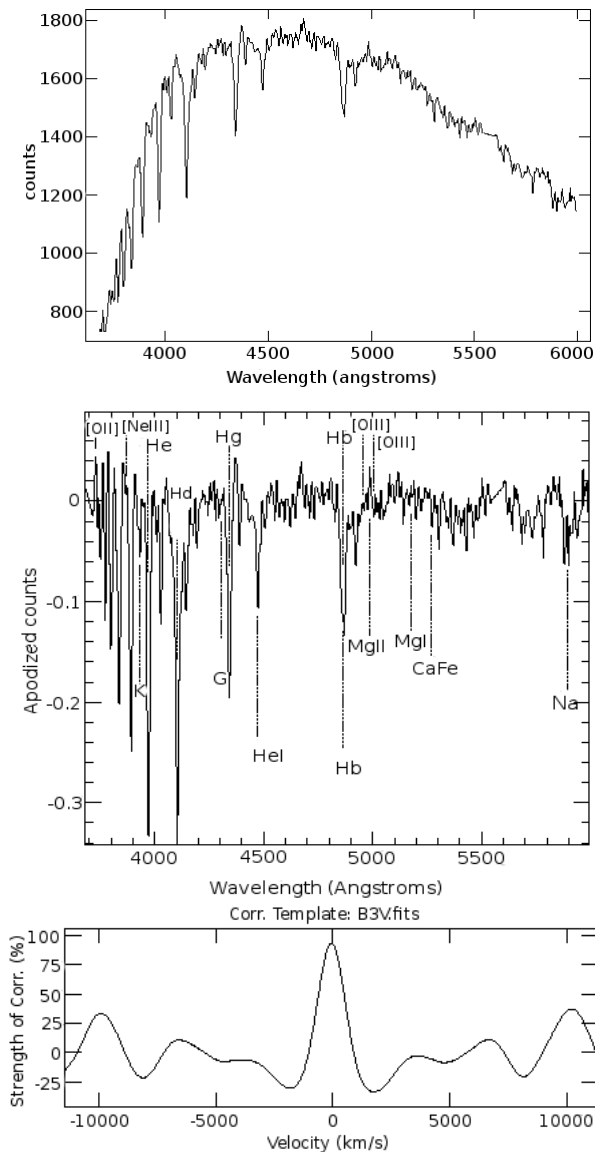


**Figure 6.** The top image shows the blue end of the RPs1326 optical spectrum prior to the removal of emission-lines and continuum. The centre frame shows the apodized and continuum subtracted spectrum, created within XCSAO and used in cross-correlation to match the best fitting template. The lower frame shows the strength of the resulting correlation, represented by the central gaussian curve, once the task has found the best-fitting template.

types are usually denoted as ‘continuum stars’ since it is virtually impossible to accurately assign a spectral type.

Due to the large number of emission-line stars to be classified in this survey, as a first step, a cross-correlation routine was employed. Although the IRAF XCSAO task was originally developed in order to cross correlate galactic spectra against templates and gain redshifts (Tonry and Davis, 1979), it works equally as well as a spectral classification tool with stellar templates. The task identifies the closest spectrum in terms of line strengths and widths found and then returns a velocity along with the name of the best matching

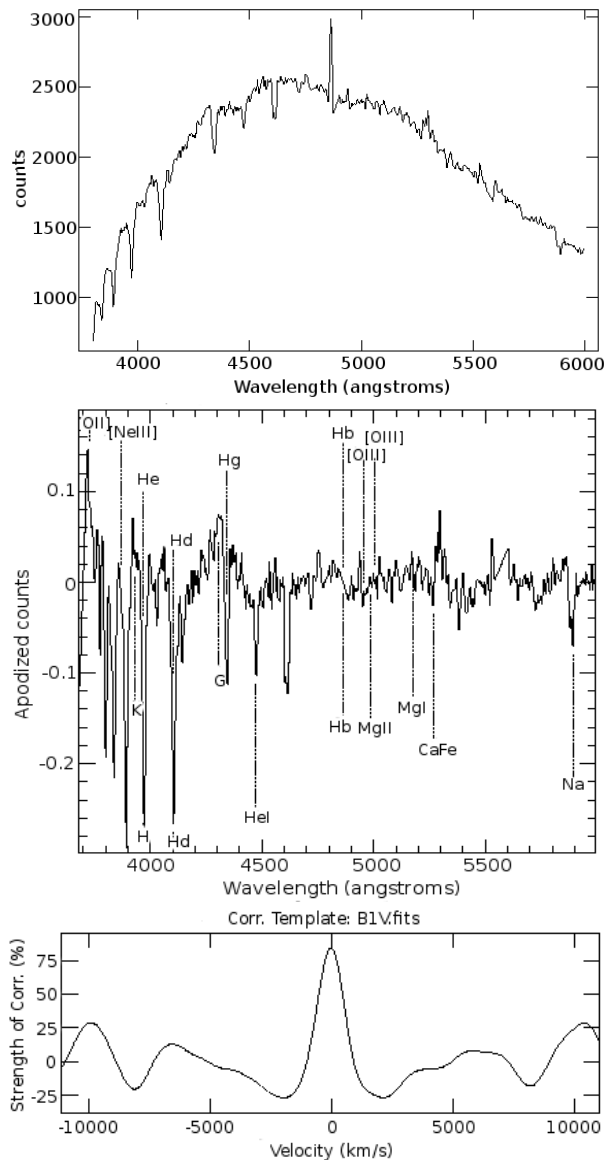


**Figure 7.** The same as Figure 6 but showing the blue end of the RPs1262, a B1V optical spectrum with top: the original blue end including emission-lines and continuum prior to their removal, middle: the continuum-subtracted and apodised spectrum with detected lines identified automatically by the software, bottom: the correlation.

template through cross-correlation based on fourier transformations.

In order to produce the most accurate result, emission-lines (mainly the Balmer series and any residual telluric sky lines which can effect the cross-correlation) were removed. The continuum was then removed using the IRAF CONTINUUM task in order to cross-correlate the absorption lines alone. This negated the influence of the continuum where it was either stronger or weaker than the best matching spectrum in the templates, which were also continuum subtracted. Apodization within XCSAO uses a cosine bell to attenuate data on the ends of the spectrum, reducing high wave number fourier components that would be produced by abrupt cutoffs at the ends of the spectra, effectively smooth-

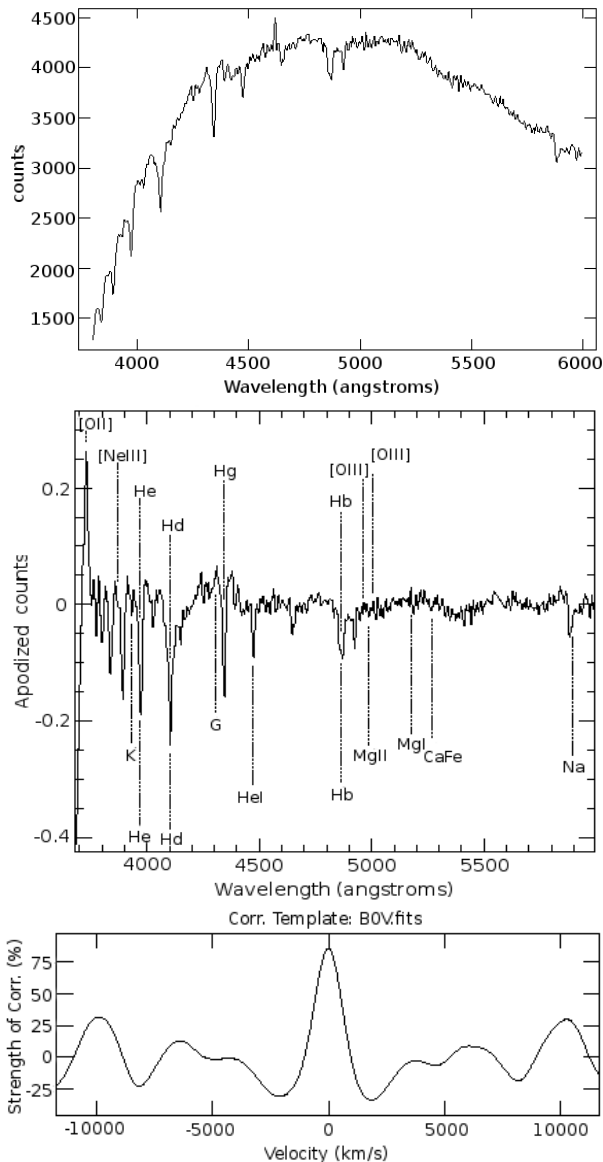


**Figure 8.** The same as Figure 6 but showing the blue end of RPs1367, a B0V optical spectrum with top: the original blue end including emission-lines and continuum prior to their removal, middle: the continuum-subtracted and apodized spectrum, bottom: the correlation.

ing out the continuum across the full length of the spectrum. Examples are shown in figures 6, 7 and 8 using only the blue end of the optical spectrum which contains the main diagnostic lines for spectral classification. The same is not true for late-type G to SC stars. For these stars, removal of emission-lines is still necessary but the overall shape of the spectrum becomes increasingly important with decreasing spectral type. By late K types it was already necessary to match the continuum with the templates using the wider optical spectrum ( $\lambda 3700$  to  $\lambda 8000$ ).

Having run the above-mentioned tasks, the raw spectra, including the emission lines, were then inspected and measured. B-type stars are strongly characterised by He and Balmer emission-lines. HeI lines show a very broad intensity maximum by B2 and B3. The intensity of Balmer lines

remains almost constant for Supergiant stars from B0 Ia through to A0 Ia but strengthens in late B giants. For main sequence stars, however, the Balmer lines strengthen from B0V to A0V. A more precise spectral type can therefore be confirmed by defining the ionisation temperature of Si and He supplemented by C II and C III. The main luminosity criteria are summarised in Table 2. In early B and late A main sequence through to F stars, line ratios are much easier to use for identification due to the larger number of lines available. The luminosity class can be tested by assessing the wings of the Balmer lines, which widen from classes I to V.

By applying these criteria, we re-classified 40 Be stars which were automatically classified as luminosity class I supergiants in the cross-correlation routine. Most of these were re-identified as giants or subgiants. Fast rotation of the Be stars causes the Balmer lines to broaden thereby matching spectra to supergiant stellar templates. This effect was countered by examining each spectrum with reference to the ratios as shown in Table 2.

## 6.2 Results of spectral classification

Although this paper is presenting the hot emission-line stars, it is important to note that the UKST  $H\alpha$  survey also uncovered a large number of cooler G to SC stars which either emit strongly or are bright at  $H\alpha$ . These late stellar objects, which will be the subject of a second paper of this series, are listed briefly here in order to compare detection rates.

The majority of emission stars found have been classed as Be, [Be] (V - III) stars and M (III) giant stars. The letter ‘e’ indicates that, at the very least, the first member of the Balmer series ( $H\alpha$ ) is in emission. Although we identified 13 supergiant B stars with  $H\alpha$  emission, these types are not generally known as Be stars, a classification reserved for luminosity classes V, IV and III. Table 3 provides a quick breakdown of the various emission-line stars found in the central  $25\text{deg}^2$  LMC survey. Of these stars, 64 Be stars are previously known variable stars.

Figure 9 shows the spectral classification of the identified B to K emission-line stars in our survey. The number of stars found is subdivided by luminosity class according to the Morgan-Keenan system (Morgan et al. 1943) where the width of absorption lines are a measure of the size of the star and thus the total luminosity. As per the standard convention, class I are supergiants, class III are giants and class V are main sequence stars. It is clear that the largest number of emission-line stars found belong to class B and, of those, the supergiants are mainly found at B0. These supermassive stars again dominate our detections from classes G5 to K5. The largest spectral class of Be stars represented in our sample are those on the main sequence.

## 6.3 Types of emission-line stars found

Of the 468 newly discovered emission-line stars, we identified 107 B[e] stars that exhibit forbidden emission-lines. They were found in spectral types B0-B9. The most common forbidden emission-lines found in the B[e] stars were [Fe II] $\lambda 4244, 4287, 4415, 5273, 7155$ , [O I] $\lambda 6300, 6363$ , [N I] $\lambda 5755, 6548, 6584$ , [S I] $\lambda 4068, 6717, 6730$ , [O II] $\lambda 7320, 7330$ , and [O III] $\lambda 4959, 5007$ , the most frequent being



**Table 2.** The most important lines examined to assist in follow-up spectral classification after cross-correlation. These include the ratios and equivalent widths of the Balmer lines and the ratios of classification lines in the  $\lambda$ 3500-4800 region of B-type stars. It should be noted that the ratios shown in columns 2-5 more or less depend on the luminosity. For example, He I is only weakly visible in A0 supergiants.

Class	Ratios & EW	Ratios	Ratios (later types)	Ratios (latest types)
<b>Supergiants</b>				
B0 Ia-B2 Ia	$H\alpha/H\beta/H\gamma$	He II 4542/He I 4471 He II 4200/He I 4144	Si III 4552/Si IV 4089	C III 4068/[O II] 4076 C II 4267/He I 4121
B2 Ia-B5 Ia	$H\alpha/H\beta/H\gamma$	Si III 4552/Si IV 4089	C III 4068/[O II] 4076	C II 4267/He I 4121
B5 Ia-A0 Ia	$H\alpha/H\beta$	Si II 4128,31/He I 4121	Si II 4128,31/He I 4026	Si II 3856, 63/He I 3820, 4026
<b>Giants</b>				
O5 III-B0 III	$H\alpha/H\beta/H\gamma$	He II 4200, 4542/He I 4471	Si IV 4089/H $\delta$	He I 4388/H $\gamma$
B0 III-B5 III	$H\alpha/H\beta/H\gamma$	Si IV 4089/Si III 4553	C III 4647-51/He I 4388	Mg II 4481/He I 4471
B5 III-A0 III	$H\alpha/H\beta$	Mg III 4481/He I 4471	Si II 4128,31/He I 4144,4026	
<b>Main Sequence</b>				
O4 V-B0 V	$H\alpha/H\beta/H\gamma$	He II 4542/He I 4471	He II 4686/He I 4922	Si IV 4089/He I 4144
B0 V-B5 V	$H\alpha/H\beta/H\gamma$	Si IV 4089,4116/He I 4121	He II 4686/He I 4713	C III 4068-70/He I 4009 C III 4647-51/He I 4713
B5 V - A0 V	$H\alpha/H\beta$	Si II 4128,31/He I 4144,4026	Mg II 4481/He I 4471*	C II 4267/Mg II 4481

\* The He I  $\lambda$ 4471 line is all but gone in main sequence stars by B8 V.

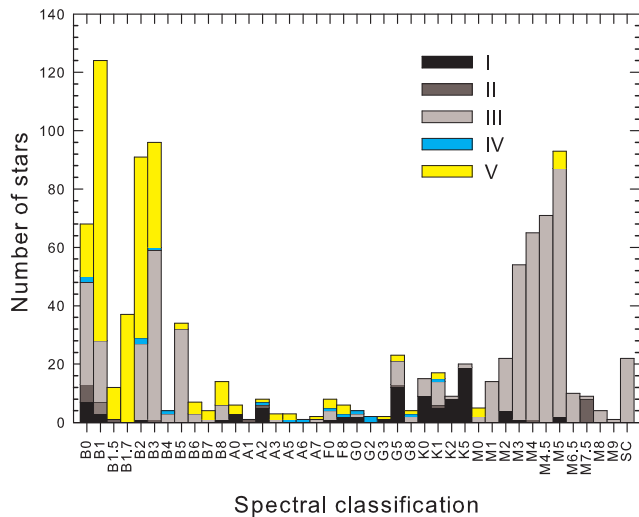


**Figure 9.** Distribution of all types of emission-line stars found within our survey region of the LMC according to number and spectral classification. The number of stars in each class is subdivided in order to express the luminosity class of the star according to the Morgan-Keenan system. It is clear that there are more main sequence stars, bright in  $H\alpha$  emission, within the B spectral class. Class SC may be divided into  $4 \times$  SC4/9 stars,  $1 \times$  S4/2,  $1 \times$  S4/6 and 16 carbon stars, 13 of which are C6.

[Fe II] and [O I]. The ionisation potentials of the last two, less than 25eV, place them lower than the ion energies found in planetary nebulae.

We have also identified early B-type stars with anomalies (weak or strong) in carbon, nitrogen and usually oxygen. These were first labelled CNO stars by Jaschek & Jaschek (1967). The stars with anomalies in their heavier elements are called Bp stars, where ‘p’ designates ‘peculiar’. We have identified 5 Bp candidates. They are particularly enhanced in Si- $\lambda$ 4200, Mn II, Cr II, Eu II and Sr II.

As the cores of intermediate mass stars ( $M_* = 1-8M_\odot$ )

**Table 3.** Classification of stellar emission sources for the whole catalogue. The numbers provided in column 4 are not additional but represent the number of stars previously known as variable.

Object Type	Previously known	Newly discovered	known variable
O stars		1	
Be stars	82	306	55
B[e] stars	23	107	9
Ae stars	3	29	
F stars	3	25	
G stars		29	
K stars		49	
M stars	86	315	33
WR stars	33	6	
Carbon stars		16	
CVs	4		4
Eclipsing Binaries	3		3
LBVs		2	
Bp stars	2	5	
AGB stars	4		
Symbiotic stars		18	
hot stars without id.		14	
cool stars without id.		7	

become too depleted in hydrogen for fusion reactions, they leave the main sequence to ascend the Red Giant Branch (RGB) and Asymptotic Giant Branch (AGB). At this point, the stars are seen as Miras or OH/IR stars with maser activity (Winckel, 2003). Although these stars will become the central stars of planetary nebulae, they are not yet hot enough to ionise a potential vast halo of expelled material. Nevertheless, the dense, complex atmospheric matter, including possible extended circumstellar envelopes, is ionised sufficiently to be detected in  $H\alpha$  and [N II].

The second largest group of stars uncovered in this survey are the M giants. Due to their cooler temperature, these stars have a spectral energy distribution (SED) that peaks towards the red end of the spectrum. They often exhibit strong excess  $H\alpha$  emission originating from the chromo-

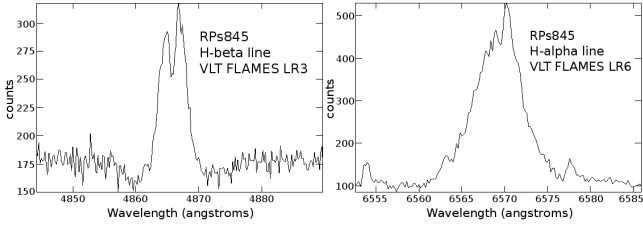


**Figure 10.** An example of Balmer line splitting where we can see fine structure components. These profiles often feature three or more emission peaks and minute detailed features extending down to the continuum. The example shown is RPs845 with H $\beta$  left (FLAMES LR3 grating) and H $\alpha$  right (FLAMES LR6 grating). The absorption wings of the H $\beta$  line are also greatly broadened by the Stark effect indicating that these are main sequence stars where the gravity and electron pressure is large.

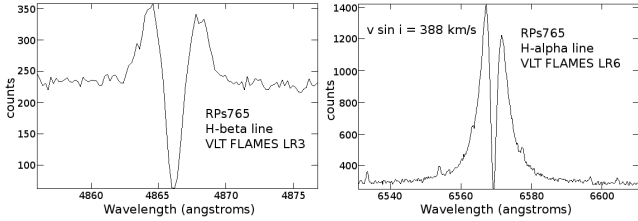


**Figure 11.** An example of Balmer line splitting, typical of a ‘shell star’ or more correctly, a star going through a shell phase, where the central absorption on the H $\alpha$  line extends below the stellar continuum. The example shown is RPs765 with H $\beta$  left (FLAMES LR3 grating) and H $\alpha$  right (FLAMES LR6 grating).

sphere which strengthens with increasing spectral type or decreasing luminosity. For this reason the H $\alpha$  line cannot be used as a classification criteria and was removed prior to cross-correlation.

Late-type M giants feature TiO and VO bands which strengthen with decreasing temperature. They also feature Mg  $\lambda$ 5167,5173,5184 until M4III and M6.5V as well as NaI  $\lambda$ 5890,5896 although the latter can be overwhelmed by TiO absorption in stars later than M2III.

Our survey uncovered 401 M giant stars with emission, 315 of which are newly identified. Of the 86 previously known M giants, 33 have been found to have variable luminosity. These M giants, together with a number of G and K emission-line stars will be the subject of the next paper in this series.

#### 6.4 Observed emission line profiles

The emission line profiles can represent a combination of instrumental broadening, small absorption features which are often broadened by rotation originating from the photosphere of the star, and the emission-line profile produced by the star’s circumstellar envelope. Both emission and absorption lines may include kinematic and non-kinematic broadening from effects such as radiative transfer and Thomson scattering which affect the envelope (eg. Hanuschik, 1989). Absorption lines are generally less affected by such effects leaving emission lines to provide important information about the rotation and physical conditions affecting the star and it’s circumstellar envelope.

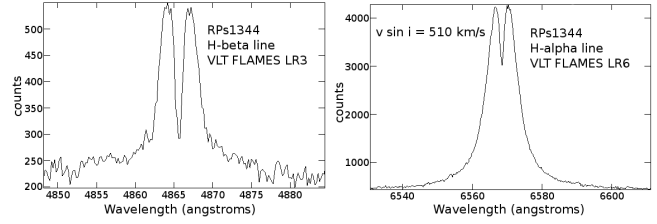


**Figure 12.** An example of Balmer line splitting in the high velocity circumstellar emission of RPs1344 with H $\beta$  left (FLAMES LR3 grating) and H $\alpha$  right (FLAMES LR6 grating). The narrow profile of the shell absorption line indicates its origin closer to the outer, slowly rotating parts of the shell.

The Balmer emission lines demonstrate the most diverse range of profiles. Profile variations are believed to be dependent on the observer’s angle of inclination to the star’s pole. According to the model of Struve (1931), shell profiles occur where the star is viewed equatorially ( $i = 90$  deg), double peaked profiles occur at mid-inclination angles and singly peaked profiles occur by viewing towards the pole ( $i = 0$  deg). The measurement of accurate inclination angles, however, is complicated by other influences on the emission profile such as temperature, density and rotational velocity (Underhill & Doazan, 1982; Quirrenbach et al. 1997; Miroshnichenko et al. 2001).

We present some representative examples of Balmer emission profiles using our VLT observations. Several of the Be stars in our VLT-observed sample show some shallow double reversal more or less central to the H $\alpha$  line. Some stars also have emission profiles with three emission peaks. It is these fine structure components (see Figure 10) that are known to show the greatest variability, down to the order of hours (Hubert & Floquet, 1998). Stars whose emission lines have sharp, very deep absorption cores such as the example shown in Figure 11 have come to be known as *shell* stars. The intrinsic variability of Be stars, however, has proven that over time these stars can lose and regain these shell characteristics (Underhill & Doazan, 1982). We therefore refer to them as going through a ‘shell phase’ at the time of our observation. Following the convention proposed by Hanuschik et al. (1996), we formally identify a shell star where the central absorption extends below the stellar continuum.

Further to this definition, we add that this only applies to absorption on the H $\alpha$  line. The H $\beta$  line is more dramatically affected by the atomic absorption since the reversal feature is not dependent or correlated to the strength of any individual Balmer emission line. For example, a medium absorption of H $\alpha$  resulting in a small reversal feature will correspondingly extend very deeply into the H $\beta$  emissive flux (see Figure 12).

Asymmetry is a sub-feature found in a small percentage of Be star profiles. This is currently thought to arise from one-armed density waves in the circumstellar disk, also known as the global disk oscillation model (Silaj et al. 2010). In Figure 13 we show asymmetry where the reversal is left of centre while Figure 14 shows reversal to the right of centre, affecting both H $\beta$  (left example) and H $\alpha$  (right example) Balmer lines the same way. The resulting emission peak on the left is known as the Violet (V) component and the emis-

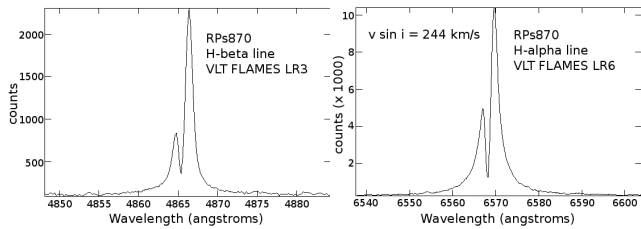


**Figure 13.** RPs870 is an example of Balmer line splitting which appears to the left of centre with H $\beta$  left (FLAMES LR3 grating) and H $\alpha$  right (FLAMES LR6 grating). The peak R>V affects both hydrogen emission lines and arises from one-armed density waves in the circumstellar disk.

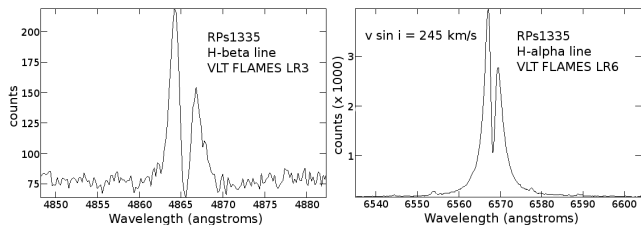


**Figure 14.** RPs1335 is an example of Balmer line splitting which appears to the right of centre with H $\beta$  left (FLAMES LR3 grating) and H $\alpha$  right (FLAMES LR6 grating). In this case V>R.

sion peak on the right is known as the Red (R) component. These asymmetries are also seen in single emission-lines and are probably the result of minor or isolated density waves.

A more unusual feature among the Be star emission line profiles is the ‘wine-bottle’ shape, often produced by viewing the star near to the pole. The example shown in Figure 15 is possibly broadened by a combination of disk rotation and Thomson scattering.

In attempting to classify the profiles of H $\alpha$  emission according to the particular features mentioned above, it is prudent to refer only to the higher resolution VLT FLAMES data. Figures 16 and 17 provide a comparison of the VLT FLAMES LR6 and 2dF 1200R spectra for the one object. In the first comparison (Figure 16) the strong absorption feature seen in RPs1343 using LR6 on FLAMES is only de-

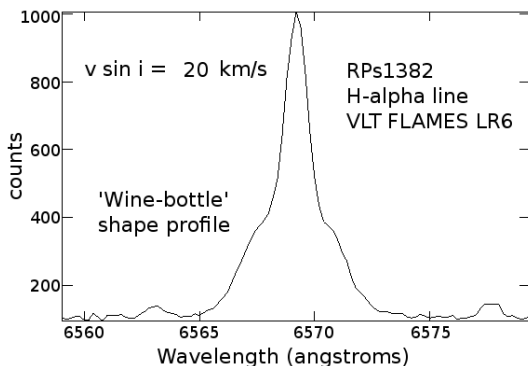


**Figure 15.** RPs1382 is an example of a ‘wine-bottle’ profile which may occur by viewing the rotating star close to pole-on ( $i = 0$  deg angle). The low rotation velocity is a direct result this viewing angle and is measured using the central profile of the H $\alpha$  line (see section 7). The broadening is circumstellar.

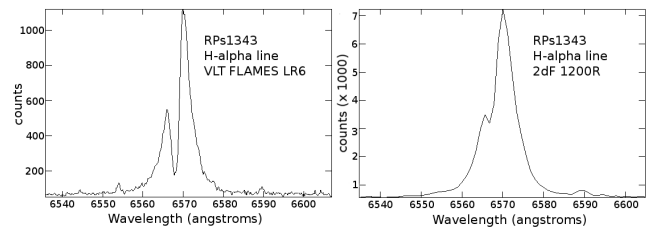


**Figure 16.** A comparison of H $\alpha$  Balmer line splitting in emission-line star RPs1343 as seen with the FLAMES LR6 R8600 grating (left) and the 2dF 1200R grating (to the right). The VLT spectrum with its increased detail provides the clear detection of line splitting and some microstructure. The 2dF spectrum is able to detect the presence of line splitting but the amplitude of the same is unable to be measured due to the lower resolution of the 1200R grating. No microstructure can be seen in the 1200R spectrum.

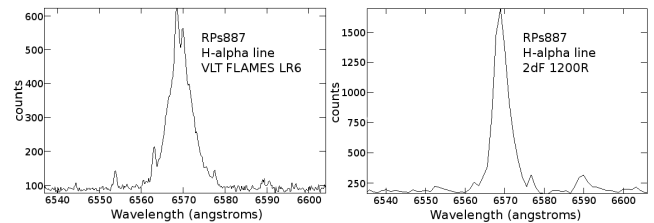


**Figure 17.** A comparison of H $\alpha$  Balmer line splitting in emission-line star RPs887 as seen with the FLAMES LR6 R8600 grating left and the 2dF 1200R grating to the right. The VLT spectrum shows fine line splitting to the top right but this cannot be seen in the 2dF 1200R spectrum which has a dispersion of 1.105Å/pixel. In this case the peaks at the top of the H $\alpha$  line are separated by 1.4Å, making fine detail impossible to detect at the lower resolution.

**Table 4.** H $\alpha$  profile features found in 122 emission-line stars observed with VLT FLAMES using the LR6 grating. Micro features are miniature peaks identified on the sides and at the top of a main peak.

Main feature	Total number	% of total	Number of micro features	Number of bottle shape
Single peak	100	82	11	9
Double peak V=R	10	8	2	
Double peak R>V	6	5	3	
Double peak V>R	4	3	3	
Shell	2	2	2	

tectable to a limited extent in the 2dF spectrum to the right. In the second comparison (Figure 17) the absorption feature is too narrow to be detected at a resolution of 1200R.

Using only the 122 emission-line stars observed on the VLT, the features shown in Table 4 were present. All 122 stars in this table reside within a 3 deg<sup>2</sup> region on the main optical bar of the LMC. With 100 detections, the single peak profile is the most common. At the time of spectroscopic observation, 11 stars were found to exhibit micro features such as miniature structures on the sides and/or at the peak. In time these may develop into separate peaks or disappear completely. Since emission-line stars are constantly evolving, a table such as this can only provide a snapshot of the percentage of features found at that time.

## 7 ROTATIONAL VELOCITIES

Classical Be stars undergo rapid rotation and possess geometrically thin, circular gaseous disks resulting in hydrogen Balmer emission (Jaschek et al. 1981; Porter & Rivinius 2003). Typical rotation compared to critical velocity ( $v_{eq}/v_{crit}$ ) has been estimated at  $\sim 70\%$ - $80\%$  (Porter 1996; Porter & Rivinius 2003). A lower estimate of  $40\%$ - $60\%$  of the critical breakup velocity for such stars was found by Cranmer (2005) but this set of data is not homogeneous. It is likely that both of these estimates may not take all the physical conditions into account. Due to fast rotation it is expected that the star is flattened, causing a variation in temperature and density from pole to equator. This is expected to result in a gravitational darkening of the stellar disk. Based on this theory, Townsend et al. (2004), employing the effects of equatorial gravity darkening, suggest that a degeneracy in the measurement of rotational rates allows Be stars to be rotating at or near their critical breakup velocity. An estimate of rotational velocity for the LMC set of emission-line stars will provide vital information for future studies.

Although the fine structure across the top of the Be star emission-line profile makes FWHM rather complex to untangle, the strength of the  $H\alpha$  line negates any underlying photospheric biases or broadening. This is also true in cases where emission is weak. To derive the projected rotational velocity ( $v \sin i$ ) we used the correlation found by Dachs et al. (1986, Equation (7)) with improvements made by Hanuschik (1989). Their three parameter correlation between FWHM ( $H\alpha$ ),  $v \sin i$  and equivalent width (EW) lead them to the relation:

$$\log[\text{FWHM}(H\alpha)/1.23 (v \sin i + 70\text{kms}^{-1})] = -0.08 \log EW + 0.14 \quad (1)$$

which was presented as equation (5) in Hanuschik (1989). We used this equation in the form:

$$v \sin i = [(\text{FWHM}(H\alpha) + 10^{0.08 \log EW + 0.14})/1.23] - 70 \quad (2)$$

to derive  $v \sin i$  for all stars in our sample. The resulting relation between  $\text{FWHM}(H\alpha)$  and  $v \sin i$  is shown in Figure 18. The scatter is mainly due to the equivalent width of the individual line although there will inevitably be a contribution from non-kinematic line broadening due to radiation transfer (Poeckert and Marlborough, 1978), electron scattering, possible turbulence and measurement errors. The median fit to the data in Figure 18 yields

$$\text{FWHM}(H\alpha) = 0.89 v \sin i + 79\text{kms}^{-1}. \quad (3)$$

A histogram giving the frequency of  $v \sin i$  for all hot emission-line stars in our LMC sample is shown in Figure 19. The distribution covers in excess of  $500 \text{ km s}^{-1}$  with a maxima at around  $200 \text{ km s}^{-1}$ . With the exception of 30 stars measured using 6dF, all the measurements were taken using the highest resolution 2dF, AAOmega and VLT data. The 30 stars measured using the 6dF red arm  $0.62 \text{ \AA/pixel}$  data cover a large range from  $73 < v \sin i < 489$ , indicating that the 6dF data is not introducing any bias to the overall results.

The number of stars found in the  $50 \text{ km s}^{-1}$  bin appears to be overstated in relation to the general trend seen in the histogram. This isolated rotational velocity peak probably has little to do with the spectral type or luminosity class,

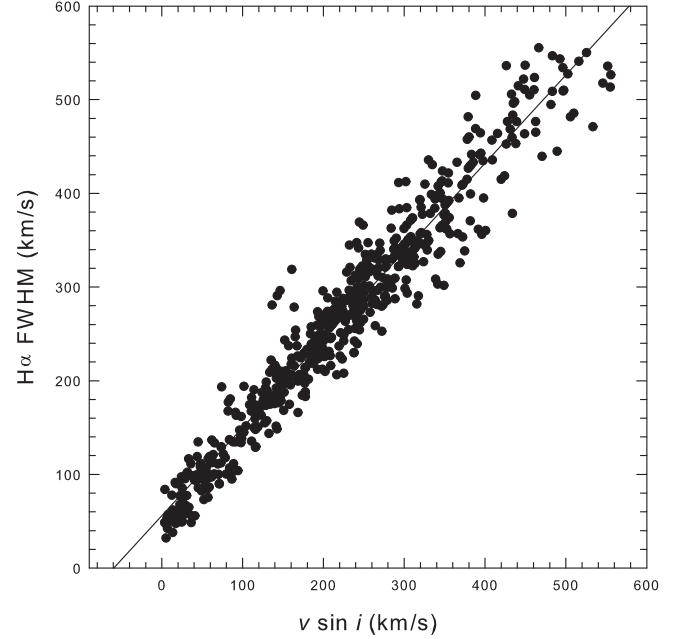


**Figure 18.** The relation between FWHM measured on the  $H\alpha$  line and the rotational velocity ( $v \sin i$ ) using equation (3) for all emission-line stars in our sample. The variations away from the line of equality are mainly due to the equivalent width, used to determine  $v \sin i$ .

both of which are quite evenly distributed across the histogram. It most likely reflects the number of stars we are viewing close to pole-on (see section 6.4), many of which do not display a strong wine-bottle  $H\alpha$  emission profile. As with all surveys, the reason may also partly lie in our selection criteria, as we specifically targeted faint stars with relatively strong  $H\alpha$  emission.

The process of estimating rotational velocities using FWHM and EW on  $H\alpha$  emission lines which display a strong wine-bottle profile is somewhat complex. Measurement of these parameters using a line such as  $\text{He}\lambda 4471$  is generally considered more accurate because it is less affected by circumstellar rotation. The extra-wide (wine-bottle profile) wings on these particular  $H\alpha$  lines substantially increase both measurements, thereby giving these stars a typical rotational velocity between  $200 < v \sin i < 300 \text{ km s}^{-1}$ .

We have found that by measuring FWHM and EW on the  $\text{He}\lambda 4471$  absorption line, or by fitting a gaussian curve to the  $H\alpha$  wine-bottle profile, the rotational velocity readings drop substantially to levels below  $100 \text{ km s}^{-1}$ . Since both methods of measurement yield similar results ( $5 < v \sin i < 40 \text{ km s}^{-1}$ ), we prefer to fit a Gaussian profile to the  $H\alpha$  line. This is expected to produce the most accurate measurement of FWHM, EW and  $v \sin i$  using these peculiar profiles. It not only constrains all FWHM and EW measurements to the  $H\alpha$  line for direct comparison across the table (Appendix Table 1) but improves reliability due to the strength of  $H\alpha$  compared to the  $\text{He}\lambda 4471$  absorption line, which is weak, difficult to fit and often perturbed by the envelope.

After selecting LMC Be stars between classes B0 and

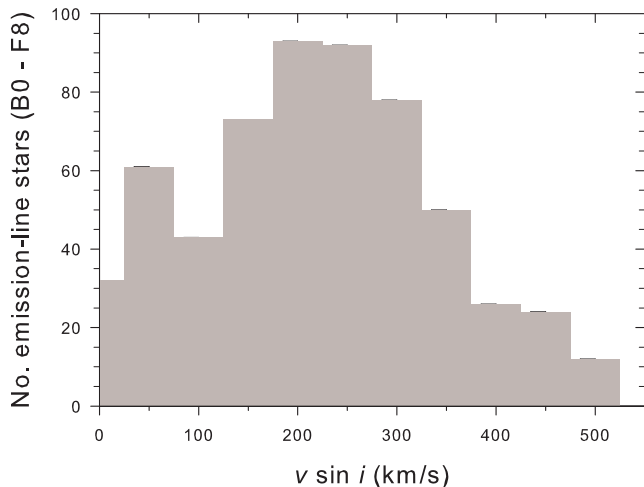


**Figure 19.** The distribution of estimated rotational velocities ( $v \sin i$ ) for all the hot emission-line stars (B0 - F8) in our survey. The large number of stars occupying the bin at  $50 \text{ km s}^{-1}$  is most likely due to their near pole-on angle to our line of sight.

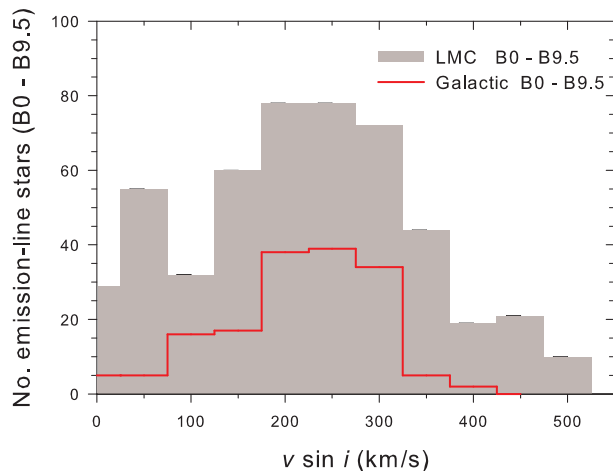


**Figure 20.** The distribution of rotational velocities ( $v \sin i$ ) for all Be stars (B0 - B9.5) in our LMC sample compared to the distribution for Galactic Be stars (B0 - B9.5) found by Slettebak (1982).

B9.5, we have compared their distribution to the distribution found in the Galaxy for the same Be classes using data from Slettebak (1982). From the histogram in Figure 20 we find a correlation coefficient of 0.88 between the LMC and Galactic data sets. Although both data sets are not complete in any sense, the plot indicates that, based on a random selection, the majority of Be stars have a projected rotational velocity between  $200 < v \sin i < 300 \text{ km s}^{-1}$ .

## 8 NEBULA CONTRIBUTION

Approximately 15 percent of the emission-line stars in our sample are B[e] stars which show evidence of forbidden nebula emission lines such as [Fe II]  $\lambda 4244, 4287, 4415, 5273, 7155$ , [N II]  $\lambda 6583, 6548$ , [O I]  $\lambda 6300, 6363$ , [O II]  $\lambda 7320, 7330$  and [S II]  $\lambda 6716, 6731$  in their spectrum. Importantly, not all of these lines are necessarily to be found in every B[e] star but the most common are [Fe II] and [O I]. These stars are often associated with ambient or extended nebula emission which is ionised by the central star with surface temperatures of between 10,000 K and 33,000 K. This means that the H $\alpha$  line may be a combination of central star and nebula emission, making them difficult to separate when the RVs of each component are similar and/or when spectral resolution is not sufficient to distinguish the components.

Since the strength of the H $\alpha$  line in each star and the ambient background H $\alpha$  emission affecting the spectrum are constantly changing with location in the LMC, a general sky subtraction may be insufficient in some cases. Each object located in an area of diffuse H II emission must therefore be individually assessed for ambient nebula contribution on the basis of H $\alpha$  emission within a 10 arcsec radius of the star, which provides a fair estimate in the crowded regions of the LMC. This can be closely approximated using our deep H $\alpha$  map. The measurement of H $\alpha$  intensities on and off the emission-line star produces a ratio which roughly indicates the percentage of H $\alpha$  spectral flux emitting from the star. If the background emission is deemed to be contributing more than 10% of the measured flux, a special note about the B[e] status is made in the comments column of Appendix Table 1. If there is no ambient emission surrounding or in the immediate vicinity of the star, we may safely assume that the star is of the B[e] variety, where we expect to find emission-lines of [N II], [S II], [O II] and even [O III].

In Figure 21 we show an example of a B[e] star with a very significant contribution of emission lines normally associated with nebulae. Where emission lines are this strong we examine the immediate environment for ambient nebula emission. If the deep H $\alpha$  image shows us that much of the emission is environmental, we flag (in the comments column) that the other emission lines in the spectrum may be the result of ambient emission. In Figure 22 we show a regular B[e] star with some nebula lines present but no apparent environmental contribution requiring correction. Finally in Figure 23 we show a Be star requiring no nebula subtraction for environmental reasons and no nebula lines. All of these stars are located within a 1 degree radius of each other, emphasising the importance of surveying the immediate location of each star.

## 9 NEW ACCURATE POSITIONS FOR LMC EMISSION-LINE STARS

We found that emission-line star positions provided by many earlier surveys (mostly using the FK4 system) were not sufficiently accurate when converted to the J2000 equinox and compared to positions across our astronomically accurate survey. As many as 138 previously identified emission-line stars were only published with an accuracy to one decimal fraction of a minute. The majority of these also gave no

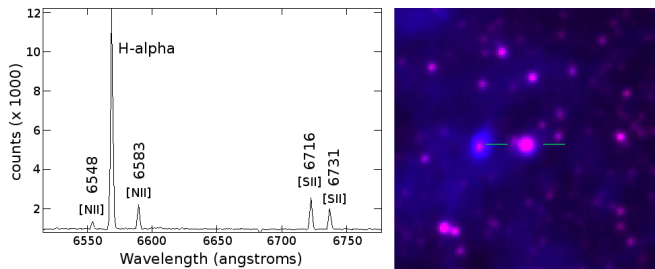


**Figure 21.** Left: A 2dF 1200R grating example of the red spectral region around the H $\alpha$  line in B[e] star RPs226 where there is strong emission from [N II] $\lambda$ 6583,6548 and [S II] $\lambda$ 6716,6731. Right: We show the H $\alpha$  (blue) and short red (red) combined UKST image, clearly showing the local environment and the contribution from ambient nebulous flux. Using the H $\alpha$  map alone we can estimate the proportion of nebula contribution by using the Starlink GAIA task to measure the ambient H $\alpha$  (sky) emission within 10 arcsec ( $\sim$ 2.4pc) of the star and compare the flux to that at the rim of the star, which represents the H $\alpha$  excess (H $\alpha$ -R) emission from the star. The object, 2 arcsec to the east of RPs226 (immediate left in the image) is RP225, a compact HII region.

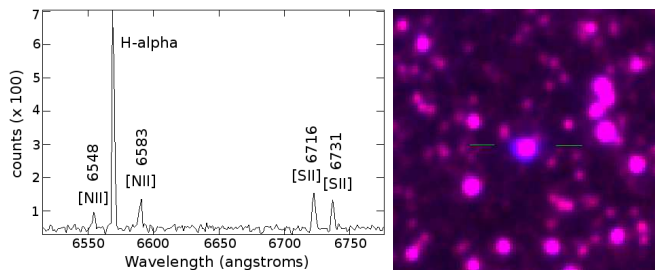


**Figure 22.** Left and right images as described in Figure 21 above. This is an example of a B[e] emission-line star (RPs161) with nebula lines present but no contribution from ambient emission at the stars location. No correction to the H $\alpha$  flux is required.

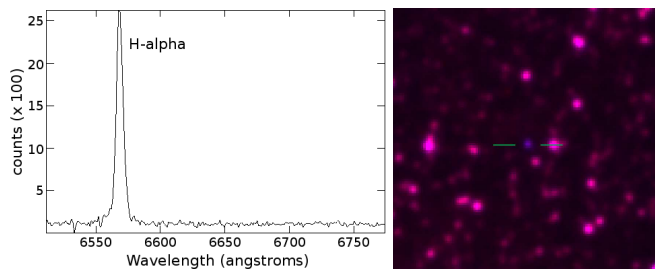


**Figure 23.** Left and right images as described in Figure 21 above. An example of a Be emission-line star (RPs634) not requiring any correction to the measured H $\alpha$  flux. No standard nebula forbidden emission-lines are detected and the environment is free of low level ambient emission.

seconds in DEC. Many true positions were uncertain given the crowded nature of the LMC. In many cases the known emission-line star had to be carefully verified as the object that was previously found. The K-view program in KARMA initially allowed us to find the position of peak intensity of any point source within the stacked H $\alpha$ /SR images allowing accurate positioning to 0.6 arcsec due to our meticulous calibration of our entire map with the SuperCOSMOS world coordinate system.

To improve the positioning and find the most accurate

positions for our new emission-line stars, we extracted red image data from the SuperCOSMOS Image Analysis Mode (IAM). The SuperCOSMOS plate measuring machine samples some 1,000 objects within 10 x 10 armin areas in order to define the xy-to-RA/Dec transformation. The resulting coordinates of a given pixel are thought to be accurate to a few tenths of an arcsec. Using both the H $\alpha$ /SR discovery images and accurate SuperCOSMOS image positions, we matched each emission-line star to the position provided by the IAM data. This match also allowed us to extract the SuperCOSMOS derived B and R broadband magnitudes for each star, as discussed in section 12.

## 10 RADIAL VELOCITIES

Stellar radial velocities for hot B stars are useful for kinematic studies within the LMC. They provide a valuable tool with which to compare young and old populations. Importantly, the radial velocities allow us to verify that our selected emission-line stars reside within the LMC.

Our stellar radial velocities were determined from the medium resolution 2dF 1200R, 6dF 425R and FLAMES spectra as described above. The largest number of velocities (92%) were measured using the 1200R 2dF grating which has an estimated accuracy of  $\pm 4$  km s $^{-1}$ . Two different methods of velocity measurement were employed in order to reduce errors arising as a result of the application of a particular technique. These techniques have been described in Reid & Parker (2006b) and will only be repeated briefly here.

Initially, we used the IRAF EMSAO technique for measuring multiple, specified emission lines. Wavelengths for 13 common emission-lines within the  $\lambda$ 6200-7350 $\text{\AA}$  range were specified to three decimal places. The program found the central position of each available line which was independent of the line width and self-absorption features. It then applied a weighted gaussian fit to each emission line dependent on its intensity, derived a weighted average across the spectrum and corrected for the heliocentric velocity. The EMSAO-derived velocity for each star was displayed and examined.

The second method of velocity determination involved the cross-correlation technique using XCSAO in IRAF (Kurtz & Mink, 1998). This method requires a list of template spectra with low internal velocities and accurately determined published radial velocities against which all the other spectra may be compared for measurement. Template emission-line velocities were based on a minimum of four lines, with at least two of these being fitted by EMSAO (Kurtz & Mink, 1998). Twenty LMC planetary nebula and emission-line star templates with well established velocities were chosen for the cross-correlation.

To derive a best possible radial velocity from our emission-line and cross-correlation methods, we examined the error and other properties (such as the fit and number of lines used) relating directly to each measurement system. From EMSAO, we used weighted velocity results where a large proportion of fitted lines were used in the compilation and error values  $\leq 13$  km s $^{-1}$ . These error values sum and weight the difference in emission line velocities for a given object. Errors larger than this value begin to result from increasingly complex shell velocity structure. Error values up to 13

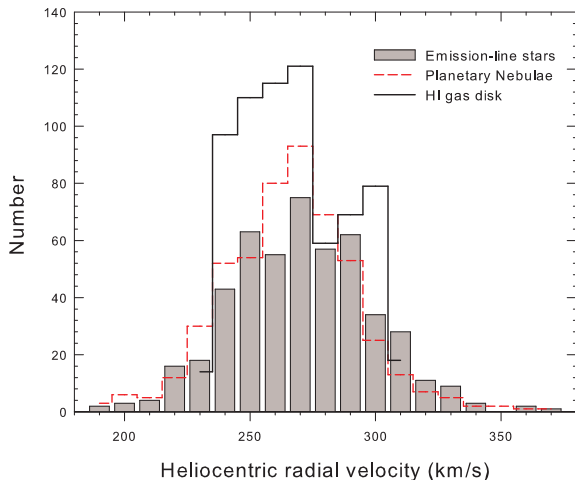


**Figure 24.** The distribution of LMC emission-line star velocities in our survey is shown by number and compared to the distribution for PNe and the HI gas disk. All sources have been placed into  $10\text{ km s}^{-1}$  heliocentric radial velocity bins. The emission-line stars lie within the range found previously for LMC PNe and H II regions which is about  $40\text{ km s}^{-1}$  wider at each end than the HI distribution. All three distributions share a mean peak number of sources at  $270\text{ km s}^{-1}$ . The HI has a sudden trough after the peak ( $280\text{ km s}^{-1}$ ) due to a warp which lies north of the main bar along the line of nodes (see Reid & Parker 2006b).

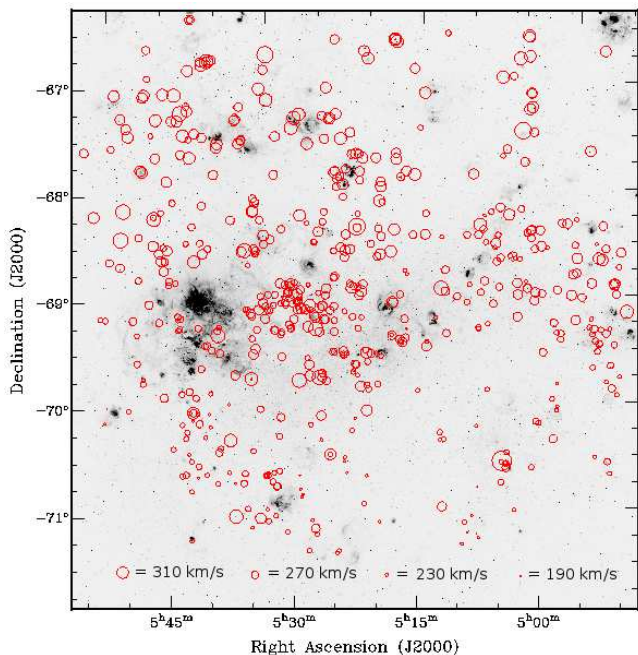


**Figure 25.** An  $\text{H}\alpha$  map of the central  $25\text{deg}^2$  region of the LMC showing the distribution of hot emission-line stars as open red circles, the size of which indicates the measured heliocentric radial velocity. The larger the diameter, the higher the velocity. The circle sizes represent a linear scale but are magnified  $10\times$  in order to emphasize similarities and contrast the deviations within selected areas. Similar to the HI gas disk, the PNe and H II populations, there is a noticeable gradient from high velocities NE of the main bar to low velocities SW of the main bar. The average velocity of  $270\text{ km s}^{-1}$  for emission-line stars is also common to all three populations on the main bar.

$\text{km s}^{-1}$  were to be expected using this technique, as velocity ratios between different lines (eg.  $\text{H}\alpha$  and  $[\text{N II}]\lambda 6583$ ) can vary depending on shock waves within the surrounding shell and/or in a few cases, ambient emission surrounding the star. In the cross-correlation technique, we looked for high correlation peaks and low error values  $\leq 2\text{ km s}^{-1}$ . In general, we favoured the cross-correlation technique since  $>50\%$  of the target stars show only Balmer lines in emission and in many cases a weighted result was not possible with EMSAO. Results from EMSAO were used where errors from the cross-correlation were above  $13\text{ km s}^{-1}$ .

A small percentage of these radial velocities will combine the true radial velocity with stellar atmospheric effects where the envelope is undergoing a phase of contraction or expansion. The contribution from these motions, unlikely to be much more than  $50\text{ km s}^{-1}$ , will not unduly displace these stars away from their location in the LMC. The Balmer and shell lines used for our radial velocities are formed in the cooler outer atmosphere. The lower order  $\text{H}\alpha$  line is formed in the outer layers of the atmosphere and is less affected by the large velocity variations which can affect the higher members of the Balmer series which are formed at the deepest layers of the envelope. According to the Struve's (1931) model, the mass flux of the star and its excitation steadily decreases towards a distance of several stellar radii where the emission lines are formed.

Our velocities, measured in the envelope, are lower than the escape velocity at the photosphere for stars with high  $v \sin i$  found from photospheric He I lines, which are in turn broad, weak and often perturbed by the envelope. Since each emission-line star is individualistic in terms of its  $v \sin i$ , shell structure, phase, periodic and non-periodic radial motions and amplitudes, a weighted average and cross-correlation of the emission line in the outer atmosphere is the most efficient and accurate means of applying a radial velocity to each emission-line star in our catalogue.

In figure 24 we show a histogram of the heliocentrically corrected radial velocities for 501 of the hot emission-line stars in our survey. These are compared with our heliocentric velocities for 515 LMC PNe (Reid & Parker, 2006b) and 686 HI gas disk pointings from the LMC map of Rohlfs et al. (1984), covering the entire  $25\text{deg}^2$  survey region. Each pointing averages an  $\sim 11.45\text{ arcmin}^2$  sub-region, ensuring an unbiased and fully representative distribution and mean can be obtained. The comparison shows that emission-line star velocities lie within the acceptable velocity boundaries and conform well with other LMC population types such as PNe and the HI gas (also see Reid & Parker, 2006b).

LMC emission-line stars and PNe have a very similar distribution but a wider range compared to the HI disk. Although 483 (89%) of the emission-line stars occupy the HI range  $230\text{ km s}^{-1}$  to  $310\text{ km s}^{-1}$ , the 52 outliers are to be expected since the HI disk has a narrow vertical velocity dispersion ranging between  $17\text{ km s}^{-1}$  and  $2.2\text{ km s}^{-1}$  with a mean of  $6\text{ km s}^{-1}$  compared to PNe ( $45\text{ km s}^{-1}$  to  $3\text{ km s}^{-1}$ ; mean  $22\text{ km s}^{-1}$ ) and emission-line stars ( $43\text{ km s}^{-1}$  to  $3\text{ km s}^{-1}$ ; mean  $23\text{ km s}^{-1}$ ), found by sampling  $37 \times 37\text{ arcmin}$  sub-regions across the survey area. A few large dispersions in HI can indicate a splitting of the gas disk, which occurs in regions such as the leading arm (see Reid & Parker 2006b). The central peak of  $270\text{ km s}^{-1}$  is common to all three distributions and indicates a strong midpoint incorpo-

rating both young and old populations. The sudden trough at  $280\text{ km s}^{-1}$  for the HI gas disk is further proof of a sharp warping of the disk which runs north of the main bar in a SE to NW direction, close to the line of nodes (see Reid & Parker 2006). This warping produces a large velocity dispersion and fewer velocities at the  $280\text{ km s}^{-1}$  level. Figure 25 clearly shows proportionally higher velocities for emission-line stars north-east of the main bar and lower velocities south-west of the main bar. This overall gradient is shared by PNe, HII regions and the HI disk but PNe, HII regions and emission-line stars have a greater vertical dispersion at any point than the HI disk.

The common peak velocity ( $270 \pm 30\text{ km s}^{-1}$ ) does not necessarily mean that each population shares the same center of rotation. In fact the rotational centre for PNe and the HI disk have been shown to be located in separate positions (Reid & Parker, 2006b). What we can see from Figure 25 is that  $270 \pm 30\text{ km s}^{-1}$  is the average velocity for emission-line stars in the main bar region.

## 11 DISTRIBUTION ACROSS THE LMC SURVEY AREA

In figure 26 we show the distribution of emission-line stars, superimposed on an  $H\alpha$  map of the central  $25\text{deg}^2$  region of the LMC. The surveyed Be stars in the region are shown as filled red circles while M giants are shown as open blue circles.

Much of the resulting distribution depends on our selection criteria since we were searching for compact emission objects and emission stars fainter than  $\text{Mag}_R = 14$ . For this reason, the most luminous emission-line stars detected in the  $H\alpha$  survey were not spectroscopically observed. Objects were selected for spectroscopic follow-up based on the strength of the  $H\alpha$  emission relative to the luminosity of the central star. Stars with low ( $<5\%$  the central star)  $H\alpha$  excess were not spectroscopically followed up as their low variability and/or emission excess over the 3 year duration of the survey indicated that they were not strong emission-line star candidates. Where the criteria were met, we extended the selection to the faintest luminosity candidates we could find. Emission-line stars found in clusters and associations were only earmarked where related velocities or previous published work make the association clear.

The densest distribution of B-F emission-line stars occurs across the main bar. From there they form a line northwards, following the line of nodes (see Reid & Parker 2006b). There is also a large number to be found along the leading arm, south of 30DOR. Being a young population of stars, they trace the more recent star formation regions and HII distribution quite well compared to the older population of PNe, which are more randomly distributed within the LMC (see Reid & Parker 2006b). The somewhat older M population, however, is more evenly distributed across the north and main bar of the LMC. There is a denser distribution of late-type stars along the leading arm which is thought to be a remnant of the LMC's close encounter with the SMC which may have occurred  $\sim 2 \times 10^8$  years ago (Murai and Fujimoto, 1980).

## 12 $H\alpha$ LUMINOSITY EFFECTS AS A FUNCTION OF SPECTRAL TYPE

The theory of equatorial darkening suggests that a degeneracy in the rotational rates allows Be stars to be rotating at or near their critical breakup velocity, Townsend et al. (2004). This implies that there will be a maximum mass and hence, luminosity, allowable for a Be star. The question then arises as to whether the intensity of  $H\alpha$  emission from these stars relates to the luminosity class for each star. In other words, does the intensity of  $H\alpha$  emission increase in hotter stars? To answer this we have constructed the first ever  $H\alpha$  luminosity histogram as a function of spectral type for Be stars, using our sample in the LMC. It is based on measuring the total flux emitted in the  $H\alpha$  line over and above the continuum level in each star.

In order to do this, measured  $H\alpha$  fluxes were converted to the  $H\alpha$  magnitude scale by correlating the  $H\alpha$  flux from known emission objects with no continuum and no [N II] contamination against well established  $H\alpha$  magnitudes for those objects. A zero point scale was then found in order to convert all  $H\alpha$  fluxes to  $H\alpha$  magnitudes. This allows comparison to other luminosity functions, such as the planetary nebulae luminosity function, which is already extensively used for distance determination.

This inaugural conversion of  $H\alpha$  fluxes to magnitudes was made by choosing PNe with published HST-derived fluxes and 2dF spectra where the PN showed no measurable [N II]  $\lambda 6548$  &  $\lambda 6583$  but were bright enough to be seen in broad-band R. PNe were chosen because the continuum level is close to zero, allowing the measurement of  $H\alpha$  emission only. Each PN was located in the  $H\alpha$  map data and an R-band image with an area of 0.1 arcmin radius around each PN was downloaded from SuperCOSMOS online. Along with the image, the IAM data 'tab' file was also downloaded. This file contains precise object positions and R magnitudes from the SuperCOSMOS sky survey and the ESO guide star catalogues. These magnitudes were graphed (see Figure 27) against our calibrated LMC PN fluxes (Reid & Parker 2010) and fluxes from the MCPN catalogue (Stanghellini et al. 2002).

The fit is sufficient to reveal the position of the line of best fit which will be used to perform the conversion. The scatter, up to half a magnitude, seen on either side of the logarithmic line of best fit is to be expected due to the limited linear response of the digitized film and characteristics of the  $H\alpha$  filter used on the UKST but does not pose any problem to the calibration of fainter objects since the AB magnitude scale is always fixed at  $2.5 \log(F_{H\alpha})$ . The logarithmic relation of flux to magnitude means that the slope of the line of best fit will always be fixed. The graph is simply used to attain the magnitude conversion value, which is the final number in the empirical relation:

$$m_{H\alpha} = -2.5 \log F_{H\alpha} - 14.15 \quad (4)$$

for the conversion of all the derived  $H\alpha$  fluxes ( $\text{ergs}^{-1} \text{cm}^{-2} \text{s}^{-1}$ ) into  $H\alpha$  apparent magnitudes ( $m_{H\alpha}$ ). A mean error estimate of  $\pm 0.27$  mag is based on line measurement and flux calibration errors at a total 7% plus 0.1 mag for uncertainties in image photometry.

To check the veracity of this calibration, we used the



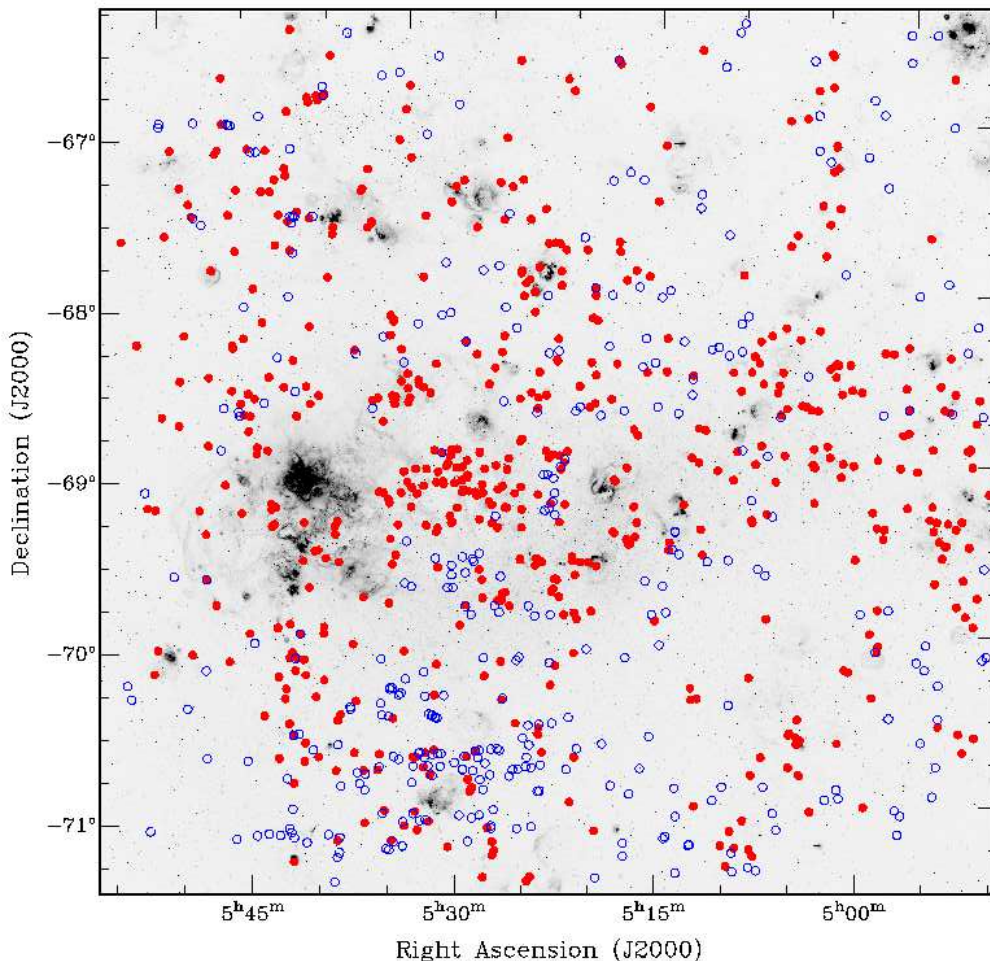


**Figure 26.** An  $H\alpha$  map of the central  $25\text{deg}^2$  region of the LMC showing the distribution of hot emission-line stars as filled red circles. The positions of late-type (mostly M-giant) stars are shown as blue open circles. Stars less than 10 arcsec apart cannot be distinctly separated by the large markers in this image. There is a significant concentration of hot emission-line stars on the immediate north-eastern side of the main bar while M-giants are concentrated to the south.

ESO magnitude-to-flux converter<sup>2</sup> to convert  $H\alpha$  fluxes in  $\text{ergs}^{-1} \text{cm}^{-2} \text{s}^{-1}$  to  $H\alpha$  magnitudes, using a variety of narrow band filters. Using the accepted flux-to-mag conversion of  $-2.5 \log F_{5007} - 13.74$  for  $[\text{O III}]\lambda 5007$  emission lines (Jacoby 1989), we simulated a variety of narrow band filters and telescopes and found that any given flux value will be between 0.4 and 0.58 mag brighter in  $H\alpha$  than in  $[\text{O III}]\lambda 5007$ . With our magnitude correction of -14.15, a given flux will be 0.41 mag brighter in  $H\alpha$  than in  $[\text{O III}]\lambda 5007$ , in basic agreement with ESO simulations, giving us added confidence in our new empirical relation.

Using this conversion we constructed the  $H\alpha$  luminosity function, which is a measure of the  $H\alpha$  emission above the continuum and is presented in terms of the each stars' spectral classification (see Figure 28), a relation which has been unknown to date. The figure shows only a modest increase in  $H\alpha$  luminosity with increasing spectral type over a 9 magnitude range. The spectral type or temperature of the star therefore does not correlate strongly with the luminos-

ity of the Balmer emission. As expected, however, classes B0 to B3 dominate the bright end while classes B6 to F9 can mainly be found at the faint end. The bright cutoff occurs at magnitude 15 (an absolute magnitude of -4.5) and the peak in the function (the largest number of stars in any particular bin) occurs at magnitude 18.6. After this peak there is a steady decrease in the distribution over the next 5 magnitudes to the faintest detection at magnitude 23.8. The lone star with a bright  $H\alpha$  magnitude of 14.6 is a luminous blue variable (LBV). The shape of the distribution is not unlike that for planetary nebulae in the LMC (see Reid & Parker 2010) but it is unlikely that this function can be used as an extra-galactic distance scale as the brightest  $H\alpha$  emission line is a magnitude fainter than the brightest  $[\text{O III}]\lambda 5007$  line from PNe in the LMC which is traditionally used for the PNLF.

### 13 PHOTOMETRY

We obtained B, V, I magnitudes from OGLE-II photometry for 54 previously known Be and B[e] stars which were

<sup>2</sup> <http://archive.eso.org/apps/mag2flux/>

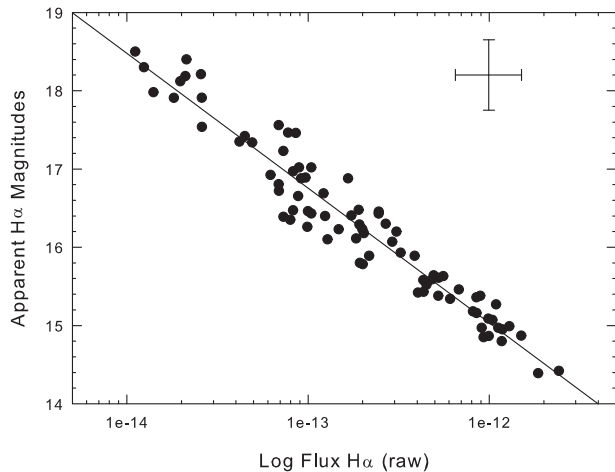


**Figure 27.** The graph, based on our LMC PN sample, used to convert  $H\alpha$  flux to  $H\alpha$  magnitude. The apparent  $H\alpha$  magnitudes for LMC PNe were measured using image photometry on the stacked  $H\alpha$  map. Only PNe with extremely low or no  $[N\text{II}]6548$ ,  $6583\text{\AA}$  lines were included in the calibration since the presence of these lines in the wings of the filter can effect the  $H\alpha$  measurement. The  $H\alpha$  fluxes are from our calibrated 2dF and longslit fluxes for the same PNe. Calibrated this way, there is no need to subtract continuum from the  $H\alpha$  line. The scatter is expected due to the limited linear response of the digitised photographic data used to create the  $H\alpha$  map. The line of best fit is shown on the graph and the underlying algorithm is provided at equation 4.

found to have strong variability. To this number we add 63 newly discovered Be stars with published OGLE-II photometry (Szymański, 2005, Udalski et al. 2002), found from the limited OGLE coverage of the main bar only. For other stars not in the OGLE data base we gained I, B and R photometry from SuperCOSMOS. The Starlink GAIA image detection option was used to detect and isolate sources by placing an ellipse around the assumed centre. For single stars found in relative isolation this works extremely well. For other sources with close companions or within clusters, the de-blending option was employed. The position of each star was manually checked against the downloaded image to ensure accuracy of positioning and non-blending.

To supplement the OGLE-II V magnitudes we also include GSC2 V magnitudes from ESO. We warn the user to use care in comparing the three photometric sets directly against each other due to intrinsic variability and the change of epoch between the three surveys. Unless specified, we only compare OGLE-II photometry in this section since the published values are an average across the survey period.

### 13.1 V vs (B-V) colour-magnitude diagram

B stars congregate at the upper left of the traditional H-R colour-magnitude diagram, close to a 0 B-V colour and where the tracks for main sequence, subgiant and giant stars converge. This area of the H-R diagram is a useful test for our Be stars for two reasons. Firstly, by separating giants from main sequence stars, we can independently test our correlated estimates for luminosity class. Secondly, we can

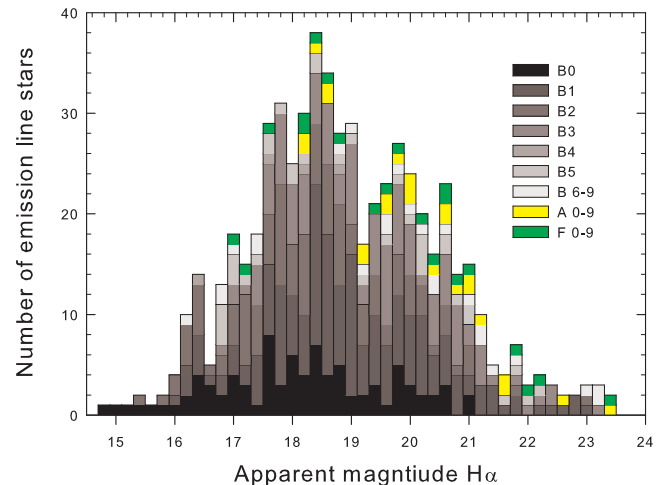


**Figure 28.** The luminosity function of  $H\alpha$  emission from hot emission-line stars found in our survey within the central  $25\text{deg}^2$  region of the LMC. The luminosity bins are 0.2 magnitudes and spectral classifications are indicated in the legend.

see if the variability of these stars is having any effect on the normal position of these stellar classes.

The V versus (B-V) magnitudes for a sample of 100 of our LMC emission-line stars is shown in Figure 29. These magnitudes are derived from OGLE-II photometry where the variability of these stars has been established. Their position on the diagram includes corrections for foreground and intrinsic reddening within the LMC. These reddenings were obtained from the Strömgren CCD photometry on LMC fields conducted by Larsen et al (2000) using B stars. Although several of the stars in this small sample exhibit a strong reddening, only 3 of them - RPs83, RPs1751 and RPs1350 - are visibly surrounded by extended emission halos ( $\geq 6$  arcsec radius). Rather than applying a small reddening to each individual object, we adopt an uncertainty of  $\pm 0.10$  for all of these stars since they are close to or on the main bar (Larsen et al. 2000). The stars are separated into main sequence (open red circles) and giants (filled black circles) in Figure 29 where the position of the intrinsic (observed) zero point for (B-V) is shown as a broken vertical line.

The plot indicates that the cross-correlation technique appears to be working very successfully. Main sequence stars appear to be spread across the plot at a broad 45 degree angle from the lower right, following the established track for main sequence stars. Giants on the other hand span across the centre of the plot to the left where they increase in V magnitude.

### 13.2 $H\alpha$ emission

A correlation has been found between the strength of  $H\alpha$  emission and the spatial extent of the emitting region of a Be star (eg. Quirrenbach et al., 1997, Tycner et al. 2005). The  $H\alpha$  emission is also thought to be correlated with the observed colour excess (Dachs et al. 1988) where an increase in both  $H\alpha$  emission and the colour excess  $E(B-V)$  will oc-

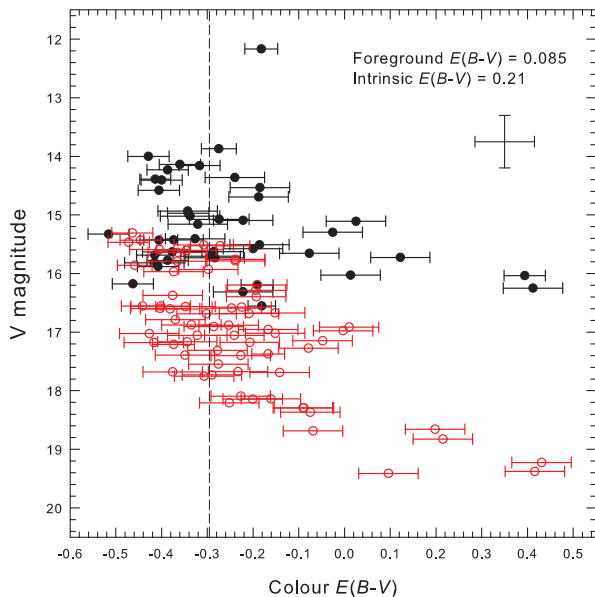


**Figure 29.** The V versus  $E(B-V)$  colour-magnitude diagram from OGLE-II photometry for 117 variable hot emission-line stars found on the LMC main bar. Main sequence stars are assigned red open circles while giant stars are represented by filled black circles. We assume a combined foreground and intrinsic reddening of  $E(B-V) = 0.295$ . Error bars are based on a combination of B and V published error estimates for B stars on or very close to the main bar. Maximum errors on both scales are shown. The observed position of  $(B-V) = 0$  is shown by the broken vertical line.

cur with a larger contribution from bound-free and free-free continuum emission (Beaulieu et al. 2001). For Be stars in our LMC sample, we also find a mild correlation between the Balmer line radiation originating from the stellar envelope as exhibited by  $H\alpha$  equivalent width  $EW(H\alpha)$  and the  $(B-V)$  colour indices. This relation is shown in Figure 30 where the correlation is strongest at low  $EW(H\alpha)$ .

The increasing scatter with increasing  $EW(H\alpha)$  is partly due to increased reddening from interstellar dust and emission from the circumstellar gas envelope, and partly due to complex variations in the  $H\alpha$  emission profiles between the time of our spectroscopic observations and the OGLE-II observations. Since the measured  $EW(H\alpha)$  is an integrated quantity, it has the tendency to be insensitive to the small-scale variations in the line profile. Effects from OGLE-II photometry, where the LMC was observed repeatedly between 1997 and 2000 will mostly correspond to our 12  $H\alpha$  stacked images, also observed between 1997 and 2000. The average of these photometric variations over 3 year timescales was applied to our spectroscopic observations conducted in 2004 and 2005. Since  $(B-V)$  has been averaged out over timescales of years, this ratio is not expected to vary greatly with variation of the star's intrinsic luminosity. For the most variant objects, our spectroscopic measurements of the  $H\alpha$  line require slightly larger error margins but re-

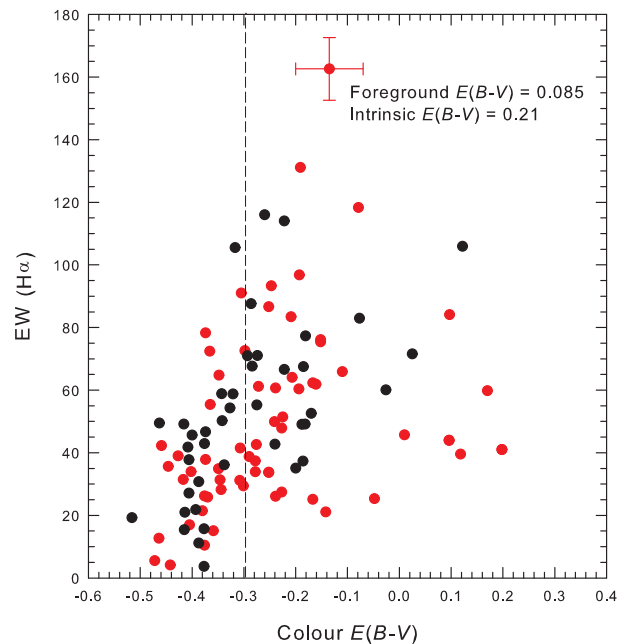


**Figure 30.** The equivalent width ( $H\alpha$ ) versus  $E(B-V)$  colour diagram using our measured  $H\alpha$  magnitudes and averaged OGLE-II photometry for 100 variable Be stars in the LMC sample. We assume a combined foreground and intrinsic reddening of  $E(B-V) = 0.295$ . Error bars are based on a  $\pm 0.10$  estimated error for B stars on or very close to the main bar. The observed position of  $(B-V) = 0$  is shown by the broken vertical line. There is a mild correlation up to  $E(B-V)$  of  $\sim -0.3$  but as the colour index increases the relation breaks down. Giant stars are again shown in black and main-sequence stars are shown in red.

main impossible to estimate without repeated spectroscopic exposures.

Despite these caveats, a mild correlation is still evident. The decrease in the maximum observed value of  $(B-V)$  with increasing  $EW(H\alpha)$  is one of the main features. It implies that cooler stars will have larger emission shells with a probable maximum size allowable for each spectral class.

In Figure 31 we replace the  $EW(H\alpha)$  with the  $H\alpha$  emission flux above the continuum. There is no correlation evident, however, the range in  $(B-V)$  appears to broaden with decreasing flux suggesting that low  $H\alpha$  flux can be present in both the brightest and faintest Be stars.

Figure 32 shows that the  $H\alpha$  magnitude is almost consistently fainter than the V magnitude of the star by a mean of  $2.72 \pm 1$  mag. The correlation coefficient between the  $H\alpha$  and V magnitudes for our set is only 0.578, implying that the V magnitude of any particular emission-line star could be associated with a wide range of  $H\alpha$  flux excess. Figure 32 shows that this could be up to 3 magnitudes either side of the mean correlation, which is  $V_{mag} = H\alpha - 2.72$ .

The main body of available V magnitudes cease at  $V=18$  due to the limit of the ESO catalogue. OGLE-II magnitudes extend to fainter limits. Stars intrinsically fainter than  $V=18$  include a wide variety of spectral types so it may be that many of them were undergoing a strong emis-

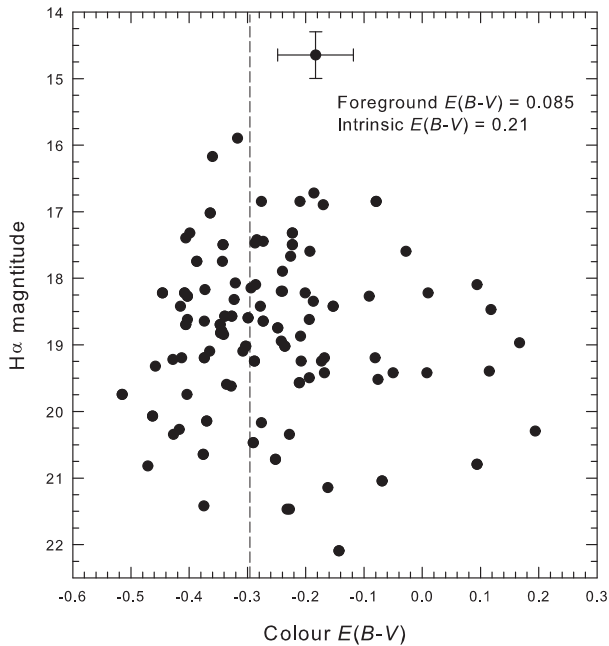


**Figure 31.** The  $H\alpha$  emission from stars in the LMC is compared with their  $E(B-V)$  colour. No real correlation between the  $H\alpha$  magnitude and colour index can be seen. The magnitude of the  $H\alpha$  emission is therefore somewhat independent of the  $E(B-V)$  colour of the host star. Similar to Figure 30, however, the minimum observed  $E(B-V)$  colour appears to increase with increasing  $H\alpha$  magnitude above magnitude 20.

sive phase at the time of our spectroscopic observations. The effect of  $H\alpha$  flux variability upon  $V$  magnitude is impossible to estimate, however we may assume that a portion of the scatter away from the line of best fit may be due to oscillations.

The emission-line stars in figure 32 have been separated into giants and main sequence classifications in order to investigate their positions on the H-R diagram according to luminosity class. As expected, the giants dominate the bright end and the main sequence stars dominate the faint end of the plot. The overlap region of  $\sim 2$  magnitudes from  $V=14.7$  to  $V=16.7$  contains about 15 main sequence stars with rather low  $H\alpha$  emission. There is nothing peculiar that these stars have in common. Their spectral types range from B1Ve to A6IVe. The size separation either side of the overlap region ( $V_{mag}$  16.7-14.7) is very robust, permitting a secure size assessment to be made based on  $V$  magnitude alone.

## 14 VARIABILITY

The variable nature of Be and B[e] stars is an important feature which relates to the physical stability of the star. As a phenomenon, it has been known for more than a century and may be due to various combinations of physical properties, one or more of which may undergo a transition. Suggested mechanisms are mass loss through stellar winds, rapid ro-

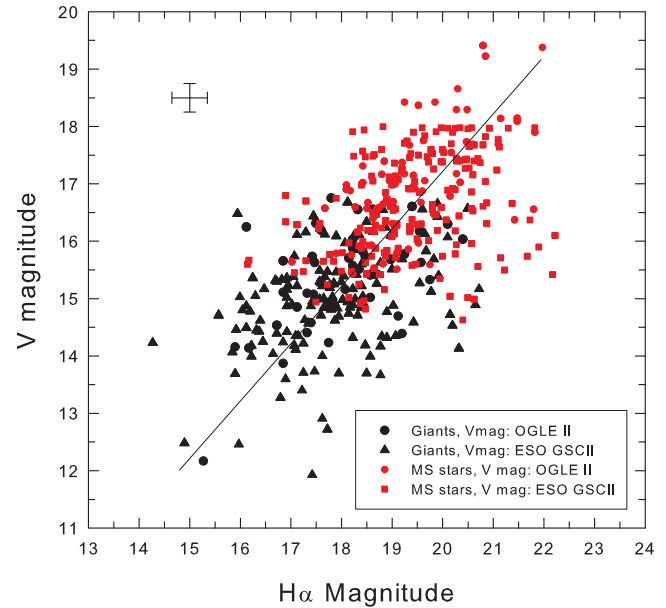


**Figure 32.** The luminosity of  $H\alpha$  emission from stars in the LMC is compared with their  $V$  magnitude. Giants and main-sequence stars are separated and assigned black and red colours respectively. A mild correlation can be seen down to the faint cut-off of  $V=18$  for the ESO dataset. The linear line of regression indicates that  $H\alpha$  magnitudes are generally 2.72 magnitudes fainter than the visual magnitude for these stars. The correlation coefficient is 0.578 and the equation:  $V_{mag} = H\alpha - 2.72$ , may be used as a rough estimate. Maximum expected errors based on published (for  $V$ ) and measurement/calibration (for  $H\alpha$ ) are shown.

tation and/or non-radial pulsations (see Porter & Rivinius, 2003). These mechanisms, individually or in combination are usually proposed to explain disc formation and outbursts in Be stars. Sudden brightening and fading episodes are thought to be connected with discrete mass ejection at the surface of Be and B[e] stars. The most notable variations are time dependent variations, known as E/C variations (Hubert-Delplace et al. 1982) where there may be either a change in the emission line intensity or in the continuum level. The latter occasionally cause a veiling effect in the intensity of early-type Be stars.

The jury is still out regarding the mechanism that triggers short-period line profile variability. The possibility of non-radial pulsations has been proposed by several authors (see Rivinius et al. 2003). If the modeling codes (see Townsend, 1997) are observationally confirmed, up to 80% of early-type Be stars may pulsate in one or more modes. Large numbers of spectroscopic observations to detect multi-periodicity will help to decide this issue. Lastly, and related, are the time variations in the intensities of violet and red components (V/R) as seen in double-peaked emission-line profiles. These probably arise from one-armed density waves in the circumstellar disk.

The classification of Be stars in terms of their light curves was initiated by Mennickent et al. (2002) based on their discovery of 1056 Be star candidates in the Small Magellanic Cloud (SMC) using OGLE II data. Having observed

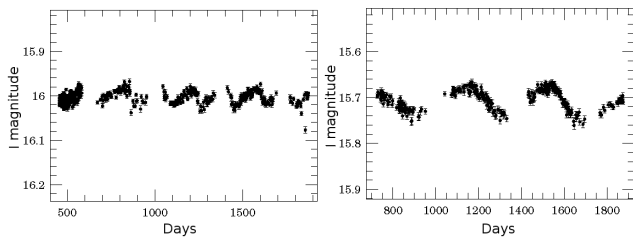


**Figure 33.** Light curves for RPs1383 (B0Ve, H $\alpha$ : Single Peak,  $v \sin i$ :  $243 \pm 12 \text{ km s}^{-1}$ ) and RPs1794 (B2V[e], H $\alpha$ : Single Peak,  $v \sin i$ :  $185 \pm 9 \text{ km s}^{-1}$ ) from the OGLE-II database. These examples show regular variability, with a steady central magnitude.

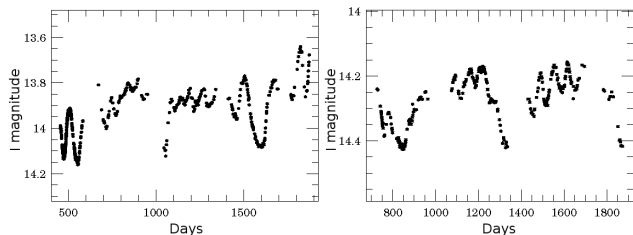


**Figure 34.** Light curves for RPs870 (B2IV[e], H $\alpha$ : Double Peak R>V,  $v \sin i$ :  $245 \pm 12 \text{ km s}^{-1}$ ) and RPs2197 (H $\alpha$ : Double Peak R>V,  $v \sin i$ :  $82 \pm 4 \text{ km s}^{-1}$ ) from the OGLE-II database. These examples show semi-regular variability interspersed with minor variations.

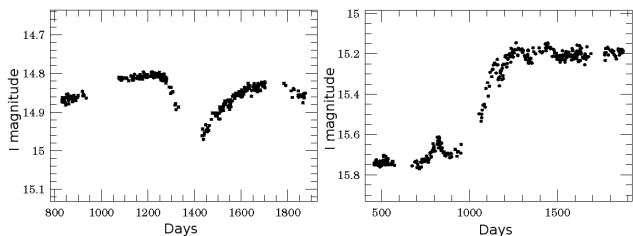


**Figure 35.** Light curves for RPs1173 (B1IIIe, H $\alpha$ : Single Peak,  $v \sin i$ :  $356 \pm 18 \text{ km s}^{-1}$ ) and RPs1382 (B1Ve, H $\alpha$ : Double Peak V>R,  $v \sin i$ :  $319 \pm 16 \text{ km s}^{-1}$ ) from the OGLE-II database. These examples are long period variables which may also include micro features such as that seen at period 1200 days in the right image.

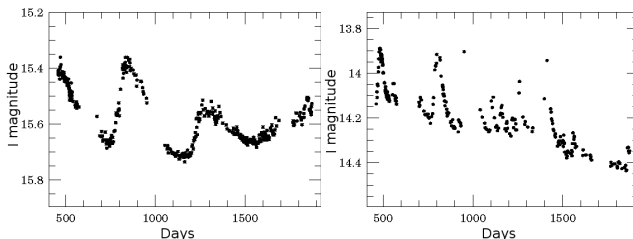


**Figure 36.** Light curves for RPs1381 (B1Ve, H $\alpha$ : Single Peak,  $v \sin i$ :  $184 \pm 9 \text{ km s}^{-1}$ ) and RPs1348 (B1IIIe, H $\alpha$ : Single Peak,  $v \sin i$ :  $133 \pm 79 \text{ km s}^{-1}$ ) from the OGLE-II database. RPs1381 shows quasi-non-regular periods where the brightening can be quite sudden at times. RPs1348 shows semi-regular variability on a broad decline over a long period.

several light curves not seen in Galactic Be stars, they classified four types. Type-1 show outbursts; Type-2 show sudden high and low oscillations; Type-3 show periodic or near periodic variations; Type-4 show the type of light curves seen in Galactic Be stars.

In our data, variability is usually easy to detect by comparing an image taken at a single epoch with our 12 stacked and combined images taken over a 3 year period. While this method strongly indicates variability, the length of the periods can only be measured with repeat exposures over regular intervals.

Although the OGLE photometry currently available does not cover the outer regions of the LMC, there is sufficient data available to find variable stellar candidates within the inner bar region of the LMC. A careful search has found 117 stars with OGLE II data available from our selection of Be stars in the area. Some representative examples of the light curves from these stars are shown in Figures 33 to 36. Periods vary between a few days and over 2,000 days. Magnitude variations range from 0.05 mag (Figure 33 left) to 0.6 mag (Figure 33 right). Many stars show inconsistent variations in both magnitude and period. For example, Figure 34 left shows several 100 day periods followed by a general 0.2 mag increase. The brighter magnitude is accompanied by short bursts which broaden out and increase to 0.3 magnitudes after 900 days. The light curve of RPs1382 (Figure 35 right) shows a short 0.15 mag burst after 400 days (from the start of observations) which precedes and may possibly have pre-cursed a large 0.5 mag increase which was maintained for at least 700 days to the end of the observations. Examples not shown here also include long-term fading episodes such as large decreases over 0.5 in magnitude followed by a wave of short period bursts.

For our LMC data, the larger magnitude variability (>0.2 mag) is mainly confined to early spectral type Be stars (brighter than  $\sim B4$ ). These variations include regular, semi-regular and sporadic outbursts in stars with moderate to high  $v \sin i$ . Short and mid-term variability on scales of days to weeks can produce amplitudes of up to 0.3 mag. Long-term variability (years to decades) can be accompanied by amplitudes up to 0.8 mag. It is noteworthy that the 2 long period examples with major fading and brightening events shown in Figure 35 have high rotational velocities which are among the highest 20% of  $v \sin i$  measurements in our sample.

Figure 36 left shows RPs1381, an example of a Be star which features recurrent outbursts (100 days) which slowly decrease over much longer periods, typically about 400 days in this example. Each outburst has a decreasing amplitude which culminates in a gradual brightening after at least 1000 days.

An interesting phenomenon observed in some variable stars is multiple period oscillations. Low amplitude oscillations are superimposed on much slower and often irregular periods. For example, we find  $\sim 100$  day luminosity bursts or minor periods occurring as stars experience an overall decrease in magnitude lasting in excess of 2000 days (Figure 36 right). The variability of emission-line stars is now recognised as one of the main Be star diagnostics; hence further spectroscopic follow-up has been planned.

## 15 THE CATALOGUE OF EMISSION-LINE STARS

The full catalogue of emission-line stars uncovered in the stacked H $\alpha$  survey of the central 25deg<sup>2</sup> of the LMC is provided in the Appendix as Tables 1 and 2. In Table 1 we present our measured and derived data whereas in Table 2 we present a compendium of catalogue identifications and magnitudes where available for each star.

In the first column of Table 1 we give the Reid & Parker (RPs) catalogue number where the ‘s’ is added to clearly identify and separate stars from other objects such as PNe, SNRs and H II regions which included in the larger RP catalogue. Columns 2 and 3 give the accurate RA and Dec in J2000 world coordinates to 2 decimal places in RA and 1 decimal place in DEC with reference to SuperCOSMOS and verified against 2MASS astrometry. Column 4 provides a published catalogue reference where a star has been previously identified. Please note that this reference does not necessarily indicate that the star was known as an emission-line star. Column 5 shows our estimate of spectral classification and luminosity class as derived from the cross-correlation described in section 6.1.

Column 6 gives the emission flux from H $\alpha$   $\lambda$ 6563 which was measured from our flux-calibrated spectra. All measurements of the H $\alpha$  line including the flux, FWHM (column 7) and the EW (column 8) were measured using the highest quality, medium to high resolution spectra ( $R > 1,000$ ) available in our data set. Individual measurements were made using standard IRAF tasks. The heliocentric velocity shown in column 9 represents the measurement which produced the lowest errors, obtained from our high resolution spectra using the IRAF (EMSAO and XCSAO) tasks. Details are provided in section 10. The estimated rotational velocity ( $v \sin i$ ) is shown in column 10 and described in section 7.

In column 11 we provide comments on each star including a list of which H lines were observed in emission. In the majority of cases, forbidden lines indicate that the star is a B[e] type, however, in several cases, the presence of both low [S II] emission and ambient H $\alpha$  emission (detected in our H $\alpha$  stacked image) suggest that these forbidden lines are not intrinsic to the star itself. In such cases we present the star as a normal Be star but comment on the low [S II] found in the spectrum. Standard abbreviations include ‘SP’ and ‘DP’ indicating an H $\alpha$  line with a single peak or a double peak respectively. The ‘DP’ abbreviation is usually followed by either ‘V>R’, ‘R>V’, or ‘centre’ indicating the position of the absorption feature (see section 6.4).

The second table presented in the appendix contains a compilation of the B, V, I and R photometry available for each object in this work. In the first three columns we again provide the RP number, RA and DEC of each object to make identification and cross-referencing easier. The fourth column lists the GSC2.2 catalog reference number while column 5 gives the linear distance in arcmins between our position and the GSC2.2 position. Positional errors at the plate epoch are estimated to be in the 200-250 mas range. Column 6 gives the OGLE catalog reference where the matching position has been found in the OGLE II database. Column 7 gives the USNO-A2.0 catalog reference with the linear distance in arcmins between our position and the best matching USNO position shown in column 8. It is estimated that the

positional error at plate epoch is near 250 mas. Column 9 then provides the position angle (PA) for each object published in the USNO catalog.

The remaining columns, 10 to 18 provide the magnitudes where available for each star. Since emission-line stars are variable, we should expect a comparison of surveys to reveal minor variations in overall flux estimates. These modulations are confirmed by the data presented here.

In columns 10 to 12 we present the B magnitudes from OGLE, SuperCosmos (SC) and USNO respectively. Columns 13 and 14 give the V magnitudes from GSC2.2 and OGLE. Columns 15 and 16 give the I magnitudes from SC and OGLE and columns 17 and 18 give the R magnitudes from SC and USNO.

Our online database to be hosted at Macquarie University will contain extra information relating to each star. We will provide optical spectra for each object as well as  $1 \times 1$  arcmin H $\alpha$ /Short Red thumbnail images. At the time of writing, the web site is under construction.

## 16 SUMMARY

Using our deep H $\alpha$  and SR maps centered on the central 25deg<sup>2</sup> of the LMC, we have uncovered 1,003 stars which exhibit H $\alpha$  emission. A series of follow-up spectroscopic observations were performed, mostly using 2dF on the AAT during December 2004. The majority of the stars have been assigned a spectral classification using the IRAF cross-correlation technique and spectral class templates. In addition to the 111 previously known Be stars we have added 468 newly discovered Be, B[e], A and F stars. Most of these stars fall between spectral classes B1 and B3. Analysis of the survey data has also allowed us to identify 315 M (late-type) stars exhibiting chromospheric emission.

For the hot emission-line stars, we provide new, accurate positions, radial and rotational velocities. The distribution of radial velocities has been plotted and compared to the heliocentric distributions for PNe and the H I gas disk in the LMC. The good agreement not only indicates that all our emission-line star candidates are located in the LMC, but traces the overall inclination of the LMC’s main disk. The distribution of rotational velocities has been plotted and compared to a Galactic sample, revealing a 200-300 km s<sup>-1</sup> agreement in the peak of the distributions. We have also briefly discussed the various H $\alpha$  emission-line profiles identified in our LMC sample.

Emission from the hot B to F stars has been measured and flux calibrated in order to provide the first ever luminosity function for the H $\alpha$  emission from these stars. This included the first ever derived conversion from H $\alpha$  fluxes to magnitudes, with its associated formula, which can be used generally for emission objects in the LMC. The emission has a bright cut-off at magnitude 14.8 (absolute -4.5) and covers a 9 magnitude range. The function shows a steady rise to a distribution peak at 18.5 followed by a decrease over 5 magnitudes to magnitude 23.6. We find a mild correlation between the H $\alpha$  and V magnitudes of the hot stars in our sample. Main sequence stars in our sample are only found at magnitudes below 14.5 in V whereas giants extend to magnitude 12 in V. A compilation of B,V,I and R magnitudes

from OGLE II, SuperCOSMOS, ESO GSC 2.2 and USNO are provided in Table 2 of the Appendix.

A plot of the distribution of emission-line stars within the survey area shows that approximately 40% lie on the main bar. As many as 130 (25%) of the B-class stars are found to be of the B[e] variety, emitting forbidden lines in [S II], [N II], [O I] and even [O III]. Many of these are located in areas of strong ambient emission or H II regions so care is needed to removed these contributions if only emission associated with or emitting from the star is to be measured. These stars with probable contamination have been labeled accordingly within the tables.

## 17 ACKNOWLEDGEMENTS

The authors wish to thank the AAO board for observing time on the AAT and UKST. The authors also thank the European Southern Observatory for observing time on the VLT and Australian National University along with their telescope time allocation committees for supporting our programme of follow-up spectroscopy. We thank the anonymous referee for very helpful comments and suggestions while carefully reviewing the paper. Lastly we would like to thank Suzanne Reid from Kalidus Systems for lending her database design skills to create a repository for the emission-line star data.

## REFERENCES

- Acke B., van den Ancker M.E., Dullemond C.P. 2005, *A&A*, 436, 209
- Andrews A.D., Lindsay E.M., 1964, *IrAJ*, 6, 241
- Andrillat Y., & Houziaux L. 1991, *IAUC*, 5164, 3
- Beaulieu J-P., et al., 2001, *A&A* 380, 168
- Bohannon B.E., Epps H.W., 1974, *A&AS*, 18, 47
- Böhm T., & Catala C. 1994, *A&A*, 290, 167
- Böhm T., & Hirth G.A. 1997, *A&A*, 324, 177
- Bowyer S., Sasseen T.P., Wu X., Lampton M., 1995, *AJ* suppl. ser. 96, 461
- Bjorkman J.E., Cassinelli J.P., 1993, *ApJ*, 409, 429
- Bjorkman K. S., Miroshnichenko A.S., McDavid D., Pogrosheva T.M. 2002 *ApJ*, 573, 812
- Bland-Hawthorn J., Shopbell P.L., Malin D., 1993, *AJ*, 106, 2154B
- Butler C.J., Wayman P.A., 1974, *DunOP*, 1, 193
- Cassinelli J.P., Brown J.C., Maheswaran M., Miller N.A., Telfer D.C., 2002, *ApJ*, 578, 951
- Cohen M., Kuhl L., 1979, *ApJS*, 41, 743
- Corcoran M., Ray T.P., 1998 *A&A*, 331, 147
- Cranmer S.R., 2005, *ApJ*, 634, 585
- Dachs J., Hanuschik R.W., Kaiser D., & Rohe D., 1986, *AA*, 159, 276
- Dachs J., Kiehling R., Engels D., 1988, *A&A*, 194, 167
- Draper H., 1924, *Ann. Astron. Obs. Harvard* 91-100, 1-6
- Feast M. W.; Thackeray, A. D.; Wesselink, A. J. 1960, *MNRAS* 121, 337
- Frew D., Parker Q., 2010, *PASA*, 27, 129
- Gordon K.D., Clayton G.C., Misselt K.A., Landolt A.U., Wolff M.J., 2003, *ApJ*, 594, 279
- Grebel E.K., 1997, *A&A*, 317, 448
- Grebel E.K., Chu Y., 2000, *AJ*, 199, 787
- Gullbring E., Hartmann L., Briceno C., Calvet N., 1998, *ApJ*, 492, 323
- Hamann F., 1994, *ApJS*, 93, 485
- Hambly N. C., et al., 2001, *MNRAS*, 326, 1279H
- Hanuschik R.W., 1989, *Ap&SS*, 161, 61
- Hanuschik R.W., Hummel W., Sutorius E., Dietle O., Thimm G., 1996, *A&AS*, 116, 309
- Hartigan P., Edwards S., Ghandour L., 1995, *ApJ*, 452, 736
- Hartmann L., Hewett R., Calvet N., 1994, *ApJ*, 426, 669
- Heney L.G., Lelevier R., Levée R.D., 1955, *PASP* 67, 154
- Henize K.G., 1956, *ApJS*, 2, 315
- Hubert-Delplace A. M., Hubert H., Chambon M. T., Jaschek M. 1982 *IAUS: Be stars; Proceedings of the Symposium, Munich, West Germany, 1981, Dordrecht, D. Reidel*, 98, 125
- Hubert A.M., Floquet M., 1998, *A&A*, 335, 565
- Herbig G.H., 1960, *ApJS*, 4, 337
- Hernández J., Calvet N., Briceño C., Hartmann L., Berlind P., 2004, *AJ*127, 1682
- Hillenbrand L.A., Strom S.E., Vrba F.J., Keene J., 1992, *ApJ*, 397, 613
- Hubrig S., Schöller M., Yudin R.V. 2004, *A&A*, 428, L1
- Hughes S.M.G., 1989, 97, 1634
- Hummel W., Szeifert T., Gässler W., Muschielok B., Seifert W., Appenzeller I., Rupprecht G., 1999 *A&A* 352, L31
- Hutsemékers D. 1985, *A&AS*, 60, 373
- Jaschek M., Jaschek C., 1967, *ApJ*, 150, 355
- Jacoby G.H., Hunter, D.A., Christian C.A., 1984, *ApJS*, 56, 257
- Jacoby G.H., 1989. Planetary nebulae as standard candles. I. Evolutionary models. *ApJ*, 339, 39
- Jaschek M., Jaschek C., 1967, *ApJ*, 150, 355
- Jaschek M., Slettebak A., Jaschek C., 1981 *Be Star Newsl.*, 4, 9
- Kaler J.B., 1997, *Stars and their spectra*, Univ. press Cambridge. ISBN 0 521585708 p 192
- Keller S.C., Wood P.R., Bessell M.S., 1999, *A&AS*, 134, 489
- Keller S.C., Bessell M.S., Da Costa G.S., 2000, *AJ*, 119, 1748
- Keller S.C., Bessell M.S., Cook K. H., Geha M., Syphers D., 2002, *AJ*, 124, 2039
- Königl A., 1991, *ApJ*, 370, L39
- Kontizas E., Dapergolas A., Morgan D. H., Kontizas M., 2001, *A&A*, 369, 932
- Kurtz M.J., Mink D.J., 1998, *PASP*, 110, 934
- Lada C.J., Adams F.C., 1992, *ApJ*, 393, 278
- Larsen S.S., Clausen J.V., Storm J., 2000, *A&A*, 364, 455
- Le Borgne J.-F., Bruzual G., Pelló R., Lançon A., Rocca-Volmerange B., Sanahuja B., Schaerer D., Soubiran C., Vílchez-Gómez R., 2003, *A&A* 402, 433
- Lewis I.J., et al., 2002, *MNRAS*, 333, 279
- Lindsay E.M., 1963, *IrAJ*, 6, 127
- Lindsay E.M., 1974, *MNRAS* 166, 703
- Lumb D.H., Guainazzi M., Gondoin P., 2001, *A&A*, 376, 387
- Melchior A.-L., Hughes S. M. G., Guibert J., 2000, *A&AS*, 145, 11
- Mennickent R.E., Pietrzyński G., Gieren W., Szewczyk O., 2002, *A&A*, 393, 887

- Miroshnichenko A.S., Fabregat J., Bjorkman K.S., Knauth D.C., Morrison N.D., Tarasov A.E., Reig P., Negueruela I., Blay P., 2001, *A&A*, 371, 600
- Morgan W. W., Keenan P.C., Kellman E. 1943, “An atlas of stellar spectra, with an outline of spectral classification”, Chicago, Ill., The University of Chicago press
- Murai T., Fujimoto M., 1980, *PASJ*, 32, 581
- Muzerolle J., Calvet N., Hartmann L., 1998, *ApJ*, 492, 743
- Muzerolle J., Calvet N., Hartmann L., 2001, *ApJ*, 550, 944
- Muzerolle J., D’Alessio P., Calvet N., Hartmann L., 2004, *ApJ*, 617, 406
- Olsen K.A.G., Kim S., Buss J.F., 2001 *AJ*, 121, 3075
- Parker Q.A., Bland-Hawthorn J., 1998, *PASA*, 15, 33p
- Parker Q.A., Malin D., 1999, *PASA*, 16, 288P
- Parker Q.A., et al., 2005 *MNRAS* 362, 689
- Pasquini L., et al., 2002, *Msngr.* 110, 1
- Poeckert R., Marlborough J.M., 1978, *A.J.suppl.* 38, 229
- Porter J.M., 1996, *MNRAS*, 280, 31
- Porter J.M., Rivinius T., 2003 *PASP*, 115, 1153
- Pickles A.J., 1998, *PASP*, 110, 863
- Quirrenbach A., Bjorkman K.S., Bjorkman J.E., Hummel C.A., Buscher D.F., Armstrong J.T., Mozurkewich D., Elias N.M.II, Babler B.L., 1997, *ApJ*, 479, 477
- Reid N., Glass I.S., Catchpole R.M., 1988, *MNRAS*, 232, 53
- Reid W.A., Parker Q.A. 2005, *AIPC*, 804, 12
- Reid W.A., Parker Q.A. 2006a, *MNRAS*, 365, 401
- Reid W.A., Parker Q.A. 2006b, *MNRAS*, 373, 521
- Reid W.A., Parker Q.A. 2010, *MNRAS*, 405, 1349
- Rivinius Th., Baade D., Štefl S., Townsend R.H.D., Stahl O., Wolf B., Kaufer A., 2001, *A&A*, 369, 1058
- Rivinius Th., Baade D., Štefl S., 2003, *A&A*, 411, 229
- Rohlfs K., Kreitschmann J., Feitzinger J.V., Siegman B.C., 1984, *A&A*, 137, 343
- Sabogal B.E., Mennickent R.E., Pietrzyński G., Gieren W., 2005, *MNRAS*, 361, 1055
- Schwering P.B.W., 1989, *A&A Suppl. Ser.* 79, 105
- Silaj J., Jones C.E., Tycner C., Sigut T.A.A., Smith A.D., 2010, *ApJS*, 187, 228
- Silva D.R., Cornell M.E., 1992, *ApJS*, 81, 865
- Skrutskie M.F., et al., 2006, *AJ.*, 131, 1163
- Slettebak A., 1982, *AJ. Supp. Series*, 50, 55
- Stanghellini L., Shaw R.A., Mutchler M., Palen S., Balick B., Blades J.C., 2002, *ApJ*, 575, 178
- Struve O., 1931, *ApJ*, 73, 94
- Szymański M.K., 2005, *Acta Astron.*, 55, 43
- Telting J.H., 2000 in *ASP Conf. Proc.* 214, The Be Phenomenon in Early-Type Stars, ed. M.A. Smith & H.F. Henrichs (San Francisco: ASP), 422
- Tonry J.L., Davis M., 1979, *AJ.* 43, 393
- Townsend R.H.D., 1997, *MNRAS*, 284, 839
- Townsend R.H.D., Owocki S.P., Howarth I.D., 2004, *MNRAS*, 350, 189
- Turnshek D.E., Turnshek D.A., Craine E.R., Boeshaar, P.C., 1985, *An atlas of digital spectra of cool stars* Astronomy and Astrophysics Series, v.1, Tucson: Western Research Company, ISBN 0-934525-00-5
- Tycner C., et al., 2005, *ApJ*, 624, 359
- Uchida Y., Shibata K., 1985, *PASJ*, 37, 515
- Udalski A., Szymański M., Kubiak M., Pietrzyński G., Soszyński I., Woźniak P., and Zeburuń K., 2000, *Acta Astron.*, 50, 307
- Underhill A., Doazan V., 1982, “B STARS with and without emission” NASA SP-456, Washington DC.: NASA
- Van Winckel H., 2003, *ARA&A*, 41, 391
- Viera S.L.A., Corradi W.J.B., Alencar S.H.P., Mendes L.T.S., Torres C.A.O., Quast G.R., Guimarães M.M., da Silva L. 2003, *AJ*, 126, 2971
- Waters L.B.F.M., Waelkens C., 1998, *ARA&A*, 36, 233
- Wade G.A. et al., 2005, *A&A*, 442, L31
- Wisniewski J.P., Bjorkman K.S., 2006 *ApJ*, 652, 458

This paper has been typeset from a  $\text{\TeX}$ / $\text{\LaTeX}$  file prepared by the author.



## 1 APPENDIX: TABLE 1

Basic data for all hot emission-line stars in the LMC UKST H $\alpha$  survey. Please refer to section 15 for more detailed information. Column 1 gives the Reid Parker (RPs) number for the star (s). Columns 2 and 3 give the RA and Dec in J2000 coordinates. Column 4 gives the published catalogue and number where a star has been previously identified. Column 5 gives our estimate of spectral classification and luminosity class. Column 6 gives a log of the H $\alpha$  emission flux obtained from our flux calibrated spectra. Column 7 gives the Full Width at Half Maximum (FWHM) in km/s as measured from our data. Column 8 gives the Equivalent Width (EW) of the H $\alpha$  line in Angstroms. Column 9 gives the heliocentric radial velocity and column 10 gives the rotational velocity ( $v \sin i$ ). In column 11 we provide comments where em=emission, A.Em=ambient emission, SP=single peak, DP=double peak, sh=shell. Notes on column 4 are given at the end of the table.

RP Object	RA J2000	DEC J2000	Other Catalog Reference	Spec Type	Log F H $\alpha$	FWHM H $\alpha$ km/s	EW H $\alpha$ Å	Vel. (helio) km/s	$v \sin i$ km/s	Comments
RP1741	04 52 55.41	-70 42 12.3		B7Ve	-13.92	464 ± 23	70 ± 3	326 ± 6	449 ± 22	H $\alpha$ , $\beta$
RP1647	04 53 01.03	-70 42 12.3		B3Ve	-13.97	342 ± 17	18 ± 1	241 ± 1	243 ± 12	H $\alpha$ , [S II] from faint, diffuse local emission
RP1701	04 53 02.01	-69 47 04.1		B2Ve	-13.73	333 ± 17	55 ± 2	236 ± 5	296 ± 15	H $\alpha$ , $\beta$
RP1699	04 53 06.86	-69 57 24.7		B1.7V[e]	-13.33	56 ± 3	59 ± 2	242 ± 1	22 ± 1	H $\alpha$ , $\beta$ , $\gamma$ , [S II], [N II], [O II]
RP1671	04 53 25.43	-70 35 39.7		B0III[e]	-12.78	247 ± 12	19 ± 1	262 ± 1	165 ± 8	H $\alpha$ , $\beta$ , $\gamma$ , [S II], [N II], [O III]
RP1778	04 53 43.26	-69 54 02.3		B2Ve	-13.18	282 ± 14	74 ± 3	271 ± 4	267 ± 13	H $\alpha$ , $\beta$
RP1715	04 53 54.12	-69 29 24.9		B1.5Ve	-13.64	349 ± 17	48 ± 2	260 ± 4	304 ± 15	H $\alpha$ , $\beta$
RP1704	04 54 06.45	-69 41 14.9		B1Ve	-13.36	362 ± 18	77 ± 3	261 ± 5	352 ± 18	H $\alpha$ , $\beta$
RP1844	04 54 08.72	-68 37 02.9		B3IIIe	-12.88	307 ± 15	61 ± 2	289 ± 4	278 ± 14	H $\alpha$ , $\beta$
RP1757	04 54 11.97	-69 00 53.9	BE74162	B1Ve	-13.29	357 ± 18	89 ± 4	275 ± 5	356 ± 18	H $\alpha$ , $\beta$
RP1814	04 54 12.32	-68 45 21.0		B2Ve	-13.84	345 ± 17	44 ± 2	253 ± 5	300 ± 15	H $\alpha$ , $\beta$
RP1700	04 54 23.92	-69 50 53.2		B1Ve	-13.20	336 ± 17	56 ± 2	238 ± 5	299 ± 15	H $\alpha$ , $\beta$
RP1767	04 54 26.05	-68 54 38.1		B3Ve	-13.36	260 ± 13	30 ± 1	286 ± 4	199 ± 10	H $\alpha$ , Pcyg. Profile on H $\beta$
RP1765	04 54 30.18	-68 55 25.2		B2Ve	-13.49	317 ± 16	40 ± 2	302 ± 5	264 ± 13	H $\alpha$ , $\beta$
RP1783	04 54 33.88	-69 20 35.7	L6331	B2III[e]	-12.40	129 ± 6	113 ± 5	240 ± 3	116 ± 6	H $\alpha$ , $\beta$ , $\gamma$ , $\delta$ , multiple forbidden lines. Few absorption lines. Weak correlation.
RP1766	04 54 37.11	-68 55 19.4		B2Ve	-13.62	250 ± 12	42 ± 2	280 ± 12	201 ± 10	H $\alpha$ , $\beta$
RP1784	04 54 53.95	-69 23 23.7		B0Ve	-13.08	100 ± 5	69 ± 3	277 ± 23	70 ± 4	H $\alpha$ , $\beta$ , in area of strong H $\alpha$ emission 20 x 16 arcsec with filament to NE
RP1651	04 54 54.76	-70 33 41.4		B2IIIe	-12.87	325 ± 16	78 ± 3	233 ± 5	313 ± 16	H $\alpha$ , $\beta$ , $\gamma$
RP1781	04 55 27.18	-69 29 33.1		B2Ve	-13.07	175 ± 9	41 ± 2	254 ± 3	130 ± 7	H $\alpha$ , $\beta$
RP1786	04 55 28.71	-69 21 36.5		B3IIIe	-12.57	283 ± 14	68 ± 3	253 ± 4	260 ± 13	H $\alpha$ , $\beta$
RP1780	04 55 33.97	-69 29 43.5		B2IIIe	-12.58	343 ± 17	49 ± 2	267 ± 5	298 ± 15	H $\alpha$ , $\beta$
RP1710	04 55 39.89	-69 34 09.0	L6339	B3III	-12.76	336 ± 17	45 ± 2	255 ± 4	291 ± 15	H $\alpha$ , $\beta$ , patchy emission in local area
RP1843	04 55 44.36	-68 35 42.9		B1III[e]	-12.91	57 ± 3	80 ± 3	275 ± 2	27 ± 1	H $\alpha$ , $\beta$ , [S II], [N II], centre of complex, dense stellar cluster 19 arcsec dia with strong H $\alpha$ emission surrounding all.
RP1779	04 55 58.23	-69 28 18.3	MACHO17.2472.36	B1III[e]	-13.02	192 ± 10	25 ± 1	261 ± 3	128 ± 6	H $\alpha$ , $\beta$ , faint and diffuse emission in area contributes [S II], [N II], [O II] and [O III] at low levels.
RP1829	04 55 59.94	-68 42 08.8		B2IVe	-13.97	260 ± 13	43 ± 2	308 ± 4	211 ± 11	H $\alpha$ , $\beta$
RP1703	04 56 01.98	-69 43 22.8	MACHO17.2468.63	B1Ve	-13.10	300 ± 15	56 ± 2	253 ± 4	271 ± 14	H $\alpha$ , $\beta$
RP1733	04 56 14.22	-69 21 29.6		B3IIIe	-12.80	371 ± 19	100 ± 4	274 ± 5	382 ± 19	H $\alpha$ , $\beta$
RP1857	04 56 14.37	-68 22 59.3		B3IIIe	-12.86	322 ± 16	56 ± 2	282 ± 5	293 ± 15	H $\alpha$ , $\beta$
RP1828	04 56 23.14	-68 41 34.4		B5IIIe	-13.81	288 ± 14	49 ± 2	311 ± 4	244 ± 12	H $\alpha$ , (Pcyg profile on H $\beta$ )
RP1782	04 56 23.42	-69 24 41.5		B2IV[e]	-13.18	56 ± 3	175 ± 7	253 ± 1	41 ± 2	H $\alpha$ , $\beta$ , $\gamma$ , $\delta$ , $\epsilon$ , [S II], [N II], [O II], [O III]
RP1736	04 56 37.52	-69 16 08.5		B1Ve	-13.28	351 ± 18	44 ± 2	242 ± 5	306 ± 15	H $\alpha$ , $\beta$
RP1732	04 56 44.68	-69 20 53.4		A5Ve	-13.72	147 ± 7	32 ± 1	253 ± 3	96 ± 5	H $\alpha$ , $\beta$
RP1762	04 56 54.26	-68 55 54.6		F8Ve	-13.48	237 ± 12	24 ± 1	291 ± 4	167 ± 8	H $\beta$ line suffers from low S/N
RP1928	04 57 26.91	-66 44 08.7		B3V[e]	-14.49	307 ± 15	83 ± 3	304 ± 40	302 ± 15	H $\alpha$ , $\beta$ , [S II], [N II], [O II], [O III], emission to East, star to West
RP1746	04 57 48.54	-69 04 15.6		B3Ve	-13.91	329 ± 16	43 ± 2	276 ± 3	276 ± 14	H $\alpha$ , $\beta$ , ([S II] at 2 $\sigma$ noise)
RP1884	04 58 07.26	-67 41 11.4		B0.5II[e]	-12.26	100 ± 5	125 ± 5	301 ± 21	86 ± 4	H $\alpha$ , $\beta$ , $\gamma$ , [S II], [N II], [O II], [O III]
RP1737	04 58 17.48	-69 17 20.1		B1.7Ve	-13.68	333 ± 17	48 ± 2	288 ± 4	288 ± 14	H $\alpha$ , $\beta$
RP1806	04 58 33.31	-68 50 49.9	HD268840	B0.5III[e]	-11.69	286 ± 14	71 ± 3	279 ± 4	264 ± 13	H $\alpha$ , $\beta$ , $\gamma$ , $\delta$ , $\epsilon$ , [S II], [N II], [O II], [O III]
RP1826	04 58 38.12	-68 42 26.5		B2IV[e]	-13.32	441 ± 22	45 ± 2	299 ± 9	393 ± 20	H $\alpha$ , $\beta$ , [O III]
RP1804	04 58 55.65	-68 51 45.1		B3IIIe	-12.84	408 ± 20	36 ± 1	284 ± 6	342 ± 17	H $\alpha$ , $\beta$
RP1747	04 58 56.23	-69 03 29.1		F8II[e]	-12.65	212 ± 11	76 ± 3	294 ± 3	193 ± 10	H $\alpha$ , $\beta$ , $\gamma$ , $\delta$ , low [O III], HeII 4686, [S II], [N II]
RP1839	04 58 56.52	-68 35 02.8	MACHO18.3090.104	B5IIIe	-12.76	188 ± 9	50 ± 2	262 ± 3	151 ± 8	H $\alpha$ , $\beta$ , Could appear as a B8 I star
RP1860	04 58 58.47	-68 20 32.8		B3IIIe	-13.33	266 ± 13	72 ± 3	245 ± 4	250 ± 13	H $\alpha$ , $\beta$
RP1774	04 59 35.00	-70 06 59.0		B1V[e]	-13.25	339 ± 17	33 ± 1	231 ± 1	270 ± 14	H $\alpha$ , Pcyg on H $\beta$ , [S II], [N II], [O II]. East star of double system
RP1775	04 59 37.18	-70 09 09.6	BE74499	B0.5II[e]	-12.59	49 ± 2	109 ± 4	235 ± 1	24 ± 1	H $\alpha$ , $\beta$ , $\gamma$ , $\delta$ , [S II], [N II], [O II], dense H II disk extending to 2 smaller stars to the SE
RP1717	04 59 44.89	-69 28 57.2		B0Ve	-13.13	309 ± 15	32 ± 1	259 ± 4	243 ± 12	H $\alpha$ , $\beta$
RP1724	04 59 44.90	-69 25 32.5		B3Ve	-13.06	229 ± 11	68 ± 3	261 ± 3	204 ± 10	H $\alpha$ , $\beta$

RP Object	RA J2000	DEC J2000	Other Catalog Reference	Spec Type	Log F H $\alpha$	FWHM H $\alpha$ km/s	EW H $\alpha$ Å	Vel. (helio) km/s	$v \sin i$ km/s	Comments
RP1656	04 59 46.62	-70 25 27.7		B1Ve	-13.74	509 ± 25	60 ± 2	278 ± 9	483 ± 24	H $\alpha$ only, Pcyg on H $\beta$
RP1698	04 59 48.42	-69 54 13.0	L6370	B1Ve	-12.99	290 ± 14	78 ± 3	226 ± 4	276 ± 14	H $\alpha, \beta$
RP1856	04 59 54.75	-68 23 07.4		B0.5IIIe	-13.16	410 ± 20	50 ± 2	289 ± 6	373 ± 19	H $\alpha, \beta, \gamma$
RP1777	05 00 13.12	-70 02 56.5	SVDV 284	B1.5Ve	-13.56	291 ± 15	79 ± 3	246 ± 4	277 ± 14	H $\alpha, \beta$
RP1722	05 00 14.06	-69 25 13.9	SAB2338	B2Ve	-13.01	309 ± 15	61 ± 2	250 ± 4	280 ± 14	H $\alpha, \beta$
RP1855	05 00 28.46	-68 23 04.4		B2Ve	-13.56	547 ± 27	41 ± 2	274 ± 9	483 ± 24	H $\alpha, \beta$
RP1755	05 00 28.77	-69 01 06.3	SAB1539	B3Ve	-13.23	323 ± 16	77 ± 3	277 ± 5	310 ± 16	H $\alpha, \beta$
RP1729	05 00 35.39	-69 19 53.3	SAB744	B3IIIe	-13.16	272 ± 14	50 ± 2	272 ± 4	235 ± 12	H $\alpha, \beta$
RP1662	05 01 32.53	-70 16 56.1	MACHO23.3428.997	B1Ve	-13.28	477 ± 24	54 ± 2	251 ± 6	439 ± 22	H $\alpha, \beta$
RP1707	05 01 33.25	-69 36 58.7		B1Ve	-12.79	353 ± 18	106 ± 4	274 ± 5	372 ± 19	H $\alpha, \beta$
RP1832	05 01 48.92	-68 37 33.6	SAB1625	B3IIIe	-13.00	347 ± 17	56 ± 2	238 ± 5	319 ± 16	H $\alpha, \beta, \gamma$
RP1663	05 01 50.52	-70 16 14.9		B2Ve	-13.65	363 ± 18	66 ± 3	261 ± 4	344 ± 17	H $\alpha, \beta$
RP1645	05 02 00.95	-70 42 23.7	BE74504	B1V[e]	-12.70	90 ± 5	106 ± 4	254 ± 2	71 ± 4	H $\alpha, \beta$ , [S II], [N II], [O II] (emission lines brighter than continuum).
RP1792	05 02 03.12	-68 03 40.9	SAB1656	B0V[e]	-13.28	247 ± 12	43 ± 2	271 ± 3	198 ± 10	H $\alpha, \beta$ , [S II], [N II], [O II]
RP1838	05 02 26.96	-68 36 55.8	AL56	BIIIpe	-12.09	281 ± 14	86 ± 3	292 ± 4	274 ± 14	H $\alpha, \beta$ equal to a B2IIIe
RP1854	05 02 39.99	-68 27 59.4		B1.7V[e]	-12.70	56 ± 3	140 ± 6	286 ± 2	37 ± 2	H $\alpha, \beta, \gamma$ , [S II], [N II], [O II], within a small assoc. of stars.
RP1750	05 02 45.65	-69 03 13.1		B1V[e]	-13.65	77 ± 4	18 ± 1	287 ± 2	23 ± 1	H $\alpha, \beta$ , [S II], [N II]
RP1745	05 02 50.69	-69 07 57.6	SAB236	B1.7Ve	-14.30	95 ± 5	11 ± 0	285 ± 2	29 ± 1	H $\alpha$ , (H $\beta$ with strong Pcyg profile.) Forbidden lines and 40% H $\alpha$ due to diffuse emission 20 arcsec diameter stretching NE-SW
RP1834	05 03 04.89	-68 38 35.6		B3Ve	-13.96	234 ± 12	44 ± 2	274 ± 3	191 ± 10	H $\alpha$ , (Pcyg profile on H $\beta$ )
RP1850	05 03 26.01	-68 28 24.3		F0IVe	-13.80	471 ± 24	146 ± 6	199 ± 12	533 ± 27	H $\alpha, \beta$ , weak continuum
RP1852	05 03 32.09	-68 27 56.1		B1Ve	-14.23	315 ± 16	33 ± 1	285 ± 15	249 ± 12	H $\alpha, \beta$ , ([S II] appears to be assoc. with emission to NW)
RP1845	05 03 32.94	-68 32 35.0		B1Ve	-14.62	296 ± 15	5 ± 0	272 ± 1	146 ± 7	H $\alpha$ only. Centre of faint, extended H II emission 12 x 12 arcsec.
RP1794	05 03 38.63	-69 01 21.2	SAB839	B2V[e]	-13.17	239 ± 12	37 ± 1	278 ± 3	185 ± 9	H $\alpha, \beta$ , [S II], [N II], [O III], SP
RP1793	05 03 38.94	-69 01 11.9		B1Ve	-13.76	203 ± 10	29 ± 1	283 ± 1	142 ± 7	H $\alpha$ , pcyg profile on H $\beta$ , [S II] from local diffuse nebula
RP1851	05 03 39.12	-68 28 23.7		B1Ve	-14.40	291 ± 15	5 ± 0	286 ± 1	143 ± 7	H $\alpha$ , [S II] at only 3 $\sigma$ noise
RP1614	05 03 41.74	-71 07 09.7		A7Ve	-14.36	198 ± 10	46 ± 2	235 ± 2	156 ± 8	H $\alpha$
RP1760	05 03 51.47	-68 57 25.3	BE74193	B1IIIe	-13.42	733 ± 37	17 ± 1	233 ± 24	553 ± 28	H $\alpha, \beta, \gamma$ , [S II]
RP1899	05 03 52.12	-67 32 43.6		A0Ve	-13.45	207 ± 10	61 ± 2	282 ± 15	176 ± 9	H $\alpha, \beta$
RP1945	05 04 09.07	-67 18 30.1		B2IIIe	-12.58	424 ± 21	32 ± 1	308 ± 6	347 ± 17	H $\alpha, \beta$
RP1910	05 04 17.16	-67 10 55.4		B0IIIe	-13.69	192 ± 10	38 ± 2	290 ± 6	142 ± 7	H $\alpha, \beta$ , [S II]
RP1909	05 04 18.26	-67 10 30.3		B3IIIe	-13.59	97 ± 5	20 ± 1	297 ± 17	41 ± 2	H $\alpha$ , [S II]
RP1944	05 04 24.06	-67 19 45.9		B2V[e]	-13.43	259 ± 13	73 ± 3	306 ± 23	243 ± 12	H $\alpha, \beta, \gamma$ , [S II], [N II], [O II], [O III]
RP1738	05 04 31.78	-69 17 40.9		B8Ve	-14.19	382 ± 19	22 ± 1	286 ± 5	285 ± 14	H $\alpha$
RP1817	05 04 35.61	-68 44 55.1	AL66	F0Ie	-11.84	165 ± 8	40 ± 2	253 ± 3	120 ± 6	pcyg on H $\alpha, \beta$ , central star of a compact cluster 20arcsec dia.
RP1881	05 04 37.15	-67 49 49.0		B3IIIe	-13.86	97 ± 5	7 ± 0	284 ± 2	24 ± 1	H $\alpha$ , 3 stars in a row. All bright in H $\alpha$
RP1751	05 04 37.41	-69 05 05.7		B3IIIp[e]	-13.55	94 ± 5	22 ± 1	290 ± 2	40 ± 2	H $\alpha, \beta$ , [S II], [N II], [O III] possible Bp, sh
RP1923	05 04 40.40	-66 49 49.0		B1IIIe	-13.77	187 ± 9	23 ± 1	312 ± 14	124 ± 6	H $\alpha, \beta$
RP1672	05 04 40.78	-70 42 06.0		B1.7Ve	-13.09	335 ± 17	56 ± 2	240 ± 5	306 ± 15	H $\alpha, \beta$
RP1863	05 04 44.02	-68 16 32.4		A0Ve	-13.73	181 ± 9	8 ± 0	264 ± 2	85 ± 4	H $\alpha, \beta$ , faint diffuse H II emission surrounding star
RP1795	05 04 44.85	-68 58 31.1	L63106	B2IIIe	-12.47	205 ± 10	47 ± 2	290 ± 3	163 ± 8	H $\alpha, \beta$
RP1936	05 04 47.97	-66 38 53.2			-13.91	445 ± 22	134 ± 5	302 ± 13	489 ± 25	H $\alpha, \beta$ , very weak
RP1935	05 04 51.70	-66 38 07.6		B0.5IIIe	-12.32	360 ± 18	140 ± 6	315 ± 18	401 ± 20	H $\alpha, \beta, \gamma$ , southern-most of 7 stars in a line
RP1675	05 04 54.94	-70 43 33.7		B3IIIe	-12.39	330 ± 16	46 ± 2	275 ± 8	285 ± 14	H $\alpha, \beta$
RP1650	05 04 56.74	-70 34 45.9	L63114	B1.7Ve	-13.83	288 ± 14	35 ± 1	250 ± 4	230 ± 12	H $\alpha, \beta$
RP1640	05 04 58.05	-70 41 03.0	BE74519	B1.7Ve	-13.36	335 ± 17	27 ± 1	256 ± 4	259 ± 13	H $\alpha, \beta$
RP1901	05 04 58.48	-67 32 05.2		B2Ve	-13.35	231 ± 12	69 ± 3	360 ± 11	207 ± 10	H $\alpha, \beta$
RP1639	05 05 00.69	-70 41 03.4	MACHO23.3906.30	B3Ve	-13.25	379 ± 19	170 ± 7	243 ± 8	434 ± 22	H $\alpha, \beta$
RP1818	05 05 04.09	-68 44 40.4	2MASSJ05050415-6844407	B4IVe	-12.77	335 ± 17	101 ± 4	242 ± 5	342 ± 17	H $\alpha, \beta$ , Previously identified as delta Cepheid variable
RP1820	05 05 22.28	-68 43 39.5		B5IIIe	-13.06	188 ± 9	101 ± 4	285 ± 3	177 ± 9	H $\alpha, \beta$
RP1629	05 05 25.31	-70 51 53.8		B0Ve	-13.77	298 ± 15	104 ± 4	255 ± 9	301 ± 15	H $\alpha, \beta$
RP1641	05 05 26.53	-70 39 45.2	MACHO23.4027.43							Not observed
RP1642	05 05 30.41	-70 40 22.0		B1Ve	-13.72	395 ± 20	62 ± 2	246 ± 5	368 ± 18	H $\alpha, \beta$
RP1926	05 05 33.48	-66 51 17.9		A0Ve	-13.19	303 ± 15	156 ± 6	324 ± 16	341 ± 17	H $\alpha, \beta$
RP1821	05 05 39.09	-68 43 20.2	SAB561	B5IIIe	-13.16	229 ± 11	35 ± 1	243 ± 4	176 ± 9	H $\alpha, \beta$
RP1861	05 05 56.94	-68 20 03.2		A2IIIe	-13.04	270 ± 14	48 ± 2	307 ± 4	227 ± 11	H $\alpha, \beta$ , molecular absorption
RP1915	05 06 08.53	-67 01 23.1		B3IIIe	-13.41	286 ± 14	48 ± 2	272 ± 3	242 ± 12	H $\alpha, \beta$
RP1882	05 06 26.66	-67 42 58.3		B0.5IIIe	-12.94	392 ± 20	50 ± 2	282 ± 6	355 ± 18	H $\alpha, \beta$

RP Object	RA J2000	DEC J2000	Other Catalog Reference	Spec Type	Log F H $\alpha$	FWHM H $\alpha$ km/s	EW H $\alpha$ Å	Vel. (helio) km/s	$v \sin i$ km/s	Comments
RP1822	05 06 38.01	-68 44 41.5		B1.7V[e]	-13.71	167 ± 8	27 ± 1	272 ± 1	111 ± 6	H $\alpha, \beta, \gamma$ , [S II], [N II], [O II], [O III]. Dense halo surrounding star + diffuse emission 10 arcsec radius surrounding assoc. of stars.
RP1822	05 06 38.01	-68 44 41.5		B1.7V[e]	-13.71	167 ± 8	27 ± 1	272 ± 1	111 ± 6	H $\alpha, \beta, \gamma$ , [S II], [N II], [O II], [O III]. Dense halo surrounding star + diffuse emission 10 arcsec radius surrounding assoc. of stars.
RP1754	05 06 39.31	-69 01 22.5		B1Ve	-13.54	457 ± 23	48 ± 2	268 ± 3	408 ± 20	H $\alpha, \beta$ , [S II] only 3 sigma noise
RP1879	05 06 50.97	-67 46 53.7		B1Ve	-13.94	253 ± 13	138 ± 6	247 ± 4	272 ± 14	H $\alpha, \beta$
RP1865	05 06 54.00	-68 16 08.9			-14.22	135 ± 7	36 ± 1	284 ± 1	88 ± 4	Too faint to determine accurate class.
RP1847	05 06 59.17	-68 31 56.5		B3IIIe	-13.99	319 ± 16	5 ± 0	255 ± 1	161 ± 8	H $\alpha$ only
RP1811	05 07 01.08	-68 46 60.0		B3V[e]	-14.05	94 ± 5	23 ± 1	270 ± 1	41 ± 2	H $\alpha, \beta$ , [S II], [N II]
RP1837	05 07 11.00	-68 36 31.8		B5IIIe	-12.89	174 ± 9	22 ± 1	295 ± 1	109 ± 5	H $\alpha, \beta$
RP1744	05 07 11.44	-69 10 50.0	SAB15	A7Ve	-14.60	200 ± 10	35 ± 1	271 ± 2	149 ± 7	H $\alpha, \beta$ , weak forbidden lines due to compact diffuse emission to SW
RP1914	05 07 11.54	-67 02 23.0	BE7418	B0.5IIIe	-12.88	346 ± 17	48 ± 2	318 ± 5	301 ± 15	H $\alpha, \beta$
RP1836	05 07 16.78	-68 39 06.6		B5IIIe	-13.09	339 ± 17	61 ± 2	244 ± 5	310 ± 16	H $\alpha, \beta$
RP1262	05 07 26.42	-69 59 41.5	SAB1596	B1Ve	-13.19	224 ± 11	60 ± 2	244 ± 3	193 ± 10	H $\alpha, \beta$
RP1302	05 07 41.85	-69 22 30.3		B1IIIe	-12.83	235 ± 12	49 ± 2	246 ± 4	199 ± 10	H $\alpha, \beta$
RP1132	05 07 44.47	-71 23 53.6		B7Ve	-12.49	357 ± 18	53 ± 2	221 ± 5	320 ± 16	H $\alpha, \beta$
RP1862	05 07 47.09	-68 18 59.6		B2V[e]	-14.45	78 ± 4	8 ± 0	255 ± 1	12 ± 1	H $\alpha, \beta$ , [S II], [N II], [O III], much of emission from H II region extending North
RP1136	05 08 01.19	-71 21 25.8		B0.5IIIe	-12.23	318 ± 16	35 ± 1	206 ± 5	258 ± 13	H $\alpha, \beta$
RP1171	05 08 07.04	-70 55 15.9	L63133	B2Ve	-12.20	223 ± 11	62 ± 2	213 ± 3	193 ± 10	H $\alpha, \beta$
RP1322	05 08 12.63	-68 58 15.0		B1.7V[e]	-13.53	145 ± 7	39 ± 2	277 ± 2	101 ± 5	H $\alpha, \beta$ , [S II], [N II], [O II], [O III]
RP1459	05 08 13.68	-68 36 12.8		B3Ve	-14.99	175 ± 9	50 ± 2	251 ± 1	139 ± 7	H $\alpha$ only. Possible symbiotic. SP
RP1501	05 08 29.55	-68 21 09.2		A0Ve	-13.93	168 ± 8	84 ± 3	228 ± 1	151 ± 8	H $\alpha, \beta$
RP1206	05 08 29.91	-70 20 42.6	MACHO9.4516.29	B3IIIe	-12.82	505 ± 25	48 ± 2	234 ± 7	455 ± 23	H $\alpha, \beta$
RP1473	05 08 32.37	-68 28 51.7		B1Ve	-14.07	214 ± 11	55 ± 2	265 ± 3	177 ± 9	H $\alpha, \beta$
RP1393	05 08 33.49	-69 04 48.6		B1.7Ve	-13.92	399 ± 20	38 ± 2	263 ± 6	334 ± 17	H $\alpha, \beta$
RP1151	05 08 36.12	-71 11 28.1		B3V[e]	-13.50	201 ± 10	35 ± 1	221 ± 3	150 ± 8	H $\alpha, \beta$ , [S II], [O III], weak
RP1299	05 08 38.80	-69 25 34.1	SAB1642	B3V[e]	-13.63	347 ± 17	17 ± 1	247 ± 5	241 ± 12	H $\alpha$ , [S II], [N II] within H II region and small cluster. Probably contaminated ELS
RP1298	05 08 41.11	-69 24 44.9		B3V[e]	-14.27	362 ± 18	38 ± 2	254 ± 13	300 ± 15	H $\alpha, \beta$ , [S II], [N II]
RP1483	05 08 52.73	-68 26 29.4		F0Ve	-14.43	316 ± 16	37 ± 1	323 ± 4	257 ± 13	H $\alpha, \beta$
RP1472	05 09 01.39	-68 32 12.5		B5IIIe	-13.79	57 ± 3	19 ± 1	278 ± 1	7 ± 0	H $\alpha, \beta$ , surrounded by a cloud of emission 9arcsec radius
RP1133	05 09 06.46	-71 21 10.9		B2Ve	-12.58	273 ± 14	38 ± 2	217 ± 5	217 ± 11	H $\alpha, \beta$
RP1145	05 09 29.88	-71 15 23.1	L63142	B0.5IIIe	-11.96	354 ± 18	48 ± 2	248 ± 5	308 ± 15	H $\alpha, \beta$
RP1126	05 09 41.93	-71 27 41.5	AL94	B1.7Ve	-12.15	65 ± 3	65 ± 3	229 ± 2	33 ± 2	H $\alpha, \beta$ , forbidden lines from dense emission surrounding assoc of 9 stars, cluster.
RP1531	05 09 44.24	-67 57 50.5		B5III[e]	-13.70	112 ± 6	16 ± 1	297 ± 1	48 ± 2	H $\alpha, \beta$ , [S II], [N II]
RP1326	05 09 47.58	-69 00 31.5		B3Ve	-13.96	279 ± 14	11 ± 0	245 ± 1	164 ± 8	H $\alpha$ , [S II] from ambient emission
RP1311	05 09 58.94	-69 10 39.6	MACHO79.4775.100	B5IIIe	-13.56	168 ± 8	10 ± 0	256 ± 2	82 ± 4	H $\alpha, \beta$
RP1134	05 10 08.37	-71 20 35.5				0	0			Not observed
RP1471	05 10 12.42	-68 32 31.1		B1Ve	-14.13	218 ± 11	34 ± 1	266 ± 3	160 ± 8	H $\alpha$ only
RP1312	05 11 03.97	-69 07 32.6		B2IIIe	-13.02	207 ± 10	50 ± 2	268 ± 3	170 ± 9	H $\alpha, \beta$
RP1419	05 11 56.00	-68 53 18.6		B1Ve	-13.85	237 ± 12	41 ± 2	239 ± 3	189 ± 10	H $\alpha$ only
RP1290	05 12 07.66	-69 28 35.0	MACHO5.5134.1734	B1IIIe	-13.43	256 ± 13	41 ± 2	270 ± 1	207 ± 10	H $\alpha, \beta$ , extended emission contributing [S II] and low [N II]
RP1209	05 12 08.38	-70 28 40.3		B3IIIe	-12.76	51 ± 3	35 ± 1	243 ± 1	10 ± 1	H $\alpha, \beta$ , in an assoc of stars enveloped by a disk of dense H II emission 11 arcsec radius. Cluster
RP1158	05 12 09.11	-71 06 49.9		B8Ie	-12.22	150 ± 8	52 ± 2	287 ± 3	114 ± 6	H $\alpha, \beta, \gamma$ , possibility of being a B5IIIe
RP1316	05 12 20.07	-69 04 49.5		F0IIIe	-12.73	527 ± 26	101 ± 4	282 ± 9	556 ± 28	H $\alpha, \beta$ , SP
RP1422	05 12 22.83	-68 52 38.1		B1IIIe	-12.42	307 ± 15	60 ± 2	273 ± 4	278 ± 14	H $\alpha, \beta$
RP1211	05 12 32.12	-70 29 03.3		B3IIIe	-13.60	90 ± 5	7 ± 0	236 ± 1	17 ± 1	H $\alpha$ , surrounded by huge emission disk 27 arcsec radius
RP1205	05 12 36.18	-70 24 58.6		B1Ve	-14.28	102 ± 5	10 ± 0	254 ± 1	32 ± 2	H $\alpha$ , centre of diffuse emission 6 arcsec radius
RP1597	05 12 36.69	-66 38 22.5		B5IIIe	-12.50	151 ± 8	118 ± 5	255 ± 6	141 ± 7	H $\alpha, \beta, \gamma$
RP1392	05 12 47.90	-69 03 06.4	BE74224	B5IIIe	-12.47	220 ± 11	53 ± 2	335 ± 3	183 ± 9	H $\alpha, \beta$
RP1461	05 12 49.60	-68 33 55.6		B1.7Ve	-13.47	275 ± 14	56 ± 2	240 ± 3	245 ± 12	H $\alpha, \beta$
RP1389	05 13 17.44	-69 19 55.0		B3IVe	-12.73	362 ± 18	131 ± 5	235 ± 1	392 ± 20	H $\alpha, \beta$ in H II region forbidden lines from H II
RP1348	05 14 13.05	-69 33 24.6	SAB82	B1IIIe	-12.83	209 ± 10	19 ± 1	239 ± 3	133 ± 7	H $\alpha, \beta, \gamma$ , SP
RP1350	05 14 14.90	-69 36 08.7		B1Ve	-12.97	239 ± 12	111 ± 4	294 ± 6	242 ± 12	H $\alpha, \beta$ , within a compact, dense H II region 13 x 9 arcsec, SP
RP1499	05 14 29.85	-68 20 50.9		B2IIIe	-13.02	348 ± 17	67 ± 3	263 ± 5	329 ± 16	H $\alpha, \beta$
RP1470	05 14 32.47	-68 32 46.9		A2Ve	-14.20	213 ± 11	21 ± 1	293 ± 2	142 ± 7	H $\alpha$ only
RP1574	05 14 43.41	-67 12 25.3		B3IIIe	-13.64	316 ± 16	21 ± 1	309 ± 1	229 ± 11	H $\alpha, \beta$ , Large H II disk 12 arcsec radius surrounding star and contributing [S II].
RP1563	05 15 09.95	-67 32 15.3		B1Ve	-13.19	206 ± 10	149 ± 6	251 ± 3	216 ± 11	H $\alpha, \beta, \gamma$ , SP

RP Object	RA J2000	DEC J2000	Other Catalog Reference	Spec Type	Log F H $\alpha$	FWHM H $\alpha$ km/s	EW H $\alpha$ Å	Vel. (helio) km/s	$v \sin i$ km/s	Comments
RP <sub>s</sub> 1260	05 15 10.00	-70 01 21.6		B3III[e]	-14.07	52 ± 3	61 ± 2	241 ± 1	18 ± 1	H $\alpha$ , $\beta$ , $\gamma$ , [S II], [N II], [O II]
RP <sub>s</sub> 1524	05 15 41.41	-67 58 52.4	BE74231	B4III[e]	-12.29	412 ± 21	18 ± 1	316 ± 1	302 ± 15	H $\alpha$ , $\beta$ , $\gamma$ , [S II], [N II], [O II], dense H II halo surrounding, SP
RP <sub>s</sub> 1582	05 15 45.61	-66 58 42.3		B1Ve	-14.99	42 ± 2	55 ± 2	291 ± 1	7 ± 0	H $\alpha$ , p cyg on H $\beta$
RP <sub>s</sub> 1469	05 15 48.74	-68 33 04.0		B1.7Ve	-13.92	98 ± 5	27 ± 1	272 ± 3	49 ± 2	H $\alpha$ only
RP <sub>s</sub> 1414	05 16 24.57	-68 55 27.6		B3V[e]	-12.97	302 ± 15	186 ± 7	232 ± 1	349 ± 18	H $\alpha$ , $\beta$ , $\gamma$ , [S II], [N II], [O II], Poor spectral fit
RP <sub>s</sub> 1335	05 16 27.14	-69 26 22.6	SAB1899	B1Ve	-13.41	262 ± 13	78 ± 3	219 ± 4	246 ± 12	H $\alpha$ , $\beta$ , DP V>R
RP <sub>s</sub> 1529	05 16 31.96	-67 56 50.2		B2V[e]	-13.52	102 ± 5	21 ± 1	293 ± 2	47 ± 2	H $\alpha$ , $\beta$ , $\gamma$ , [S II], [N II], [O II]
RP <sub>s</sub> 1334	05 16 33.24	-69 31 29.2		F0Ve	-13.04	188 ± 9	102 ± 4	273 ± 3	178 ± 9	H $\alpha$ , $\beta$ only
RP <sub>s</sub> 1423	05 16 39.06	-68 53 20.5		B3Ve	-14.57	95 ± 5	8 ± 0	238 ± 1	25 ± 1	H $\alpha$ only + HeI 4144 in emission
RP <sub>s</sub> 1386	05 16 39.11	-69 20 47.9	SAB899	B3Ve	-13.41	339 ± 17	79 ± 3	274 ± 4	328 ± 16	H $\alpha$ only, DP centre
RP <sub>s</sub> 1382	05 16 52.29	-69 33 56.4	SAB631	B1Ve	-13.37	76 ± 6	15 ± 1	291 ± 4	20 ± 5	H $\alpha$ , $\beta$ , SP bottle-shape
RP <sub>s</sub> 1381	05 17 01.02	-69 34 10.5	SAB138	B1Ve	-12.54	226 ± 11	48 ± 2	249 ± 4	184 ± 9	H $\alpha$ , $\beta$ , SP
RP <sub>s</sub> 1525	05 17 06.93	-68 00 27.8		B2V[e]	-13.98	134 ± 7	52 ± 2	211 ± 5	98 ± 5	H $\alpha$ , $\beta$ , [S II], [N II]strong central H $\alpha$ emission, SP
RP <sub>s</sub> 1526	05 17 07.33	-68 00 18.5		B1Ve	-13.21	356 ± 18	63 ± 3	276 ± 4	328 ± 16	H $\alpha$ , $\beta$
RP <sub>s</sub> 1331	05 17 08.13	-69 07 02.1		B1.7V[e]	-13.10	48 ± 2	80 ± 3	267 ± 1	17 ± 1	H $\alpha$ , $\beta$ , [N II], [S II], [O II], [O II], SP
RP <sub>s</sub> 2054	05 17 08.93	-69 32 21.1	SVHV 5717		-14.51	419 ± 21	86 ± 3	280 ± 4	424 ± 21	H $\alpha$ , [N II]but no [O III].
RP <sub>s</sub> 1588	05 17 31.40	-66 43 30.1		B3III[e]	-12.77	291 ± 15	149 ± 6	320 ± 1	317 ± 16	H $\alpha$ , $\beta$ , $\gamma$ , [S II], [N II], [O II]
RP <sub>s</sub> 1537	05 17 34.45	-67 50 08.8		B1IIe	-13.81	257 ± 13	42 ± 2	303 ± 4	208 ± 10	H $\alpha$ , $\beta$
RP <sub>s</sub> 1538	05 17 35.37	-67 46 40.3		B1Ve	-13.33	299 ± 15	78 ± 3	289 ± 4	285 ± 14	H $\alpha$ , $\beta$
RP <sub>s</sub> 1592	05 17 40.69	-66 42 08.8		B0III[e]	-12.82	327 ± 16	83 ± 3	196 ± 4	324 ± 16	H $\alpha$ , $\beta$ , [S II], [N II]
RP <sub>s</sub> 1591	05 17 40.80	-66 42 04.8		B3III[e]	-12.81	216 ± 11	93 ± 4	301 ± 15	209 ± 10	H $\alpha$ , $\beta$ , $\gamma$ , [S II], [N II], [O II]
RP <sub>s</sub> 1593	05 17 40.96	-66 42 08.7		B3III[e]	-12.90	208 ± 10	157 ± 6	319 ± 1	225 ± 11	H $\alpha$ , $\beta$ , $\gamma$ , [S II], [N II]
RP <sub>s</sub> 1478	05 17 46.26	-68 30 03.2		B1Ve	-13.32	351 ± 18	49 ± 2	308 ± 5	305 ± 15	H $\alpha$ , $\beta$
RP <sub>s</sub> 1374	05 17 53.26	-69 11 44.1	BE74242	B2IIe	-12.66	291 ± 15	37 ± 1	292 ± 4	233 ± 12	H $\alpha$ , $\beta$ , low [O III] 5007 from ambient emission in area
RP <sub>s</sub> 1373	05 17 57.65	-69 11 10.3	BE74242	B2IIe	-12.09	513 ± 26	106 ± 4	305 ± 10	555 ± 28	H $\alpha$ , $\beta$
RP <sub>s</sub> 1384	05 17 59.80	-69 30 07.6		A3IIe	-12.77	460 ± 23	60 ± 2	283 ± 13	433 ± 22	H $\alpha$ , $\beta$
RP <sub>s</sub> 1383	05 18 02.98	-69 29 49.1		B0Ve	-13.00	309 ± 15	32 ± 1	237 ± 3	243 ± 12	H $\alpha$ , $\beta$ , SP
RP <sub>s</sub> 1448	05 18 08.15	-68 42 39.9		B1V[e]	-13.53	99 ± 5	51 ± 2	313 ± 2	63 ± 3	H $\alpha$ , $\beta$ , [S II], [N II]
RP <sub>s</sub> 1503	05 18 59.76	-68 14 39.4		B1Ve	-13.47	301 ± 15	48 ± 2	261 ± 4	257 ± 13	H $\alpha$ , $\beta$
RP <sub>s</sub> 1514	05 19 07.79	-68 05 42.0	AL128	B1IIe	-12.63	242 ± 12	48 ± 2	303 ± 3	200 ± 10	H $\alpha$ , $\beta$
RP <sub>s</sub> 1517	05 19 07.91	-68 02 57.7		B1.5Ve	-14.17	319 ± 16	36 ± 1	288 ± 4	260 ± 13	H $\alpha$ , + [O I] 6300, 6363
RP <sub>s</sub> 1468	05 19 08.33	-68 34 01.5		B1Ve	-13.84	206 ± 10	56 ± 2	282 ± 3	170 ± 9	H $\alpha$ , $\beta$
RP <sub>s</sub> 1339	05 19 11.45	-69 41 55.9	SAB2069	B1Ve	-13.34	175 ± 9	45 ± 2	249 ± 3	134 ± 7	H $\alpha$ , $\beta$ , other weak forbidden line probably from ambient emission, SP
RP <sub>s</sub> 1437	05 19 12.83	-68 44 04.6		B5.7Ve	-14.38	363 ± 18	28 ± 1	302 ± 3	284 ± 14	H $\alpha$ only
RP <sub>s</sub> 1506	05 19 17.99	-68 13 45.0		B1Ve	-12.94	327 ± 16	67 ± 3	309 ± 4	306 ± 15	H $\alpha$ , $\beta$
RP <sub>s</sub> 1479	05 19 25.11	-68 29 36.7		B3IIIe	-13.55	73 ± 4	107 ± 4	271 ± 2	52 ± 3	H $\alpha$ , $\beta$ , [S II]. H II emission extending 1 arcsec on w side of star. Companion? To immediate E.
RP <sub>s</sub> 1149	05 19 29.28	-71 15 50.7		B1.7V[e]	-12.56	245 ± 12	53 ± 2	226 ± 3	208 ± 10	H $\alpha$ , $\beta$ weak [S II], [O III]
RP <sub>s</sub> 1436	05 19 33.68	-68 45 24.5		B1Ve	-14.10	112 ± 6	44 ± 2	274 ± 1	73 ± 4	H $\alpha$ only
RP <sub>s</sub> 1370	05 19 34.20	-69 57 50.6		B3Ve	-13.07	275 ± 14	33 ± 1	258 ± 3	212 ± 11	H $\alpha$ , $\beta$ , SP
RP <sub>s</sub> 1539	05 19 37.30	-67 49 30.5	AL136	B0.5IIIe	-13.10	384 ± 19	44 ± 2	294 ± 5	338 ± 17	H $\alpha$ , $\beta$
RP <sub>s</sub> 1340	05 19 44.00	-69 40 28.3		B1V[e]	-13.37	56 ± 3	47 ± 2	243 ± 1	18 ± 1	H $\alpha$ , $\beta$ , [O II], [O III], [S II], [N II], SP
RP <sub>s</sub> 1449	05 20 11.54	-68 37 53.7		F5IIe	-13.49	259 ± 13	107 ± 4	293 ± 14	264 ± 13	H $\alpha$
RP <sub>s</sub> 1452	05 20 12.96	-68 38 08.3		B2Ve	-13.72	95 ± 5	26 ± 1	269 ± 1	44 ± 2	H $\alpha$ only
RP <sub>s</sub> 1342	05 20 15.34	-69 40 29.0		B1Ve	-14.06	117 ± 6	6 ± 0	278 ± 1	33 ± 2	H $\alpha$ only, SP
RP <sub>s</sub> 1600	05 20 17.83	-66 52 53.6		B2Ve	-13.14	332 ± 17	69 ± 3	313 ± 1	312 ± 16	H $\alpha$ , $\beta$ , ([S II], [N II], [O II], [O III] from dense compact H II region 12 x 16 arcsec).
RP <sub>s</sub> 1265	05 20 34.34	-70 00 33.0		B8Ve	-13.41	214 ± 11	55 ± 2	259 ± 3	178 ± 9	H $\alpha$ , $\beta$
RP <sub>s</sub> 1356	05 20 39.89	-69 44 59.1	SAB2161	B1IIIe	-12.71	290 ± 14	57 ± 2	259 ± 4	260 ± 13	H $\alpha$ , $\beta$ , SP
RP <sub>s</sub> 1586	05 20 40.11	-66 48 49.2		B3Ve	-14.22	85 ± 4	13 ± 1	305 ± 1	25 ± 1	H $\alpha$ , $\beta$ , Centre star of faint emission 25 arcsec radius.
RP <sub>s</sub> 1355	05 20 45.17	-69 58 24.5		B7Ve	-14.07	371 ± 19	36 ± 1	258 ± 3	308 ± 15	H $\alpha$ only, SP
RP <sub>s</sub> 1343	05 20 47.86	-69 39 56.2		A7V[e]	-13.14	272 ± 14	60 ± 2	308 ± 3	242 ± 12	H $\alpha$ , $\beta$ , [S II], [O III], DP R>V
RP <sub>s</sub> 1238	05 20 49.08	-70 12 40.8		A3V[e]		366 ± 18	15 ± 1	305 ± 1	249 ± 12	with [O III] emission on star. No H emission. SP
RP <sub>s</sub> 1344	05 20 51.12	-69 38 28.9	BE74565	B1IIIe	-12.72	486 ± 24	101 ± 4	259 ± 7	510 ± 26	H $\alpha$ , $\beta$ , DP centre
RP <sub>s</sub> 1173	05 20 54.35	-70 49 42.1	SAB817	B1IIIe	-12.66	374 ± 19	69 ± 3	225 ± 5	356 ± 18	H $\alpha$ , $\beta$ , SP
RP <sub>s</sub> 1535	05 20 57.37	-67 49 21.1	BE74255	B3IIIe	-13.29	98 ± 5	33 ± 1	304 ± 2	51 ± 3	H $\alpha$ , p cyg on H $\beta$ , In dense H II region 20 x 14 arcsec dia
RP <sub>s</sub> 1368	05 21 05.22	-69 01 03.3		B1.5Ve	-13.46	442 ± 22	42 ± 2	281 ± 4	383 ± 19	H $\alpha$ only
RP <sub>s</sub> 1156	05 21 15.37	-71 05 29.8		B1Ve	-14.46	536 ± 27	24 ± 1	157 ± 3	426 ± 21	H $\alpha$ only
RP <sub>s</sub> 1365	05 21 16.97	-69 04 57.8		B2Ve	-13.48	324 ± 16	64 ± 3	308 ± 4	304 ± 15	H $\alpha$ , $\beta$

RP Object	RA J2000	DEC J2000	Other Catalog Reference	Spec Type	Log F H $\alpha$	FWHM H $\alpha$ km/s	EW H $\alpha$ Å	Vel. (helio) km/s	$v \sin i$ km/s	Comments
RP s1360	05 21 17.30	-69 19 53.9	BE74257	B5IIIe	-12.73	262 $\pm$ 13	38 $\pm$ 2	251 $\pm$ 4	213 $\pm$ 11	H $\alpha, \beta$
RP s1542	05 21 20.43	-67 47 06.8	IRAS-P.C05214-6749	B2IV[e]	-13.46	49 $\pm$ 2	233 $\pm$ 9	279 $\pm$ 1	36 $\pm$ 2	H $\alpha, \beta$ , [N II], [S II], [O II], SP
RP s1266	05 21 21.48	-69 59 00.2		A2Ve	-14.02	320 $\pm$ 16	30 $\pm$ 1	300 $\pm$ 1	246 $\pm$ 12	H $\alpha, \beta$ , similar size star 3 arcsec to SW.
RP s1362	05 21 29.45	-69 07 25.4		B1Ve	-14.04	256 $\pm$ 13	41 $\pm$ 2	285 $\pm$ 1	207 $\pm$ 10	H $\alpha, \beta$
RP s1494	05 21 31.88	-68 20 59.5	AL 146	B3IIIe	-12.79	287 $\pm$ 14	42 $\pm$ 2	253 $\pm$ 4	236 $\pm$ 12	H $\alpha, \beta$ , [O III] from ambient H II
RP s1367	05 21 36.06	-69 02 30.7		B0Ve	-13.79	222 $\pm$ 11	16 $\pm$ 1	262 $\pm$ 1	135 $\pm$ 7	H $\alpha$ , (H $\beta$ is fully absorbed). Forbidden [N II] & [S II] from strong H II region to south
RP s1481	05 21 36.52	-68 28 55.7	MACHO3.6722.273	B1IIIe	-13.66	217 $\pm$ 11	20 $\pm$ 1	277 $\pm$ 3	140 $\pm$ 7	strong [O III]
RP s1543	05 21 38.09	-67 46 52.1		B0V[e]	-12.75	399 $\pm$ 20	40 $\pm$ 2	300 $\pm$ 2	343 $\pm$ 17	H $\alpha, \beta$ , [S II], [N II], [O II], [O III], strong H II surrounding & North
RP s1480	05 21 38.47	-68 28 21.1		B3Ve	-13.59	477 $\pm$ 24	64 $\pm$ 3	481 $\pm$ 1	462 $\pm$ 23	H $\alpha$ only, SP,
RP s1359	05 21 40.54	-69 26 06.1	SAB2199	F5IVe	-13.18	342 $\pm$ 17	43 $\pm$ 2	257 $\pm$ 5	289 $\pm$ 14	H $\alpha, \beta$ , SP
RP s715	05 21 47.25	-69 52 33.5		F5IVe	-13.49	263 $\pm$ 13	32 $\pm$ 1	240 $\pm$ 4	202 $\pm$ 10	H $\alpha, \beta$ , SP
RP s2173	05 21 54.96	-69 46 35.9		BIIIe	-13.02	202 $\pm$ 10	35 $\pm$ 1	273 $\pm$ 4	151 $\pm$ 8	H $\alpha, \beta, \gamma$ , SP
RP s852	05 22 02.11	-69 02 05.8		A0V[e]	-14.07	121 $\pm$ 6	21 $\pm$ 1	267 $\pm$ 2	64 $\pm$ 3	H $\alpha$ only, [N II], [S II], [O II]
RP s2174	05 22 02.73	-69 46 14.5	AGPRSJ052204.08-694619.6	BIIIe	-14.02	99 $\pm$ 5	18 $\pm$ 1	274 $\pm$ 4	43 $\pm$ 2	H $\alpha, \beta$ , known variable within H II region. SP
RP s985	05 22 03.16	-67 47 04.3		B2V[e]	-13.38	210 $\pm$ 10	95 $\pm$ 4	283 $\pm$ 24	202 $\pm$ 10	H $\alpha, \beta$ , [S II], [N II], [O II], [O III], diffuse H II in area
RP s606	05 22 07.95	-70 17 01.1		B1Ve	-13.12	190 $\pm$ 10	17 $\pm$ 1	219 $\pm$ 3	114 $\pm$ 6	H $\alpha$ only
RP s718	05 22 10.51	-69 49 43.1		B0V[e]	-13.79	53 $\pm$ 3	23 $\pm$ 1	236 $\pm$ 1	6 $\pm$ 0	H $\alpha, \beta$ , [S II], [N II], bright star 5 arcsec to SE, SP
RP s1059	05 22 10.82	-67 34 50.6		B1V[e]	-13.69	77 $\pm$ 4	30 $\pm$ 1	294 $\pm$ 1	31 $\pm$ 2	H $\alpha, \beta$ , [S II]
RP s813	05 22 14.14	-69 19 30.6		B1Ve	-13.57	321 $\pm$ 16	49 $\pm$ 2	263 $\pm$ 4	276 $\pm$ 14	H $\alpha, \beta$ only, SP
RP s854	05 22 17.44	-69 03 04.8		B3Ve	-13.47	483 $\pm$ 24	44 $\pm$ 2	306 $\pm$ 3	434 $\pm$ 22	H $\alpha, \beta$ , SP
RP s716	05 22 17.90	-69 50 49.1	MACHO78.6822.56	B1Ve	-12.89	106 $\pm$ 6	14 $\pm$ 1	247 $\pm$ 2	43 $\pm$ 3	H $\alpha, \beta$ , SP, Bottle shape
RP s925	05 22 22.88	-68 41 00.8		A0IVe	-13.61	245 $\pm$ 12	41 $\pm$ 2	290 $\pm$ 3	196 $\pm$ 10	H $\alpha$ , low level $\beta$
RP s853	05 22 28.54	-69 00 43.2	MACHO80.6835.21	B1IIIe	-13.06	175 $\pm$ 9	26 $\pm$ 1	268 $\pm$ 3	113 $\pm$ 6	H $\alpha, \beta$
RP s600	05 22 30.03	-70 23 53.6	L63206	F2IIIe	-13.01	274 $\pm$ 14	29 $\pm$ 1	245 $\pm$ 3	205 $\pm$ 10	H $\alpha$ only
RP s978	05 22 39.72	-67 55 24.7		B1.7V[e]	-13.26	326 $\pm$ 16	167 $\pm$ 7	282 $\pm$ 79	369 $\pm$ 19	H $\alpha, \beta$ , [S II], [O II], [O III], [N II], SP
RP s948	05 22 48.19	-68 32 41.7		B2V[e]	-13.56	114 $\pm$ 6	28 $\pm$ 1	287 $\pm$ 1	63 $\pm$ 3	H $\alpha$ , [N II], [S II]
RP s924	05 22 54.11	-68 41 42.7		B2Ve	-13.67	260 $\pm$ 13	39 $\pm$ 2	296 $\pm$ 3	210 $\pm$ 11	H $\alpha$ only
RP s871	05 22 54.20	-69 40 09.6	SAB2268	B1V[e]	-13.10	506 $\pm$ 25	37 $\pm$ 1	248 $\pm$ 14	433 $\pm$ 22	H $\alpha, \beta$ , weak [S II], [N II], SP
RP s901	05 22 58.45	-68 45 34.6		A1Ile	-14.01	385 $\pm$ 19	37 $\pm$ 1	281 $\pm$ 6	321 $\pm$ 16	H $\alpha, \beta$ very low
RP s752	05 22 58.47	-69 44 01.5		F2III[e]	-13.36	129 $\pm$ 6	25 $\pm$ 1	274 $\pm$ 1	74 $\pm$ 4	H $\alpha, \beta$ , [S II], [O II], [O III], [N II], SP
RP s984	05 22 59.58	-68 04 07.9		B5III[e]	-13.02	108 $\pm$ 5	25 $\pm$ 1	304 $\pm$ 2	55 $\pm$ 3	H $\alpha, \beta$ , [N II], [S II], [O II], [O III], SP
RP s962	05 23 00.14	-68 11 21.3		B1V[e]	-13.08	90 $\pm$ 17	37 $\pm$ 1	270 $\pm$ 2	33 $\pm$ 17	H $\alpha, \beta$ , some portion of the forbidden lines from ambient H II environment. SP, Bottle shape
RP s814	05 23 05.25	-69 16 12.1	SAB2287	B0IIIe	-12.96	274 $\pm$ 14	41 $\pm$ 2	253 $\pm$ 4	224 $\pm$ 11	H $\alpha, \beta, \gamma$ only
RP s1054	05 23 07.93	-67 38 14.1		F0IIIe	-13.13	318 $\pm$ 16	37 $\pm$ 1	317 $\pm$ 12	259 $\pm$ 13	H $\alpha, \beta$
RP s420	05 23 12.37	-70 47 51.1		A2Ve	-14.66	469 $\pm$ 23	32 $\pm$ 1	218 $\pm$ 4	388 $\pm$ 19	H $\alpha$ alone
RP s761	05 23 17.39	-69 40 53.5		F0Ve	-14.45			269 $\pm$ 1		H $\alpha$ alone
RP s870	05 23 17.43	-69 38 50.4	BE74574	B2IV[e]	-12.18	254 $\pm$ 13	88 $\pm$ 4	286 $\pm$ 4	245 $\pm$ 12	H $\alpha, \beta, \gamma, \delta$ , He4471 in emission. Much weaker forbidden lines, DP R>V
RP s982	05 23 17.73	-67 59 38.9		B2V[e]	-13.72	59 $\pm$ 3	49 $\pm$ 2	284 $\pm$ 1	23 $\pm$ 1	H $\alpha, \beta$ , [S II], [NI], [O II], [O III], SP
RP s922	05 23 21.91	-68 39 53.9		B1.7Ve	-13.98	91 $\pm$ 5	6 $\pm$ 0	285 $\pm$ 1	16 $\pm$ 1	H $\alpha$ only in emission
RP s762	05 23 22.81	-69 41 15.3		B3III[e]	-13.63	385 $\pm$ 19	29 $\pm$ 1	243 $\pm$ 8	303 $\pm$ 15	H $\alpha, \beta$ some associated emission, SP
RP s1010	05 23 24.32	-70 39 08.0	MACHO6.6931.37	B1Ve	-13.38	237 $\pm$ 12	20 $\pm$ 1	235 $\pm$ 3	157 $\pm$ 8	H $\alpha, \beta$
RP s552	05 23 26.98	-70 41 26.9		B1IVe	-13.21	278 $\pm$ 14	38 $\pm$ 2	223 $\pm$ 4	221 $\pm$ 11	H $\alpha, \beta$
RP s1094	05 23 30.46	-66 41 53.4		B0.5IIIe	-13.04	280 $\pm$ 14	49 $\pm$ 2	287 $\pm$ 3	237 $\pm$ 12	H $\alpha, \beta$
RP s983	05 23 31.90	-68 01 00.9		B2IV[e]	-13.11	53 $\pm$ 3	72 $\pm$ 3	289 $\pm$ 2	23 $\pm$ 1	H $\alpha, \beta$ , [N II], [S II], [O II], in cocoon, SP
RP s1062	05 23 33.30	-67 24 10.2		B3III[e]	-13.34	86 $\pm$ 4	39 $\pm$ 2	302 $\pm$ 2	45 $\pm$ 2	H $\alpha$ , Pcyg on H $\beta$ , [S II], [O II], [N II], in assoc. of stars.
RP s961	05 23 40.48	-68 05 28.8		B1V[e]	-13.27	59 $\pm$ 3	30 $\pm$ 1	270 $\pm$ 1	16 $\pm$ 1	H $\alpha, \beta$ , [N II], [S II], SP
RP s966	05 23 47.74	-67 56 32.4		B2V[e]	-13.83	281 $\pm$ 14	53 $\pm$ 2	284 $\pm$ 10	244 $\pm$ 12	H $\alpha, \beta$ , [S II], [NI], [O II]
RP s964	05 23 49.64	-67 57 26.3		F5V[e]	-13.35	230 $\pm$ 11	122 $\pm$ 5	308 $\pm$ 1	238 $\pm$ 12	H $\alpha, \beta, \gamma$ , [N II], [S II], SP
RP s899	05 24 03.12	-68 56 21.3		B0V[e]	-12.93	331 $\pm$ 17	31 $\pm$ 1	279 $\pm$ 1	263 $\pm$ 13	H $\alpha, \beta$ , [N II], [O II], [S II], in cocoon
RP s928	05 24 06.36	-68 41 59.2		B2IIIe	-12.67	206 $\pm$ 10	30 $\pm$ 1	259 $\pm$ 3	150 $\pm$ 8	H $\alpha, \beta$ . Indication of forbidden lines may be H II in area.
RP s898	05 24 09.71	-68 57 04.0		B2V[e]	-13.77	322 $\pm$ 16	29 $\pm$ 1	266 $\pm$ 1	248 $\pm$ 12	H $\alpha, \beta$ , [N II], [O II], [S II], extensive H $\alpha$ emission surrounding star
RP s804	05 24 11.91	-69 21 17.8		B8V[e]	-14.32	88 $\pm$ 8	10 $\pm$ 1	259 $\pm$ 2	23 $\pm$ 5	H $\alpha, \beta$ , [S II], [N II], [O II], SP, Bottle shape
RP s1061	05 24 12.33	-67 26 37.7		B3IV[e]	-13.57	90 $\pm$ 4	110 $\pm$ 4	311 $\pm$ 16	71 $\pm$ 4	H $\alpha, \beta$ , [S II], [N II], [O II], [O III], SP
RP s1060	05 24 12.47	-67 26 32.6		B2IVe	-13.69	94 $\pm$ 5	42 $\pm$ 2	279 $\pm$ 2	52 $\pm$ 3	H $\alpha, \beta$ , [S II], [N II] mainly from surrounding nebula
RP s847	05 24 12.49	-69 13 20.5		B3IIIe	-12.78	227 $\pm$ 11	46 $\pm$ 2	275 $\pm$ 3	185 $\pm$ 9	H $\alpha, \beta$ only, SP

RP Object	RA J2000	DEC J2000	Other Catalog Reference	Spec Type	Log F H $\alpha$	FWHM H $\alpha$ km/s	EW H $\alpha$ Å	Vel. (helio) km/s	$v \sin i$ km/s	Comments
RP <sub>s</sub> 778	05 24 14.14	-69 27 40.3		B1III[e]	-13.41	101 $\pm$ 5	9 $\pm$ 0	277 $\pm$ 1	31 $\pm$ 2	H $\alpha$ , $\beta$ , [S II] & some associated [N II] emission, SP
RP <sub>s</sub> 601	05 24 17.73	-71 31 50.2	BE74580	B3V[e]	-12.45	96 $\pm$ 5	43 $\pm$ 2	238 $\pm$ 1	55 $\pm$ 3	H $\alpha$ , $\beta$ , $\gamma$ , $\delta$ , [O II] 3727, [N II], [S II], relatively low continuum levels suggest active H II region
RP <sub>s</sub> 873	05 24 23.07	-69 39 08.9	BE74579	B3V[e]	-13.04	88 $\pm$ 4	62 $\pm$ 2	272 $\pm$ 1	55 $\pm$ 3	H $\alpha$ , $\beta$ , [S II], [O II], [N II]
RP <sub>s</sub> 874	05 24 23.70	-69 38 53.6	BE74579	B3V[e]	-13.31	338 $\pm$ 17	50 $\pm$ 2	246 $\pm$ 25	301 $\pm$ 15	H $\alpha$ , $\beta$ , [S II], [O II]
RP <sub>s</sub> 1073	05 24 27.98	-67 09 10.4		B3III[e]	-12.99	86 $\pm$ 4	74 $\pm$ 3	303 $\pm$ 2	59 $\pm$ 3	H $\alpha$ , Pcyg on hb, [S II], [O II], [N II]
RP <sub>s</sub> 817	05 24 37.95	-69 15 36.8		F3Ve	-14.05	174 $\pm$ 9	33 $\pm$ 1	276 $\pm$ 3	120 $\pm$ 6	H $\alpha$ only, SP
RP <sub>s</sub> 1055	05 24 46.26	-67 38 11.1	BE74266	B3IIIe	-13.50	241 $\pm$ 12	41 $\pm$ 2	287 $\pm$ 3	193 $\pm$ 10	H $\alpha$ , $\beta$ , HeII4686
RP <sub>s</sub> 1109	05 24 57.81	-67 24 58.2		B1Ve	-12.88	287 $\pm$ 14	103 $\pm$ 4	283 $\pm$ 4	289 $\pm$ 14	H $\alpha$ , $\beta$ , $\gamma$
RP <sub>s</sub> 2147	05 24 58.51	-69 03 04.5	FAUST844	BIII[e]	-13.24	224 $\pm$ 11	36 $\pm$ 1	292 $\pm$ 4	171 $\pm$ 9	H $\alpha$ , $\beta$ , [S II], [N II], [O II], SP
RP <sub>s</sub> 944	05 25 00.39	-68 19 30.4		B2V[e]	-13.27	50 $\pm$ 2	37 $\pm$ 1	265 $\pm$ 1	10 $\pm$ 1	H $\alpha$ , $\beta$ , [N II], [S II], [O II], HeII4686.
RP <sub>s</sub> 567	05 25 01.95	-70 37 09.5		B2IIIe	-13.32	522 $\pm$ 26	37 $\pm$ 1	244 $\pm$ 11	448 $\pm$ 22	H $\alpha$ , $\beta$
RP <sub>s</sub> 2155	05 25 05.75	-69 06 56.5			-14.36	435 $\pm$ 22	53 $\pm$ 2	274 $\pm$ 4	397 $\pm$ 20	H $\alpha$ , $\beta$
RP <sub>s</sub> 943	05 25 10.22	-68 25 16.4	BE74268	B2III[e]	-13.05	60 $\pm$ 3	71 $\pm$ 3	263 $\pm$ 2	29 $\pm$ 1	H $\alpha$ , [N II], [S II], [O II]
RP <sub>s</sub> 800	05 25 10.89	-69 20 37.1		B1V[e]	-13.47	102 $\pm$ 5	33 $\pm$ 1	280 $\pm$ 1	55 $\pm$ 3	H $\alpha$ , $\beta$ , [N II], [S II], [O III], within H II region, SP
RP <sub>s</sub> 707	05 25 12.29	-69 55 26.9	SAB2388	B3IIIe	-13.21	257 $\pm$ 13	26 $\pm$ 1	273 $\pm$ 4	185 $\pm$ 9	H $\alpha$ , $\beta$ , SP
RP <sub>s</sub> 2149	05 25 20.02	-69 20 24.3		BIII[e]	-14.44	433 $\pm$ 22	34 $\pm$ 1	288 $\pm$ 4	365 $\pm$ 18	H $\alpha$ , $\beta$ , [S II], [N II], [O II] within dense H II region. DP R>V
RP <sub>s</sub> 869	05 25 25.72	-69 12 55.7		B3IIIe	-12.84	281 $\pm$ 14	59 $\pm$ 2	283 $\pm$ 27	237 $\pm$ 12	H $\alpha$ , $\beta$ , [N II], [S II] and [O III] some due to local emission. SP
RP <sub>s</sub> 724	05 25 29.68	-69 50 30.4		A2Ibe	-14.12	193 $\pm$ 10	4 $\pm$ 0	225 $\pm$ 6	74 $\pm$ 4	H $\alpha$ only, SP
RP <sub>s</sub> 725	05 25 39.77	-69 50 59.7		B1.7V[e]	-13.80	60 $\pm$ 3	45 $\pm$ 2	272 $\pm$ 1	23 $\pm$ 1	H $\alpha$ , $\beta$ , [S II], [O II], SP
RP <sub>s</sub> 942	05 25 40.09	-68 30 46.1	AL182	B1IIIe	-12.18	299 $\pm$ 15	64 $\pm$ 3	294 $\pm$ 4	278 $\pm$ 14	H $\alpha$ , $\beta$ , $\gamma$
RP <sub>s</sub> 727	05 25 44.66	-69 53 20.5		B1V[e]	-13.76	319 $\pm$ 16	28 $\pm$ 1	278 $\pm$ 1	245 $\pm$ 12	H $\alpha$ , Pcyg on Hb, [S II], [N II], [O II], [O III]
RP <sub>s</sub> 2166	05 25 46.00	-69 14 02.3		B3V[e]	-13.20	286 $\pm$ 14	49 $\pm$ 2	293 $\pm$ 4	249 $\pm$ 13	H $\alpha$ , $\beta$ , [S II], [N II], [O II], SP
RP <sub>s</sub> 2146	05 25 50.55	-69 05 29.4		BV[e]	-14.42	369 $\pm$ 18	13 $\pm$ 1	253 $\pm$ 5	244 $\pm$ 12	H $\alpha$ , $\beta$ , [S II], [N II], [O II], [O III], SP
RP <sub>s</sub> 779	05 25 50.62	-69 27 33.1	SAB2427	B3III[e]	-12.70	207 $\pm$ 10	43 $\pm$ 2	285 $\pm$ 1	160 $\pm$ 8	H $\alpha$ , $\beta$ , [N II], [S II], [O II]
RP <sub>s</sub> 672	05 25 56.58	-70 15 06.6		B3Ve	-13.35	330 $\pm$ 17	28 $\pm$ 1	288 $\pm$ 4	255 $\pm$ 13	H $\alpha$ , $\beta$ only, SP
RP <sub>s</sub> 592	05 25 58.15	-70 28 42.4		B5IIIe	-12.85	391 $\pm$ 20	52 $\pm$ 2	226 $\pm$ 4	353 $\pm$ 18	H $\alpha$ , $\beta$ only
RP <sub>s</sub> 886	05 26 00.41	-69 53 27.0	BE74581	B5IIIe	-12.47	495 $\pm$ 25	72 $\pm$ 3	337 $\pm$ 18	481 $\pm$ 24	H $\alpha$ , $\beta$ , Bpe, semi-regular pulsating star. DP R>V
RP <sub>s</sub> 988	05 26 05.58	-68 36 26.4	BE74276	B1V[e]	-12.90	338 $\pm$ 17	99 $\pm$ 4	247 $\pm$ 55	345 $\pm$ 17	H $\alpha$ , $\beta$ , [S II], [N I], [O II], [O III]
RP <sub>s</sub> 989	05 26 07.35	-68 36 35.9	BE74276	B1.7Ve	-13.29	67 $\pm$ 3	47 $\pm$ 2	260 $\pm$ 2	29 $\pm$ 2	H $\alpha$ , $\beta$ , weak forbidden lines [S II], [N II], [O III], [O II] belong to compact H II in area
RP <sub>s</sub> 2162	05 26 11.28	-69 19 21.5		BV[e]	-13.11	74 $\pm$ 8	12 $\pm$ 1	296 $\pm$ 4	14 $\pm$ 6	H $\alpha$ , $\beta$ , [S II], [N II], [O II]. SP, Bottle shape
RP <sub>s</sub> 798	05 26 13.74	-69 25 45.1		A0Ve	-13.95	482 $\pm$ 24	26 $\pm$ 1	333 $\pm$ 6	379 $\pm$ 19	H $\alpha$ only
RP <sub>s</sub> 2160	05 26 22.19	-69 18 07.4	BE74227	BIII[e]	-12.72	249 $\pm$ 12	35 $\pm$ 1	291 $\pm$ 4	195 $\pm$ 10	H $\alpha$ , $\beta$ , [S II], [N II], [O II], within dense H II region. SP
RP <sub>s</sub> 1110	05 26 30.57	-67 40 36.5		F2III[e]	-12.56	104 $\pm$ 5	144 $\pm$ 6	311 $\pm$ 2	94 $\pm$ 5	H $\alpha$ , $\beta$ , $\gamma$ , $\delta$ , possible emO with weak continuum
RP <sub>s</sub> 878	05 26 34.51	-69 06 32.3		B1Ve	-12.84	266 $\pm$ 13	64 $\pm$ 3	210 $\pm$ 25	243 $\pm$ 12	H $\alpha$ , $\beta$ , [S II] and [O III] is ambient, SP
RP <sub>s</sub> 818	05 26 44.77	-69 14 55.7		B1Ve	-13.34	202 $\pm$ 10	31 $\pm$ 1	262 $\pm$ 3	146 $\pm$ 7	H $\alpha$ , $\beta$ , SP
RP <sub>s</sub> 845	05 26 46.73	-69 11 58.3		B2Ve	-13.66	173 $\pm$ 9	34 $\pm$ 1	305 $\pm$ 2	124 $\pm$ 6	H $\alpha$ , $\beta$ , DP R>V
RP <sub>s</sub> 941	05 26 49.05	-68 25 45.5		B2V[e]	-13.29	59 $\pm$ 3	88 $\pm$ 4	244 $\pm$ 1	32 $\pm$ 2	H $\alpha$ , [N II], [S II]
RP <sub>s</sub> 859	05 26 51.89	-69 00 30.4		B3Ve	-13.80	412 $\pm$ 21	36 $\pm$ 1	232 $\pm$ 2	346 $\pm$ 17	H $\alpha$ is mostly from ambient emission, SP
RP <sub>s</sub> 858	05 26 52.67	-69 00 49.3		B9Ve	-14.14	296 $\pm$ 15	63 $\pm$ 3	244 $\pm$ 3	267 $\pm$ 13	H $\alpha$ only
RP <sub>s</sub> 542	05 26 53.39	-71 22 08.2	LI-SMC235	B0IV[e]	-12.80	339 $\pm$ 17	146 $\pm$ 6	246 $\pm$ 2	375 $\pm$ 19	H $\alpha$ , $\beta$ , $\gamma$ , $\delta$ , [O II] 3727, [N II], [S II]
RP <sub>s</sub> 1011	05 27 00.26	-71 18 54.5		B6Ve	-13.26	226 $\pm$ 11	36 $\pm$ 1	282 $\pm$ 3	173 $\pm$ 9	H $\alpha$ only
RP <sub>s</sub> 730	05 27 02.49	-69 52 17.2	MACHO77.7548.102	B2IIIe	-13.02	259 $\pm$ 13	28 $\pm$ 1	299 $\pm$ 3	192 $\pm$ 10	H $\alpha$ , $\beta$ , SP
RP <sub>s</sub> 731	05 27 02.99	-69 46 00.7	AGPRSJ052702.99-694600.7	B5IIIe	-12.85	288 $\pm$ 14	22 $\pm$ 1	289 $\pm$ 4	205 $\pm$ 10	H $\alpha$ , $\beta$ , SP
RP <sub>s</sub> 797	05 27 03.26	-69 24 26.7		B1Ve	-13.21	340 $\pm$ 17	39 $\pm$ 2	300 $\pm$ 5	287 $\pm$ 14	H $\alpha$ , $\beta$ , weak [O III], DP R>V
RP <sub>s</sub> 599	05 27 07.19	-70 20 02.1		B3Ve	-13.23	144 $\pm$ 7	110 $\pm$ 4	247 $\pm$ 2	132 $\pm$ 7	H $\alpha$ , $\beta$
RP <sub>s</sub> 820	05 27 11.02	-69 15 55.1		B3IIIe	-12.56	295 $\pm$ 15	36 $\pm$ 1	251 $\pm$ 4	237 $\pm$ 12	H $\alpha$ , $\beta$ , SP
RP <sub>s</sub> 1108	05 27 12.29	-67 23 47.9	AL 198	B0.5IIIe	-12.22	237 $\pm$ 12	80 $\pm$ 3	319 $\pm$ 4	219 $\pm$ 11	H $\alpha$ , $\beta$ , $\gamma$
RP <sub>s</sub> 765	05 27 13.11	-69 42 12.3	MACHO77.7550.54	B3Ve	-13.02	505 $\pm$ 25	21 $\pm$ 1	253 $\pm$ 7	388 $\pm$ 19	H $\alpha$ , weak H $\beta$ , DP centre, sh
RP <sub>s</sub> 2157	05 27 15.26	-69 14 36.8	L63236	BIIIe	-12.49	174 $\pm$ 9	42 $\pm$ 2	289 $\pm$ 4	129 $\pm$ 6	H $\alpha$ , $\beta$ , SP
RP <sub>s</sub> 536	05 27 20.01	-71 14 01.8		B1IIIe	-13.09	210 $\pm$ 10	29 $\pm$ 1	233 $\pm$ 3	148 $\pm$ 7	H $\alpha$ , $\beta$
RP <sub>s</sub> 821	05 27 42.74	-69 14 11.9		B1Ve	-13.01	366 $\pm$ 18	71 $\pm$ 3	296 $\pm$ 5	347 $\pm$ 17	H $\alpha$ , $\beta$ only, DP centre
RP <sub>s</sub> 1107	05 27 43.16	-67 25 47.7	AL 203	B2IV[e]	-12.64	130 $\pm$ 6	115 $\pm$ 5	328 $\pm$ 1	116 $\pm$ 6	H $\alpha$ , $\beta$ , $\gamma$ , $\delta$ , $\epsilon$ , [S II], [N II], [O II]. Ambient H II close by. Weak [O III] probably from ambient emission.
RP <sub>s</sub> 861	05 27 43.63	-69 03 21.6		B1V[e]	-13.11	330 $\pm$ 16	61 $\pm$ 2	279 $\pm$ 3	301 $\pm$ 15	H $\alpha$ , $\beta$ , [O III], [S II]
RP <sub>s</sub> 842	05 27 44.38	-69 08 32.2		B5IIIe	-12.79	469 $\pm$ 23	55 $\pm$ 2	238 $\pm$ 23	431 $\pm$ 22	H $\alpha$ , $\beta$ , SP
RP <sub>s</sub> 843	05 27 47.62	-69 09 27.6		B2IIIe	-12.74	510 $\pm$ 26	64 $\pm$ 3	247 $\pm$ 29	497 $\pm$ 25	H $\alpha$ , $\beta$ , SP

RP Object	RA J2000	DEC J2000	Other Catalog Reference	Spec Type	Log F H $\alpha$	FWHM H $\alpha$ km/s	EW H $\alpha$ Å	Vel. (helio) km/s	$v \sin i$ km/s	Comments
RP605	05 27 49.37	-71 31 19.8		A1V[e]	-13.37	251 $\pm$ 13	60 $\pm$ 2	247 $\pm$ 2	221 $\pm$ 11	H $\alpha$ , $\beta$ , $\gamma$ , $\delta$ , [O II] 3727, [N II], [S II], [O III] 5007
RP1057	05 28 02.72	-67 31 16.5	AL 207	B2IIe	-12.18	256 $\pm$ 13	72 $\pm$ 3	324 $\pm$ 4	239 $\pm$ 12	H $\alpha$ , $\beta$ some diffuse emission in area.
RP840	05 28 03.99	-69 09 57.2		B4IVe	-12.96	453 $\pm$ 23	70 $\pm$ 3	248 $\pm$ 17	438 $\pm$ 22	H $\alpha$ , $\beta$ , SP
RP2185	05 28 04.23	-69 05 26.8	SVHV 2565	B0Ve	-13.89	182 $\pm$ 9	19 $\pm$ 1	294 $\pm$ 4	111 $\pm$ 6	H $\alpha$ , $\beta$ , DP centre
RP823	05 28 04.41	-69 13 33.0		B1.7Ve	-13.17	430 $\pm$ 22	47 $\pm$ 2	241 $\pm$ 11	382 $\pm$ 19	H $\alpha$ , $\beta$ , SP
RP822	05 28 07.61	-69 14 28.4		B1V[e]	-13.12	345 $\pm$ 17	44 $\pm$ 2	286 $\pm$ 4	300 $\pm$ 15	H $\alpha$ , $\beta$ , [O III] 5007 weak. Possible symbiotic, SP
RP841	05 28 08.09	-69 10 22.6		B2Ve	-14.17	213 $\pm$ 12	25 $\pm$ 1	264 $\pm$ 16	146 $\pm$ 9	ambient emission brings in the [O III] 5007 line, SP, Bottle shape
RP702	05 28 14.06	-69 54 37.9		F0IIe	-12.52	394 $\pm$ 20	43 $\pm$ 2	335 $\pm$ 5	338 $\pm$ 17	H $\alpha$ , $\beta$ , FeII 4173, 4179
RP879	05 28 20.08	-68 59 10.4		B0IIIe	-12.50	155 $\pm$ 8	65 $\pm$ 3	258 $\pm$ 3	127 $\pm$ 6	H $\alpha$ , $\beta$ , SP
RP512	05 28 20.82	-70 59 22.4	BE74589	B2IIe	-12.63	393 $\pm$ 20	32 $\pm$ 1	216 $\pm$ 22	319 $\pm$ 16	H $\alpha$ , $\beta$
RP2186	05 28 27.04	-69 05 37.5	BE74300	BVe	-12.73	163 $\pm$ 8	45 $\pm$ 2	294 $\pm$ 4	123 $\pm$ 6	H $\alpha$ , $\beta$ , low [O III] due to ambient emission. SP
RP510	05 28 28.87	-71 00 48.5		B5V[e]	-13.95	84 $\pm$ 4	3 $\pm$ 0	225 $\pm$ 1	4 $\pm$ 0	H $\alpha$ , [N II], [S II], [O III], SP
RP796	05 28 32.24	-69 19 56.8		B1Ve	-13.83	278 $\pm$ 14	32 $\pm$ 1	280 $\pm$ 3	215 $\pm$ 11	H $\alpha$ , $\beta$ , $\gamma$
RP472	05 28 36.50	-70 56 21.4		B2IIe	-11.92	341 $\pm$ 17	49 $\pm$ 2	225 $\pm$ 5	296 $\pm$ 15	H $\alpha$ , $\beta$ , $\gamma$ , HeI absorption
RP436	05 28 36.57	-70 48 25.9		B2IIe	-13.14	401 $\pm$ 20	39 $\pm$ 2	187 $\pm$ 6	344 $\pm$ 17	H $\alpha$ , $\beta$ only
RP839	05 28 38.27	-69 11 07.6	BE74307	B0IIIe	-12.31	239 $\pm$ 12	35 $\pm$ 1	264 $\pm$ 4	185 $\pm$ 9	H $\alpha$ , $\beta$ , $\gamma$ , SP
RP688	05 28 40.90	-70 01 38.1	MACHO77.7788.54	B2IIe	-12.99	329 $\pm$ 16	59 $\pm$ 2	203 $\pm$ 5	300 $\pm$ 15	H $\alpha$ , $\beta$
RP2179	05 28 45.59	-68 59 23.7		BIVe	-12.78	157 $\pm$ 8	63 $\pm$ 3	285 $\pm$ 5	130 $\pm$ 7	H $\alpha$ , $\beta$ , close to H II region. DP centre
RP2181	05 28 48.85	-69 01 19.6		BIII[e]	-12.69	297 $\pm$ 15	56 $\pm$ 2	283 $\pm$ 5	260 $\pm$ 13	H $\alpha$ , $\beta$ , [O III], in H II region, SP
RP784	05 28 53.10	-69 24 51.4	MACHO77.7918.68	B3Ve	-13.87	129 $\pm$ 6	25 $\pm$ 1	272 $\pm$ 3	73 $\pm$ 4	H $\alpha$ , $\beta$
RP783	05 28 57.69	-69 25 09.5	MACHO77.7918.92	A7III[e]	-13.84	288 $\pm$ 14	31 $\pm$ 1	258 $\pm$ 5	224 $\pm$ 11	H $\alpha$ , $\beta$ , [O III]
RP2182	05 28 58.82	-69 03 55.0		BVe	-13.84	377 $\pm$ 19	57 $\pm$ 2	276 $\pm$ 4	349 $\pm$ 18	H $\alpha$ , $\beta$ , in H II region. SP
RP794	05 29 01.97	-69 22 50.6	BE74309	B1IIe	-12.20	184 $\pm$ 9	100 $\pm$ 4	274 $\pm$ 3	174 $\pm$ 9	H $\alpha$ , $\beta$ , $\gamma$ , Bpe
RP2183	05 29 02.92	-69 04 29.1		BIIIe	-14.11	242 $\pm$ 12	43 $\pm$ 2	281 $\pm$ 3	193 $\pm$ 10	H $\alpha$ , $\beta$ , in H II region, SP
RP880	05 29 07.24	-69 04 51.3		B1.5V[e]	-13.73	175 $\pm$ 9	88 $\pm$ 4	278 $\pm$ 2	158 $\pm$ 8	H $\alpha$ , $\beta$ , most [S II], [N II], [O II], [O III] from ambient H II emission in area. DP R>V
RP838	05 29 21.10	-69 11 17.8		B1Ve	-13.96	163 $\pm$ 8	16 $\pm$ 1	269 $\pm$ 2	92 $\pm$ 5	H $\alpha$ only but mainly from ambient emission, SP
RP887	05 29 22.39	-69 00 11.8		B3Ve	-13.88	347 $\pm$ 17	29 $\pm$ 1	272 $\pm$ 2	270 $\pm$ 14	H $\alpha$ , $\beta$ , $\gamma$ , [O III], [N II], [S II], DP V>R
RP836	05 29 22.71	-69 10 13.8	BE74313	B0.5IIe	-12.47	207 $\pm$ 10	27 $\pm$ 1	272 $\pm$ 3	146 $\pm$ 7	H $\alpha$ , $\beta$ , weak [O III], SP
RP995	05 29 28.71	-68 28 29.9		B3V[e]	-13.96	97 $\pm$ 5	52 $\pm$ 2	273 $\pm$ 1	61 $\pm$ 3	H $\alpha$ , $\beta$ ambient emission producing [S II], [N II], [O II] and [O III]
RP1056	05 29 41.19	-67 35 48.2	AL 233	B3IIe	-13.09	297 $\pm$ 15	32 $\pm$ 1	291 $\pm$ 5	232 $\pm$ 12	H $\alpha$ , $\beta$
RP864	05 29 41.40	-69 06 53.4		B5IIe	-12.83	312 $\pm$ 16	27 $\pm$ 1	217 $\pm$ 10	239 $\pm$ 12	H $\alpha$ , $\beta$ only
RP835	05 29 50.72	-69 10 32.0		B1Ve	-13.62	85 $\pm$ 11	12 $\pm$ 3	258 $\pm$ 3	23 $\pm$ 10	H $\alpha$ , $\beta$ , [O III] from ambient emission, SP, Bottle shape
RP2177	05 29 51.32	-68 59 15.5		BIIIe	-12.69	350 $\pm$ 18	48 $\pm$ 2	288 $\pm$ 4	305 $\pm$ 15	H $\alpha$ , $\beta$ , SP
RP785	05 29 55.03	-69 26 53.3		B0V[e]	-13.25	227 $\pm$ 11	57 $\pm$ 2	257 $\pm$ 3	196 $\pm$ 10	H $\alpha$ , $\beta$ , [O III], SP
RP2210	05 29 56.15	-68 38 50.1		B1V[e]	-12.73	250 $\pm$ 13	26 $\pm$ 1	318 $\pm$ 10	184 $\pm$ 9	H $\alpha$ , $\beta$ , $\gamma$ , [O III], [N II], [S II]
RP974	05 30 00.60	-67 57 30.1		B3Ve	-13.94	202 $\pm$ 10	72 $\pm$ 3	284 $\pm$ 3	181 $\pm$ 9	H $\alpha$ , $\beta$
RP786	05 30 01.22	-69 28 09.5	SAB955	B3IIe	-13.01	224 $\pm$ 11	27 $\pm$ 1	266 $\pm$ 3	161 $\pm$ 8	H $\alpha$ , $\beta$
RP740	05 30 01.79	-69 40 46.6	SAB1210	B3V[e]	-13.27	179 $\pm$ 9	56 $\pm$ 2	275 $\pm$ 2	147 $\pm$ 7	H $\alpha$ , $\beta$ , [S II], [N II], [O III], SP
RP1083	05 30 14.61	-66 49 12.7	AL243	B2IIe	-12.42	395 $\pm$ 20	88 $\pm$ 4	355 $\pm$ 6	398 $\pm$ 20	H $\alpha$ , $\beta$
RP546	05 30 19.08	-71 20 04.6		B5Ve	-12.49	453 $\pm$ 23	56 $\pm$ 2	244 $\pm$ 3	426 $\pm$ 21	H $\alpha$ , $\beta$
RP1077	05 30 24.32	-67 14 54.6	BE74, 75	B2IIe	-12.93	350 $\pm$ 17	70 $\pm$ 3	323 $\pm$ 5	330 $\pm$ 17	H $\alpha$ , $\beta$
RP667	05 30 26.08	-70 15 07.2		A4IVe	-13.77	59 $\pm$ 3	25 $\pm$ 1	275 $\pm$ 2	13 $\pm$ 1	Possible AGB star. Variable.
RP867	05 30 26.65	-69 05 35.8		B3Ve	-13.31	312 $\pm$ 16	46 $\pm$ 2	265 $\pm$ 1	268 $\pm$ 13	H $\alpha$ , $\beta$
RP1079	05 30 33.33	-66 57 41.9		A0V[e]	-14.07	246 $\pm$ 12	54 $\pm$ 2	287 $\pm$ 2	210 $\pm$ 11	H $\alpha$ + [O III]
RP788	05 30 39.18	-69 25 43.8		F8IIe	-13.89	119 $\pm$ 6	9 $\pm$ 0	270 $\pm$ 1	44 $\pm$ 2	H $\alpha$ , $\beta$ , ambient emission causing [S II] & [O III], Cepheid known, SP
RP930	05 30 39.36	-68 34 03.6		B1.7Ve	-13.17	335 $\pm$ 17	33 $\pm$ 1	280 $\pm$ 2	266 $\pm$ 13	H $\alpha$ , other forbidden lines: [N II], [S II], [O III] but thick nebula in immediate area.
RP2203	05 30 39.43	-68 35 28.5					0			Not observed
RP787	05 30 40.67	-69 25 31.1	MACHO77.8160.6	B3IIe	-12.69	422 $\pm$ 21	38 $\pm$ 2	276 $\pm$ 6	355 $\pm$ 18	H $\alpha$ , $\beta$
RP834	05 30 41.64	-69 11 34.6		B1.5IIe	-13.10	99 $\pm$ 5	15 $\pm$ 1	256 $\pm$ 1	38 $\pm$ 2	H $\alpha$ , $\beta$ , DP centre
RP587	05 30 43.25	-70 25 57.9		B3Ve	-13.11	294 $\pm$ 15	42 $\pm$ 2	256 $\pm$ 4	243 $\pm$ 12	H $\alpha$ , $\beta$
RP556	05 30 55.02	-70 45 28.2	MACHO7.8140.15	B2IIe	-12.18	214 $\pm$ 11	55 $\pm$ 2	255 $\pm$ 3	178 $\pm$ 9	H $\alpha$ , $\beta$ , SP
RP1075	05 31 04.25	-67 08 22.3		B2IIe	-12.89	362 $\pm$ 18	77 $\pm$ 3	315 $\pm$ 5	352 $\pm$ 18	H $\alpha$ , $\beta$
RP881	05 31 10.07	-69 05 25.0		B1V[e]	-13.62	68 $\pm$ 3	28 $\pm$ 1	263 $\pm$ 25	22 $\pm$ 1	H $\alpha$ , $\beta$ , $\gamma$ , [O III], [N II], [S II]. Within ambient H II which contributes to nebula lines, SP
RP824	05 31 10.86	-69 14 16.9		B8V[e]	-13.77	199 $\pm$ 10	21 $\pm$ 1	270 $\pm$ 3	129 $\pm$ 7	H $\alpha$ , $\beta$ , [S II], [O III]
RP444	05 31 15.62	-70 53 48.4	XMMUJ053115.4-705350	B0Ie	-13.13	345 $\pm$ 17	14 $\pm$ 1	269 $\pm$ 4	232 $\pm$ 12	H $\alpha$ , $\beta$ , high mass X-ray binary
RP2209	05 31 16.89	-68 40 05.9		B3III[e]	-13.07	194 $\pm$ 10	11 $\pm$ 0	295 $\pm$ 8	102 $\pm$ 5	H $\alpha$ , $\beta$ , [O III], [N II], [S II]
RP443	05 31 18.75	-70 54 07.7	BE74595	B3IVe	-12.51	415 $\pm$ 21	84 $\pm$ 3	268 $\pm$ 4	420 $\pm$ 21	H $\alpha$ , $\beta$

RP Object	RA J2000	DEC J2000	Other Catalog Reference	Spec Type	Log F H $\alpha$	FWHM H $\alpha$ km/s	EW H $\alpha$ Å	Vel. (helio) km/s	$v \sin i$ km/s	Comments
RPs992	05 31 21.06	-68 31 34.3		B2V[e]	-12.13	32 $\pm$ 2	108 $\pm$ 4	302 $\pm$ 1	5 $\pm$ 0	H $\alpha$ , $\beta$ , $\gamma$ , [S II], [N II], [O II], [O III] within compact dense H II cloud. SP
RPs915	05 31 22.11	-68 36 42.0		B2V[e]	-13.24	82 $\pm$ 4	57 $\pm$ 2	275 $\pm$ 2	49 $\pm$ 3	H $\alpha$ , $\beta$ , [S II], [O III], [O II] in cocoon, SP
RPs2208	05 31 24.25	-68 41 33.6	BE74334		-11.81	374 $\pm$ 19	34 $\pm$ 1	278 $\pm$ 19	310 $\pm$ 16	H $\alpha$ , $\beta$ , Late-type star characteristics
RPs832	05 31 30.75	-69 11 52.0	MACHO82.8284.23	B3IIIe	-12.84	258 $\pm$ 13	31 $\pm$ 1	265 $\pm$ 4	197 $\pm$ 10	H $\alpha$ , $\beta$ [O III] from ambient emission
RPs432	05 31 33.11	-70 46 17.9	MACHO7.8260	B3Ve	-13.49	383 $\pm$ 19	26 $\pm$ 1	246 $\pm$ 0	294 $\pm$ 15	H $\alpha$ , H $\beta$
RPs507	05 31 36.20	-71 10 42.9		B8Ve	-15.02	95 $\pm$ 5	24 $\pm$ 1	246 $\pm$ 1	44 $\pm$ 2	H $\alpha$ only
RPs825	05 31 36.24	-69 18 45.6		B2III[e]	-13.07	273 $\pm$ 14	73 $\pm$ 3	286 $\pm$ 4	258 $\pm$ 13	H $\alpha$ , $\beta$ , [S II], [O III], in H II region, SP
RPs938	05 31 40.51	-68 22 44.1		B9Ve	-13.80	96 $\pm$ 5	46 $\pm$ 2	270 $\pm$ 2	58 $\pm$ 3	H $\alpha$ only, forbidden lines [O III], [N II], [S II] due to H II mainly local.
RPs453	05 31 45.97	-70 51 22.9	MACHO14.8259.18	B1V[e]	-13.37	410 $\pm$ 20	29 $\pm$ 1	257 $\pm$ 6	326 $\pm$ 16	H $\alpha$ , $\beta$ with strong [O III], DP centre
RPs2207	05 31 46.25	-68 33 59.9		F2III[e]	-12.66	300 $\pm$ 15	38 $\pm$ 2	281 $\pm$ 10	242 $\pm$ 12	H $\alpha$ , $\beta$ , [O III], [N II], [S II]
RPs831	05 31 46.26	-69 09 57.2	L278	B2IIIe	-12.55	279 $\pm$ 14	85 $\pm$ 3	290 $\pm$ 4	272 $\pm$ 14	H $\alpha$ , $\beta$ , low level [O III] from ambient emission
RPs868	05 31 57.78	-69 06 10.8	AL290	B3IIIe	-12.98	266 $\pm$ 13	36 $\pm$ 1	264 $\pm$ 4	210 $\pm$ 11	H $\alpha$ , $\beta$ , weak [O III] only 3 $\sigma$ noise
RPs953	05 32 02.67	-68 11 59.5		B3Ve	-13.71	323 $\pm$ 16	33 $\pm$ 1	270 $\pm$ 4	255 $\pm$ 13	H $\alpha$ only
RPs937	05 32 05.19	-68 12 46.4		A0Ve	-13.93	274 $\pm$ 14	55 $\pm$ 2	287 $\pm$ 3	238 $\pm$ 12	H $\alpha$
RPs830	05 32 13.66	-69 13 39.6		B5IIIe	-13.09	219 $\pm$ 11	50 $\pm$ 2	291 $\pm$ 3	183 $\pm$ 9	H $\alpha$ , $\beta$ [O III] from ambient emission, SP
RPs975	05 32 14.81	-68 10 25.6		B2Ve	-13.93	182 $\pm$ 9	35 $\pm$ 1	273 $\pm$ 2	132 $\pm$ 7	H $\alpha$ only
RPs912	05 32 15.68	-68 40 14.5		B3V[e]	-13.28	111 $\pm$ 6	83 $\pm$ 3	276 $\pm$ 2	89 $\pm$ 4	H $\alpha$ , $\beta$ , [N II], [O II], [O III], [S II], SP
RPs448	05 32 17.29	-70 47 34.0		B2Ve	-12.81	267 $\pm$ 13	41 $\pm$ 2	215 $\pm$ 6	217 $\pm$ 11	H $\alpha$ , $\beta$ , DP centre
RPs935	05 32 18.75	-68 17 30.9		B3Ve	-13.51	242 $\pm$ 12	97 $\pm$ 4	302 $\pm$ 3	238 $\pm$ 12	H $\alpha$ , $\beta$
RPs914	05 32 18.77	-68 41 59.2		B2V[e]	-13.25	58 $\pm$ 3	48 $\pm$ 2	254 $\pm$ 1	20 $\pm$ 1	H $\alpha$ , $\beta$ , [O II], [O III], [N II], [S II], DP centre
RPs936	05 32 22.20	-68 17 33.8		B3Ve	-14.21	498 $\pm$ 25	41 $\pm$ 2	310 $\pm$ 20	437 $\pm$ 22	H $\alpha$ only.
RPs911	05 32 26.47	-68 39 03.9		B1V[e]	-13.54	183 $\pm$ 9	106 $\pm$ 4	285 $\pm$ 2	178 $\pm$ 9	H $\alpha$ , $\beta$ , [N II], [O II], [O III], [S II], SP
RPs1014	05 32 26.98	-70 47 44.3		B8Ve	-14.46	267 $\pm$ 13	34 $\pm$ 1	253 $\pm$ 3	205 $\pm$ 10	H $\alpha$ only, DP V>R
RPs447	05 32 27.03	-70 47 44.0		B3Ve	-13.57	409 $\pm$ 20	49 $\pm$ 2	227 $\pm$ 6	371 $\pm$ 19	H $\alpha$ only
RPs449	05 32 28.35	-70 47 28.6		B2V[e]	-14.93	464 $\pm$ 23	46 $\pm$ 2	252 $\pm$ 3	415 $\pm$ 21	H $\alpha$ , $\beta$ , [O II], [O III], [N II], [S II]
RPs532	05 32 30.10	-71 13 30.2		B2V[e]	-12.65	443 $\pm$ 22	49 $\pm$ 2	252 $\pm$ 2	395 $\pm$ 20	H $\alpha$ , $\beta$ , [N II], [S II]
RPs790	05 32 33.61	-69 24 56.0		F2III[e]	-13.68	117 $\pm$ 6	20 $\pm$ 1	269 $\pm$ 18	57 $\pm$ 3	H $\alpha$ , $\beta$ , [O II], [O III], [N II], [S II]
RPs502	05 32 34.68	-71 06 49.8	MACHO14.8497.6	B3Ve	-13.19	208 $\pm$ 10	25 $\pm$ 1	229 $\pm$ 2	141 $\pm$ 7	H $\alpha$ , $\beta$
RPs682	05 32 41.08	-70 09 51.6		B2Ve	-14.13	46 $\pm$ 2	36 $\pm$ 1	262 $\pm$ 1	6 $\pm$ 0	in diffuse emission 8 arcsec dia.
RPs773	05 32 50.20	-69 35 35.6		B3Ve	-13.43	436 $\pm$ 22	21 $\pm$ 1	289 $\pm$ 26	330 $\pm$ 17	H $\alpha$ , $\beta$
RPs826	05 33 02.38	-69 16 55.9	BE74352	B0.5IIIe	-12.50	294 $\pm$ 15	24 $\pm$ 1	274 $\pm$ 3	217 $\pm$ 11	H $\alpha$ , $\beta$ , forbidden lines at <3 $\sigma$ noise are due to ambient emission
RPs744	05 33 05.02	-69 38 47.3	MACHO81.8519.32	B1IIIe	-13.10	429 $\pm$ 21	49 $\pm$ 2	294 $\pm$ 4	381 $\pm$ 19	H $\alpha$ , $\beta$
RPs1102	05 33 05.55	-67 37 15.6		B0Ie	-12.62	349 $\pm$ 17	35 $\pm$ 1	280 $\pm$ 15	288 $\pm$ 14	H $\alpha$ , $\beta$ , $\gamma$ , weak [O III]
RPs1101	05 33 06.23	-67 36 49.2		B5IIIe	-12.54	227 $\pm$ 11	72 $\pm$ 3	287 $\pm$ 3	208 $\pm$ 10	H $\alpha$ , $\beta$ , Weak forbidden lines mainly due to ambient H II emission
RPs827	05 33 07.23	-69 15 27.7		B1Ve	-13.47	286 $\pm$ 14	88 $\pm$ 4	283 $\pm$ 4	279 $\pm$ 14	H $\alpha$ , $\beta$ [O III] from ambient emission, SP
RPs1001	05 33 07.49	-68 47 55.1		F8IV[e]	-13.02	285 $\pm$ 14	54 $\pm$ 2	243 $\pm$ 2	248 $\pm$ 12	H $\alpha$ , $\beta$ , $\gamma$ , [S II], [N II], [O II], [O III], SP
RPs1098	05 33 07.61	-67 18 05.5	AL 312	B0.5IIIe	-12.85	179 $\pm$ 9	50 $\pm$ 2	280 $\pm$ 3	143 $\pm$ 7	H $\alpha$ , $\beta$ , $\gamma$ , SP
RPs791	05 33 07.62	-69 29 46.1			-13.96	220 $\pm$ 11	52 $\pm$ 2	260 $\pm$ 19	183 $\pm$ 9	weak
RPs1100	05 33 22.24	-67 38 48.5		B9V[e]	-13.36	197 $\pm$ 10	75 $\pm$ 3	301 $\pm$ 3	177 $\pm$ 9	H $\alpha$ , $\beta$ , $\gamma$ , [S II], [N II], [O II]
RPs908	05 33 23.24	-68 39 34.8		B1V[e]	-14.03	390 $\pm$ 19	54 $\pm$ 2	334 $\pm$ 21	352 $\pm$ 18	H $\alpha$ , $\beta$ , [O III], [O II], [N II], [S II], DP centre
RPs529	05 33 24.93	-71 11 38.9		B5Ve	-14.16	211 $\pm$ 11	31 $\pm$ 1	301 $\pm$ 2	154 $\pm$ 8	H $\alpha$ only
RPs829	05 33 25.56	-69 13 11.7		B1Ve	-13.19	286 $\pm$ 14	35 $\pm$ 1	254 $\pm$ 4	228 $\pm$ 11	H $\alpha$ , $\beta$ [O III] from ambient emission
RPs697	05 33 29.21	-69 52 33.0		B1V[e]	-13.43	345 $\pm$ 17	64 $\pm$ 3	217 $\pm$ 11	325 $\pm$ 16	H $\alpha$ , $\beta$ , [S II], [N II], [O II]
RPs698	05 33 29.89	-69 52 28.8		B3IIIe	-12.91	237 $\pm$ 12	46 $\pm$ 2	322 $\pm$ 15	195 $\pm$ 10	weak
RPs1106	05 33 33.12	-67 24 54.0		O7V[e]	-13.13	90 $\pm$ 4	8 $\pm$ 0	298 $\pm$ 18	21 $\pm$ 1	H $\alpha$ , $\beta$ , [O III], [N II], [S II]
RPs1105	05 33 37.50	-67 25 39.3	GRV0533-6727	A0III[e]	-12.91	134 $\pm$ 7	15 $\pm$ 1	296 $\pm$ 2	65 $\pm$ 3	H $\alpha$ , $\beta$ , $\gamma$ , [S II], [N II], [O II], [O III]
RPs828	05 33 40.24	-69 12 50.6		F2III[e]	-12.79	341 $\pm$ 17	44 $\pm$ 2	252 $\pm$ 40	296 $\pm$ 15	H $\alpha$ , $\beta$ , $\gamma$ , [S II], [N II], [O II], [O III]
RPs909	05 33 44.06	-68 40 15.2		B0.5IIIe	-12.07	366 $\pm$ 18	64 $\pm$ 3	296 $\pm$ 5	347 $\pm$ 17	H $\alpha$ , $\beta$ , $\gamma$ , $\delta$ , SP
RPs574	05 33 44.39	-70 33 21.2		B1Ve	-13.54	280 $\pm$ 14	31 $\pm$ 1	251 $\pm$ 3	217 $\pm$ 11	H $\alpha$ , $\beta$
RPs495	05 34 26.46	-71 16 31.2		B2Ve	-12.83	366 $\pm$ 18	36 $\pm$ 1	232 $\pm$ 4	303 $\pm$ 15	H $\alpha$ , $\beta$
RPs934	05 34 39.65	-68 21 55.7		B2Ve	-13.09	111 $\pm$ 6	39 $\pm$ 2	280 $\pm$ 2	69 $\pm$ 4	H $\alpha$ , $\beta$ , forbidden lines from 6 arcsec radius disk surround star.
RPs500	05 34 47.82	-71 05 48.9		B2Ve	-12.65	511 $\pm$ 26	45 $\pm$ 2	252 $\pm$ 5	461 $\pm$ 23	H $\alpha$ , $\beta$ , HeI absorption
RPs419	05 34 52.63	-70 45 45.8	MACHO11.8865.7	B1Ve	-13.24	182 $\pm$ 9	52 $\pm$ 2	258 $\pm$ 3	146 $\pm$ 7	H $\alpha$ , $\beta$ only
RPs471	05 35 05.47	-70 51 14.8		B3Ve	-14.08	254 $\pm$ 13	16 $\pm$ 1	264 $\pm$ 5	166 $\pm$ 8	H $\alpha$ only. Strong HeI lines
RPs696	05 35 13.68	-69 49 46.9	SAB1373	B1IIIe	-13.07	268 $\pm$ 13	30 $\pm$ 1	289 $\pm$ 3	200 $\pm$ 10	H $\alpha$ , $\beta$ , SP
RPs362	05 35 29.44	-66 50 33.8		A3V[e]	-14.10	378 $\pm$ 19	42 $\pm$ 2	288 $\pm$ 37	322 $\pm$ 16	H $\alpha$ , $\beta$ , [S II], [N II], [O II]
RPs326	05 35 30.21	-67 38 05.9		B1.7Ve	-13.55	101 $\pm$ 5	53 $\pm$ 2	308 $\pm$ 15	65 $\pm$ 3	faint, ambient H II
RPs304	05 35 35.23	-67 40 22.1	AL345	B0.5IIIe	-11.04	280 $\pm$ 14	59 $\pm$ 2	302 $\pm$ 4	250 $\pm$ 13	H $\alpha$ , $\beta$ , $\gamma$



RP Object	RA J2000	DEC J2000	Other Catalog Reference	Spec Type	Log F H $\alpha$	FWHM H $\alpha$ km/s	EW H $\alpha$ Å	Vel. (helio) km/s	$v \sin i$ km/s	Comments
RP364	05 35 49.19	-66 51 26.0		B1.5Ve	-13.86	329 ± 16	28 ± 1	302 ± 5	254 ± 13	H $\alpha$
RP365	05 35 53.94	-66 52 32.3		F8Ve	-13.58	399 ± 20	65 ± 3	262 ± 6	382 ± 19	H $\alpha, \beta$ , some local faint H II emission
RP368	05 35 55.73	-66 51 08.6		B2IVe	-13.33	271 ± 14	28 ± 1	335 ± 4	203 ± 10	H $\alpha, \beta$
RP369	05 35 57.84	-66 50 53.7	AL350	B7IIIe	-13.56	281 ± 14	30 ± 1	282 ± 4	217 ± 11	H $\alpha, \beta$
RP1033	05 36 04.27	-67 55 37.0	BE74385	B2IVe	-11.05	263 ± 13	54 ± 2	289 ± 4	227 ± 11	H $\alpha, \beta$ , LBV poss
RP487	05 36 04.46	-70 51 01.4	BE74605	B2IIe	-12.89	394 ± 20	49 ± 2	223 ± 16	347 ± 17	H $\alpha, \beta, \gamma$
RP684	05 36 09.68	-70 06 08.0	SAB1386	B7Ve	-13.59	464 ± 23	34 ± 1	224 ± 5	394 ± 20	H $\alpha$ only
RP1005	05 36 16.32	-70 26 21.9	MACHO11.9112.61	B3V[e]	-13.18	223 ± 11	110 ± 4	322 ± 3	223 ± 11	H $\alpha, \beta$ , [O III], SP
RP531	05 36 16.96	-71 09 41.9		B2Ve	-13.98	524 ± 26	41 ± 2	329 ± 2	461 ± 23	H $\alpha, \beta$
RP348	05 36 28.63	-66 53 02.5	AL359	B5IIIe	-12.46	509 ± 25	67 ± 3	312 ± 9	497 ± 25	H $\alpha, \beta$
RP370	05 36 33.18	-66 51 18.6		B1Ve	-13.65	379 ± 19	45 ± 2	286 ± 5	332 ± 17	H $\alpha, \beta$
RP639	05 36 37.12	-69 22 09.4		B3IIIe	-12.87	135 ± 7	40 ± 2	245 ± 3	92 ± 5	H $\alpha, \beta$ [O III] is ambient emission
RP557	05 36 39.75	-70 44 37.4		B3Ve	-14.18	433 ± 22	45 ± 2	238 ± 4	385 ± 19	H $\alpha, \beta$
RP258	05 36 43.71	-69 36 44.6	MACHO81.9125.21	B3III[e]	-12.87	180 ± 9	32 ± 1	274 ± 3	126 ± 6	H $\alpha, \beta, \gamma$ , [O III], [O II], [N II], [S II]. Within H II region, SP
RP259	05 36 48.63	-69 26 44.6		B3V[e]	-13.54	218 ± 11	62 ± 2	333 ± 18	187 ± 9	H $\alpha, \beta, \gamma$ , [O III], [O II], [N II], [S II]
RP231	05 36 49.38	-69 23 55.2		B2V[e]	-13.09	246 ± 12	53 ± 2	265 ± 22	210 ± 11	H $\alpha, \beta, \gamma$ , [O III], [O II], [N II], [S II]
RP2163	05 36 54.13	-66 30 04.1		B3Ve	-13.59	176 ± 9	62 ± 2	320 ± 7	145 ± 7	H $\alpha, \beta$
RP330	05 36 57.68	-67 34 02.6		B1Ve	-13.83	166 ± 8	15 ± 1	291 ± 2	91 ± 5	H $\alpha$ , (pc on H $\beta$ ), faint, ambient H II
RP284	05 37 12.85	-68 37 11.8		B1Ve	-12.89	465 ± 23	74 ± 3	265 ± 15	463 ± 23	H $\alpha, \beta$
RP353	05 37 14.27	-66 26 59.2		B3IV[e]	-13.08	212 ± 11	91 ± 4	263 ± 5	199 ± 10	H $\alpha, \beta, \gamma$ , [O III], [O II], [N II], [S II]
RP352	05 37 14.60	-66 26 52.6		B1V[e]	-12.80	38 ± 2	129 ± 5	291 ± 1	13 ± 1	strong [S II] + [N II] but low [O III]. Strong [O II]
RP27	05 37 25.41	-70 30 47.9		A4Ve	-13.58	166 ± 8	136 ± 5	254 ± 3	168 ± 8	H $\alpha, \beta$ , DP V>R
RP298	05 37 28.44	-68 12 34.7		A2IVe	-13.09	518 ± 26	101 ± 4	278 ± 8	546 ± 27	H $\alpha, \beta$
RP257	05 37 35.37	-69 34 59.5	LI-SMC302	B2IIe	-12.11	282 ± 14	172 ± 7	268 ± 5	315 ± 16	H $\alpha, \beta$ , Low level [S II], [O III] probably ambient
RP29	05 37 38.98	-70 32 46.3		B1.7Ve	-13.50	555 ± 28	31 ± 1	271 ± 65	466 ± 23	H $\alpha, \beta$
RP1043	05 37 40.59	-67 31 37.1		B1Ve	-14.01	111 ± 6	8 ± 0	293 ± 1	36 ± 2	H $\alpha$ only. Centre of faint elliptical emission 20.7 x 42 arcsec
RP283	05 37 48.30	-68 39 54.6		B3V[e]	-13.16	496 ± 25	41 ± 2	292 ± 19	435 ± 22	H $\alpha, \beta, \gamma$ , [O III], [N II], [S II], DP V>R
RP372	05 37 50.31	-66 55 40.2		B4IIIe	-12.98	394 ± 20	41 ± 2	306 ± 5	338 ± 17	H $\alpha, \beta$
RP285	05 37 58.73	-68 33 39.2	BE74411	B2IVe	-12.50	352 ± 18	38 ± 2	261 ± 4	290 ± 15	H $\alpha, \beta$
RP226	05 38 03.07	-69 31 58.9		B1.7V[e]	-12.85	49 ± 2	25 ± 1	267 ± 2	4 ± 0	H $\alpha, \beta$ , forbidden lines from ambient emission
RP81	05 38 03.78	-70 50 28.3		B0IVe	-12.70	307 ± 15	27 ± 1	251 ± 18	234 ± 12	H $\alpha, \beta$
RP634	05 38 04.67	-69 59 18.4		B6Ve	-13.54	226 ± 11	96 ± 4	242 ± 3	220 ± 11	H $\alpha, \beta$ , SP
RP2198	05 38 07.83	-70 01 37.8								Not observed
RP338	05 38 12.92	-67 18 27.8		B2Ve	-13.81	205 ± 10	42 ± 2	303 ± 2	159 ± 8	H $\alpha, \beta$ , low levels (2 $\sigma$ noise) due to faint ambient emission.
RP337	05 38 15.55	-67 15 49.2		B3IIIe	-13.03	276 ± 14	60 ± 2	267 ± 4	246 ± 12	H $\alpha, \beta$
RP224	05 38 17.32	-69 32 05.0		B0.5I[e]	-12.41	141 ± 7	41 ± 2	260 ± 3	98 ± 5	H $\alpha, \beta$ , [S II], [N II], [O III], [O II]
RP335	05 38 17.82	-67 34 39.8		B2IIe	-13.03	240 ± 12	46 ± 2	256 ± 3	198 ± 10	H $\alpha, \beta$
RP301	05 38 19.82	-67 45 01.5		B1V[e]	-13.36	135 ± 7	76 ± 3	314 ± 2	111 ± 6	H $\alpha, \beta$ , [S II], [N II], [O II]
RP1952	05 38 22.79	-71 15 13.5		B9Ve	-14.25	511 ± 26	42 ± 2	201 ± 1	449 ± 23	H $\alpha$ only
RP91	05 38 22.87	-70 18 01.5		B1Ve	-14.32	335 ± 17	26 ± 1	233 ± 2	252 ± 13	H $\alpha$ only
RP146	05 38 26.35	-70 10 50.0		B2Ve	-14.02	534 ± 27	51 ± 2	223 ± 2	496 ± 25	H $\alpha$ only
RP290	05 38 40.83	-68 24 00.7		BVp[e]	-11.92	148 ± 7	124 ± 5	267 ± 3	143 ± 7	H $\alpha, \beta$ , [O III]
RP311	05 38 44.16	-68 43 53.9		B1IVe	-12.58	264 ± 13	53 ± 2	317 ± 4	227 ± 11	H $\alpha, \beta$ , forbidden lines due top strong ambient emission
RP325	05 38 49.92	-67 32 04.5		B2Ve	-13.73	285 ± 14	29 ± 1	317 ± 4	215 ± 11	H $\alpha, \beta$
RP256	05 38 51.35	-69 44 51.1		B0.5Ve	-13.47	48 ± 2	24 ± 1	267 ± 1	4 ± 0	H $\alpha, \beta$ , [S II], [O III], large halo probably associated.
RP248	05 38 51.39	-69 21 42.5		B2V[e]	-13.10	151 ± 8	56 ± 2	264 ± 2	119 ± 6	H $\alpha, \beta, \gamma$ , [S II], [N II], [O II], [O III] at least, SP 50% forbidden lines from ambient emission
RP339	05 38 55.12	-67 19 31.7		B1Ve	-12.38	346 ± 17	57 ± 2	340 ± 4	317 ± 16	H $\alpha, \beta$
RP104	05 39 03.10	-70 23 43.9		B1V[e]	-12.80	198 ± 10	38 ± 2	241 ± 3	147 ± 7	H $\alpha$ , [N II] and [S II]
RP1034	05 39 12.67	-67 42 49.9		B3Ve	-12.72	310 ± 16	50 ± 2	286 ± 4	273 ± 14	H $\alpha$
RP66	05 39 14.02	-70 45 03.7		B1Ve	-13.66	226 ± 11	31 ± 1	245 ± 2	168 ± 8	H $\alpha, \beta$
RP340	05 39 16.59	-67 23 42.9	BE74141	B5IIIe	-12.42	289 ± 14	59 ± 2	304 ± 4	260 ± 13	H $\alpha, \beta$
RP391	05 39 19.80	-67 08 55.7		B3Ve	-12.83	249 ± 12	70 ± 3	325 ± 2	225 ± 11	H $\alpha, \beta$
RP286	05 39 25.87	-68 33 16.2	BE74426	B1Ve	-13.48	458 ± 23	31 ± 1	253 ± 3	378 ± 19	H $\alpha, \beta, \gamma$
RP390	05 39 36.81	-67 08 33.6		B3IIIe	-13.92	244 ± 12	35 ± 1	295 ± 2	190 ± 10	H $\alpha$ , [S II]
RP92	05 39 37.63	-70 15 43.9	SAB507	B0IIIe	-13.12	357 ± 18	104 ± 4	269 ± 6	366 ± 18	H $\alpha, \beta$
RP141	05 39 40.03	-70 10 16.7		B1Ve	-14.19	143 ± 11	30 ± 1	240 ± 2	93 ± 5	H $\alpha$ , Bottle shape
RP632	05 39 44.61	-70 01 00.9		B1Ve	-13.87	102 ± 24	11 ± 2	262 ± 5	36 ± 21	H $\alpha, \beta$ , SP, Bottle shape
RP341	05 39 48.49	-67 23 23.5		B2Ve	-13.28	184 ± 9	41 ± 2	295 ± 3	139 ± 7	H $\alpha, \beta$

RP Object	RA J2000	DEC J2000	Other Catalog Reference	Spec Type	Log F H $\alpha$	FWHM H $\alpha$ km/s	EW H $\alpha$ Å	Vel. (helio) km/s	$v \sin i$ km/s	Comments
RP83	05 40 04.53	-70 39 44.9	SAB1449	B0IIe	-13.38	108 ± 5	16 ± 1	255 ± 2	48 ± 2	H $\alpha, \beta$ , Forbidden lines due to surrounding thick H II disk 16arcsec radius
RP8138	05 40 10.00	-70 09 20.1		B3Ve	-13.50	62 ± 3	22 ± 1	270 ± 1	14 ± 1	H $\alpha$ only
RP8139	05 40 12.00	-70 09 15.1		F0III[e]	-13.84	411 ± 21	43 ± 2	314 ± 5	354 ± 18	H $\alpha$ , [S II], SP
RP8625	05 40 15.33	-70 46 13.2		B1Ve	-13.51	543 ± 27	44 ± 2	221 ± 9	493 ± 25	H $\alpha, \beta$
RP8288	05 40 19.60	-68 29 19.9			-13.42	515 ± 26	37 ± 1		441 ± 22	H $\alpha, \beta$
RP821	05 40 19.65	-70 13 47.3		A6IVe	-14.98	50 ± 2	114 ± 5	220 ± 2	25 ± 1	Low emission levels at time of observation
RP8160	05 40 24.80	-69 57 15.5		B8Ie	-12.51	311 ± 16	37 ± 1	268 ± 2	252 ± 13	H $\alpha$ , ([S II] from large H II disk R=18 arcsec)
RP8387	05 40 25.58	-67 07 55.6		B3Ve	-13.35	271 ± 14	40 ± 2	310 ± 4	221 ± 11	H $\alpha, \beta$
RP82197	05 40 26.74	-70 07 18.5			-14.25	177 ± 9	8 ± 0		82 ± 4	H $\alpha$ , DP R>V
RP81029	05 40 26.95	-68 09 40.3		A3Ve	-13.68	281 ± 14	73 ± 3	261 ± 4	266 ± 13	H $\alpha, \beta$
RP8629	05 40 37.20	-70 09 09.8		B1V[e]	-13.26	74 ± 4	26 ± 1	241 ± 2	26 ± 1	H $\alpha, H\beta$ absorbed, bright emission extending 6 arcsec around star with [S II], [N II][O II]
RP8239	05 40 39.38	-69 15 29.8	BE74441	B0.5IIIe	-12.57	264 ± 13	68 ± 3	260 ± 4	241 ± 12	Pcyg on H $\alpha, \beta$
RP81032	05 40 49.76	-67 57 22.5		B1.7V[e]	-13.93	195 ± 10	40 ± 2	301 ± 2	149 ± 8	H $\alpha, \beta$ , [S II], [O II]
RP8236	05 40 50.29	-69 21 26.3	BE74443	B0V[e]	-13.14	118 ± 6	49 ± 2	254 ± 2	79 ± 4	H $\alpha, \beta$ , [S II], [N II], [O II], [O III]
RP8115	05 40 50.99	-70 36 37.9		B3IIIe	-14.20	281 ± 14	5 ± 0	247 ± 1	136 ± 7	H $\alpha$ , low level [S II]
RP8306	05 40 51.97	-68 55 09.9		B0.5III[e]	-12.58	122 ± 6	37 ± 1	252 ± 2	76 ± 4	H $\alpha, \beta, \gamma$ , [S II], [N II], [O II], [O III] in H II
RP8240	05 40 55.46	-69 14 09.9		B0.5V[e]	-13.06	159 ± 8	40 ± 2	259 ± 17	115 ± 6	H $\alpha, \beta$ , [S II], [N II], [O II], [O III]
RP8238	05 40 55.93	-69 16 14.5	BE74444	B0.5III[e]	-12.10	293 ± 15	116 ± 5	246 ± 28	304 ± 15	H $\alpha, \beta$ , [S II]
RP8237	05 41 00.76	-69 22 05.1	BE74443	B1V[e]	-13.01	152 ± 8	35 ± 1	251 ± 3	104 ± 5	H $\alpha, \beta$ , [S II], [N II], [O II], [O III]
RP896	05 41 04.59	-70 19 58.4	SAB973	B8V[e]	-13.87	374 ± 19	35 ± 1	252 ± 1	310 ± 16	H $\alpha, \beta$ , [S II], [N II]
RP8113	05 41 05.19	-70 32 31.0		B1Ie	-13.77	206 ± 10	29 ± 1	228 ± 1	145 ± 7	H $\alpha$ only
RP856	05 41 10.12	-70 53 38.7		B1Ie	-13.24	135 ± 7	5 ± 0	244 ± 99	45 ± 2	H $\alpha$ only
RP895	05 41 13.73	-70 23 24.7		B9V[e]	-13.96	84 ± 4	72 ± 3	254 ± 16	56 ± 3	H $\alpha, \beta$ , [S II], [N II], [O II], [O III](diffuse emission at location)
RP8159	05 41 15.29	-69 58 10.3		B3IIIe	-13.32	347 ± 17	23 ± 1	255 ± 2	255 ± 13	H $\alpha$ , [S II] centre of large H II disk 22 arcsec radius
RP8343	05 41 20.97	-67 22 02.9		B1.5Ve	-14.01	358 ± 18	56 ± 2	315 ± 4	321 ± 16	H $\alpha, \beta$
RP81022	05 41 22.94	-68 36 24.9		F0IIIe	-12.71	482 ± 24	95 ± 4	292 ± 12	506 ± 25	H $\alpha, \beta$
RP81036	05 41 30.41	-68 53 44.0		B2IIIe	-12.21	342 ± 17	60 ± 2	268 ± 4	313 ± 16	H $\alpha, \beta$
RP820	05 41 31.63	-70 15 31.4		B1.7Ve	-13.15	241 ± 12	40 ± 2	249 ± 3	192 ± 10	H $\alpha$ on star
RP8260	05 41 34.57	-68 56 02.7		F8V[e]	-14.96	148 ± 7	59 ± 2	257 ± 2	116 ± 6	H $\alpha, \beta$ , [S II], [N II], [O II], [O III]
RP8355	05 41 36.91	-66 41 57.3		B5IIIe	-13.05	190 ± 9	28 ± 1	276 ± 3	130 ± 7	H $\alpha, \beta$ with Pcyg profile.
RP863	05 41 40.07	-70 43 55.4		B2Ve	-13.47	541 ± 27	56 ± 2	262 ± 6	516 ± 26	H $\alpha, \beta$ , continuum very weak
RP81963	05 41 42.41	-71 21 18.5		B0Ive	-11.44	75 ± 4	119 ± 5	241 ± 2	57 ± 3	H $\alpha, \beta, \gamma, \delta, \epsilon$ connected to H II region to north
RP81027	05 41 43.34	-68 14 48.7		B1Ve	-13.55	284 ± 14	70 ± 3	259 ± 4	262 ± 13	H $\alpha, \beta$
RP8300	05 41 45.26	-67 43 41.2	AL395	B0Ive	-12.95	370 ± 19	67 ± 3	293 ± 5	352 ± 18	H $\alpha, \beta$
RP8282	05 41 45.42	-68 42 30.4		B3IIIe	-12.76	221 ± 11	51 ± 2	266 ± 3	184 ± 9	H $\alpha, \beta$
RP81023	05 41 45.82	-68 34 32.0	BE74451	A5Ve	-13.94	537 ± 27	31 ± 1	260 ± 3	450 ± 23	H $\alpha, \beta$
RP8377	05 41 49.44	-66 58 20.1		A3Ve	-14.07	194 ± 10	43 ± 2	261 ± 15	148 ± 7	H $\alpha$
RP8276	05 41 57.35	-68 47 46.8		B1.7Ve	-13.35	341 ± 17	57 ± 2	290 ± 4	313 ± 16	H $\alpha, \beta$
RP8354	05 41 58.11	-67 30 39.0		B1Ve	-13.09	379 ± 19	56 ± 2	247 ± 1	351 ± 18	H $\alpha$ , H $\beta$ , H $\gamma$
RP8124	05 42 03.05	-70 44 21.9	SAB678	B0.5IIIe	-13.19	174 ± 9	40 ± 2	254 ± 3	129 ± 7	H $\alpha, \beta, \gamma$
RP8280	05 42 08.95	-68 41 50.8		B2IIIe	-12.50	326 ± 16	63 ± 3	293 ± 5	298 ± 15	H $\alpha, \beta$
RP8386	05 42 15.04	-67 07 25.9		B1Ve	-11.75	322 ± 16	56 ± 2	307 ± 3	293 ± 15	H $\alpha, \beta$ Pcyg profile on both.
RP81020	05 42 18.08	-68 37 51.4		B1Ve	-13.15	550 ± 28	60 ± 2	286 ± 8	526 ± 26	H $\alpha, \beta, \gamma$
RP81112	05 42 19.59	-67 18 58.0		B1Ve	-13.47	536 ± 27	86 ± 3	310 ± 2	552 ± 28	H $\alpha, \beta$
RP8385	05 42 25.60	-67 08 42.0		B1Ve	-13.68	279 ± 14	37 ± 1	299 ± 3	223 ± 11	H $\alpha$ only
RP8293	05 42 27.21	-68 17 46.0		B1Ve	-12.76	356 ± 18	144 ± 6	334 ± 5	396 ± 20	H $\alpha, \beta$
RP81949	05 42 28.75	-68 16 48.2		B0Ve	-13.85	242 ± 12	78 ± 3	256 ± 4	225 ± 11	H $\alpha$ . At outer rim of globular cluster
RP811	05 42 47.38	-70 28 48.9		B0IIIe	-12.49	364 ± 18	65 ± 3	251 ± 4	345 ± 17	H $\alpha, \beta$
RP81026	05 42 47.40	-68 32 57.4		F0Ve	-14.05	415 ± 21	50 ± 2	299 ± 7	378 ± 19	H $\alpha$
RP8249	05 42 57.60	-69 16 32.9		B1.7V[e]	-12.19	100 ± 5	99 ± 4	270 ± 1	80 ± 4	H $\alpha, \beta, \gamma$ [S II], [N II], [O II], [O III]. Very strong emission lines
RP8307	05 43 12.41	-67 50 53.4		B1.5V[e]	-13.25	189 ± 9	28 ± 1	305 ± 19	130 ± 7	H $\alpha, \beta$ , [S II], [N II], [O II], [O III]
RP8161	05 43 14.37	-69 59 10.4		B1.7V[e]	-13.21	320 ± 16	43 ± 2	278 ± 1	268 ± 13	H $\alpha, \beta$ , [S II], [N II], [O II]
RP8309	05 43 20.77	-67 49 44.6		B1.7V[e]	-12.99	181 ± 9	35 ± 1	304 ± 2	131 ± 7	H $\alpha, \beta$ , [S II], [N II], [O II], [O III]
RP8204	05 43 51.09	-69 05 54.9	SHV0544120 -690705	B2V[e]	-13.25	137 ± 7	11 ± 0	280 ± 2	62 ± 3	H $\alpha, \beta$ , [S II], [N II], [O II], [O III]
RP8287	05 44 12.00	-68 27 27.1	BE74468	B0Ve	-12.87	330 ± 16	66 ± 3	270 ± 4	310 ± 16	H $\alpha, \beta$
RP8322	05 44 14.25	-67 29 59.9		B2Ive	-13.18	305 ± 15	69 ± 3	307 ± 4	283 ± 14	H $\alpha, \beta$
RP8321	05 44 20.90	-67 25 33.8		B3Ive	-12.58			295 ± 1		H $\alpha, \beta$ , pcyg on H $\beta$ , extended diffuse emission

RP Object	RA J2000	DEC J2000	Other Catalog Reference	Spec Type	Log F H $\alpha$	FWHM H $\alpha$ km/s	EW H $\alpha$ Å	Vel. (helio) km/s	$v \sin i$ km/s	Comments
RPs274	05 44 41.56	-68 51 29.3		B1Ve	-12.63	527 $\pm$ 26	61 $\pm$ 2	259 $\pm$ 6	502 $\pm$ 25	H $\alpha$ , $\beta$
RPs344	05 44 47.54	-67 19 33.8	IRAS - P.C05448-6720	B1.5V[e]	-13.27	95 $\pm$ 5	160 $\pm$ 6	294 $\pm$ 2	87 $\pm$ 4	H $\alpha$ , $\beta$ , [S II], [N II], [O II]
RPs131	05 44 49.65	-70 08 26.1				-13.49	212 $\pm$ 11	19 $\pm$ 1	262 $\pm$ 11	136 $\pm$ 7
RPs383	05 45 08.11	-67 05 58.1		B2Ve	-13.25	293 $\pm$ 15	45 $\pm$ 2	306 $\pm$ 4	250 $\pm$ 13	H $\alpha$ , $\beta$
RPs244	05 45 19.02	-69 48 02.4		B3Ve	-13.65	330 $\pm$ 16	43 $\pm$ 2	243 $\pm$ 24	277 $\pm$ 14	H $\alpha$ , $\beta$ , ([S II] ambient)
RPs174	05 45 24.39	-69 50 09.8		B3V[e]	-13.90	107 $\pm$ 5	90 $\pm$ 4	254 $\pm$ 4	84 $\pm$ 4	H $\alpha$ , $\beta$ , [S II], [N II], [O II], Very low [O III]
RPs255	05 45 29.40	-69 22 37.3	BE74474	B0.5IIIe	-12.28	136 $\pm$ 7	46 $\pm$ 2	249 $\pm$ 3	97 $\pm$ 5	H $\alpha$ , $\beta$ , $\gamma$
RPs294	05 45 29.63	-68 11 45.8			B0.5IIIe	-11.88	308 $\pm$ 15	143 $\pm$ 6	340 $\pm$ 4	339 $\pm$ 17
RPs262	05 45 44.23	-69 14 05.1		B2IVe	-12.55	230 $\pm$ 11	122 $\pm$ 5	274 $\pm$ 3	238 $\pm$ 12	H $\alpha$ , $\beta$ , own emission but within H II region
RPs636	05 45 48.11	-69 38 32.6		B5III[e]	-13.66	349 $\pm$ 17	50 $\pm$ 2	263 $\pm$ 4	312 $\pm$ 16	H $\alpha$ , $\beta$ , [N II], [O II], [O III], Very low [S II]
RPs261	05 45 58.15	-69 08 57.5		B0.5III[e]	-12.50	112 $\pm$ 6	30 $\pm$ 1	231 $\pm$ 19	62 $\pm$ 3	H $\alpha$ , $\beta$ , $\gamma$ , [S II], [N II], [O II], [O III] dense emission halo + some diffuse in area
RPs305	05 46 01.62	-67 35 54.9		B5IIIe	-12.54	270 $\pm$ 13	56 $\pm$ 2	265 $\pm$ 157	233 $\pm$ 12	H $\alpha$
RPs1948	05 46 04.82	-68 27 41.1		B3IIIe	-13.63	460 $\pm$ 23	31 $\pm$ 1	342 $\pm$ 4	380 $\pm$ 19	H $\alpha$ , central star of faint diffuse emission 20 arcsec radius
RPs1017	05 46 27.15	-68 43 15.9		B1Ve	-12.82	388 $\pm$ 19	49 $\pm$ 2	282 $\pm$ 2	350 $\pm$ 18	H $\alpha$ , $\beta$
RPs1041	05 47 19.53	-70 04 31.4		B3Ve	-14.08	296 $\pm$ 15	17 $\pm$ 1	244 $\pm$ 1	199 $\pm$ 10	H $\alpha$ , [S II] from faint, extended emission
RPs1947	05 47 29.74	-68 39 46.0		B3IIIe	-12.75	229 $\pm$ 11	38 $\pm$ 2	273 $\pm$ 3	176 $\pm$ 9	H $\alpha$ , $\beta$
RPs1950	05 48 32.75	-68 13 10.8		B0Ve	-13.67	439 $\pm$ 22	116 $\pm$ 5	306 $\pm$ 5	471 $\pm$ 24	H $\alpha$ , $\beta$
RPs211	05 48 40.08	-69 12 00.8		B5IIIe	-12.64	301 $\pm$ 15	42 $\pm$ 2	255 $\pm$ 5	250 $\pm$ 13	H $\alpha$ , $\beta$
RPs1035	05 48 43.48	-67 36 10.6		B8III[e]	-10.03	229 $\pm$ 11	47 $\pm$ 2	284 $\pm$ 3	187 $\pm$ 9	H $\alpha$ , $\beta$ , $\gamma$ , $\delta$ , $\epsilon$ , [S II], [N II], [O III], LBV poss, SP
RPs210	05 49 10.14	-69 11 03.9		B2Ve	-12.87	265 $\pm$ 13	37 $\pm$ 1	248 $\pm$ 4	209 $\pm$ 10	H $\alpha$ , $\beta$
RPs633	05 49 41.16	-70 01 36.3		B5IIIe	-13.38	98 $\pm$ 5	22 $\pm$ 1	209 $\pm$ 1	44 $\pm$ 2	H $\alpha$ , $\beta$ , [O III] from triangular-shaped H II region to N and west
RPs17	05 50 08.52	-70 09 49.4		B1.7Ve	-13.21	200 $\pm$ 10	58 $\pm$ 2	219 $\pm$ 3	168 $\pm$ 8	H $\alpha$ , $\beta$ , some low [O III] from diffuse local H II

notes: AL: Andrews A.D., Lindsay E.M., (1964); AGPRS: Melchior A.-L., Hughes S.M.G., Guibert J., (2000); BE74: Bohannan B., Epps H. W., (1974); FAUST: Bowyer S., Sasseen T.P., Wu X., Lampton M., (1995); GRV: Reid N., Glass I.S., Catchpole R.M., (1988); HD: Draper H., (1924); IRAS: <http://irsa.ipac.caltech.edu/IRASdocs/iras.html>; KDM: Kontizas E., Dapergolas A., Morgan D. H., Kontizas M., (2001); L63: Lindsay E.M., (1963); LI: Schwering P.B.W., (1989); MACHO: Keller S.C., Bessell M.S., Cook K. H., Geha M., Syphers D., (2002); S: Henize K.G., (1956); SAB: Sabogal B.E., Mennickent R.E., Pietrzynski G., Gieren W., (2005); SV (DV, HV): Butler C.J., Wayman P.A., (1974); SHV: Hughes S.M.G., (1989); XMMU: Lumb D.H., Guainazzi M., Gondoin P., (2001); 2MASS: Skrutskie M.F. et al. (2006)



RP Object	RA J2000	DEC J2000	GSC2.2 Catalog Reference	d mins GSC2.2	OGLE Catalog Reference	USNO Catalog Reference	d mins USNO	PA deg.	B Mag Ogle	B Mag SC	B Mag USNO	V Mag GSC2.2	V Mag OGLE	I Mag SC	I Mag OGLE	R Mag SC	R Mag USNO
RP1722	05 00 14.06	-69 25 13.98			SC15 5854	U0150-02382843	0.016	312	15.815		15.8		15.759		15.498	14.639	15.4
RP1855	05 00 28.46	-68 23 04.41	S013201139687	0		U0150-02388956	0.007	161		16.75	17.6	16.3		15.408	15.498	15.656	16.9
RP1755	05 00 28.77	-69 01 06.37	S013203017314	0.01	SC15 31595				16.637			16.44	16.589		16.363	14.215	
RP1729	05 00 35.39	-69 19 53.36	S013202266654	0.02	SC15 9370	U0150-02391673	0.027	307	15.377			14.71	15.409		15.236	14.067	14.6
RP1662	05 01 32.53	-70 16 56.11	S013202335246	0.01		U0150-02416226	0.001	0		16.796	17.7	16.35		15.38	15.583	16.8	
RP1707	05 01 33.25	-69 36 58.72	S013202252033	0.01		U0150-02416553	0.005	302		16.037	17.6	15.65		15.094	15.049	15.9	
RP1832	05 01 48.92	-68 37 33.62	S013203044129	0						15.183		14.85		14.393	14.385		
RP1663	05 01 50.52	-70 16 14.93								16.814		16.55		16.101	16.027		
RP1645	05 02 00.95	-70 42 23.74	S013202322779	0.01		U0150-02428478	0.015	339		14.256	12.9	14.95		14.816	13.233	13.5	
RP1792	05 02 03.12	-69 03 40.94	S013203014882	0.02	SC15 197045				16.771			16.74	16.685		16.269	15.402	
RP1838	05 02 26.96	-68 36 55.82	S013203044797	0.01		U0150-02439738	0.006	25		14.136	14.8	13.69		13.266	13.554	13.4	
RP1854	05 02 39.99	-68 27 59.41	S013203051299	0		U0150-02445341	0.023	35		14.235	12.5	14.84		14.465	13.481	13.1	
RP1750	05 02 45.65	-69 03 13.12	S013203015506	0						17.593		16.64		15.786	15.763		
RP1745	05 02 50.69	-69 07 57.67			SC14 28777	U0150-02449700	0.035	328	16.292		16		16.373		16.489	13.695	14.5
RP1834	05 03 04.89	-68 38 35.68	S013203043414	0						16.98		16.86		15.848	15.967		
RP1850	05 03 26.01	-68 28 24.34	S013203051028	0						18.899				16.639	16.261		
RP1852	05 03 32.09	-68 27 56.18				U0150-02468002	0.006	282		17.13	16.9			16.611	16.456	17.1	
RP1845	05 03 32.94	-68 32 35.00	S013203048338	0.01						15.288		16.1		15.325	15.154		
RP1794	05 03 38.63	-69 01 21.29	S013203017726	0.02	SC14 96680				15.926			14.92	15.929		15.71	14.782	
RP1793	05 03 38.94	-69 01 11.94	S013203017983	0.02	SC14 96683	U0150-02471264	0.031	27	15.139		15	15.3	15.308		15.45	14.998	14.1
RP1851	05 03 39.12	-68 28 23.75	S013203051077	0.01		U0150-02471310	0.007	79		15.466	14.5	15.74		15.218	15.062	15.9	
RP1614	05 03 41.74	-71 07 09.71								19.35					18.733		
RP1760	05 03 51.47	-68 57 25.33	S013203022554	0.01	SC14 170011	U0150-02477203	0.016	85	13.867		15.6	13.54	14.001		13.942	13.47	13.7
RP1899	05 03 52.12	-67 32 43.67				U0150-02477437	0.004	101		17.813	17.6	17.75			16.431	17.8	
RP1945	05 04 09.07	-67 18 30.14	S013201319463	0.01								14.63	14.852		14.75	14.561	
RP1910	05 04 17.16	-67 10 55.46	S013201325440	0.01						16.451		16.66		16.168	15.928		
RP1909	05 04 18.26	-67 10 30.36	S013201325741	0.02						14.245		16.13		15.145	15.158		
RP1944	05 04 24.06	-67 19 45.92	S013201318296	0.02		U0225-01559820	0.055	62			12.2		18.424		18.532	14.688	17.1
RP1738	05 04 31.78	-69 17 40.92	S01320303957	0						15.481		15.71		15.004	14.688		
RP1817	05 04 35.61	-68 44 55.12	S0132030108	0.01	SC14 252731	U0150-02498427	0.009	215	12.281		13.3	12.2	12.168		11.832	11.5	
RP1881	05 04 37.15	-67 49 49.07	S013201121296	0		U0150-02499356	0.018	79		13.259	10.8	14.13		15.839	14.874	13.5	
RP1751	05 04 37.41	-69 05 05.71	S013203013936	0.02	SC14 225625				16.008			15.77	16.176		16.316	15.289	
RP1923	05 04 40.40	-66 49 49.01	S01320108396	0		U0225-01563865	0.01	299		15.399	14.2	16.07		15.711	15.014	16.3	
RP1672	05 04 40.78	-70 42 06.04								18.817				16.477	17.387		
RP1863	05 04 44.02	-68 16 32.41	S013201143367	0						15.735		15.74		15.017	14.897		
RP1795	05 04 44.85	-68 58 31.15	S013203021281	0	SC14 234471				13.891			13.65	13.871		13.636	13.426	
RP1936	05 04 47.97	-66 38 53.27	S013201014337	0		U0225-01565871	0.011	68		17.804	16.6	17.27		15.919	15.999	17.3	
RP1935	05 04 51.70	-66 38 07.62	S013201015047	0								15.17					
RP1675	05 04 54.94	-70 43 33.73	S013202322514	0.02						13.073		14.04		12.836	12.874		
RP1650	05 04 56.74	-70 34 45.95	S013202326272	0.01						15.46		15.78		15	15.358		
RP1640	05 04 58.05	-70 41 03.03	S013202323504	0.02						14.928		14.35		13.102	13.147		
RP1901	05 04 58.48	-67 32 05.25	S013201345991	0.03						15.706		17.9		15.52	16.112		
RP1639	05 05 00.69	-70 41 03.41	S013202323456	0.02						15.94		16.23		15.524	14.855		
RP1818	05 05 04.09	-68 44 40.42	S013203037602	0	SC13 35171				16.298			16	16.194		15.766	15.069	
RP1820	05 05 22.28	-68 43 39.52	S013203038776	0.01	SC13 35194				16.667			15.7	16.553		16.228		
RP1629	05 05 25.31	-70 51 53.88								17.641				14.826	16.373		
RP1641	05 05 26.53	-70 39 45.27	S013202324083	0.01		U0150-02523108	0.02	319		15.844	17.1	15.69		15.678	15.205	15.9	
RP1642	05 05 30.41	-70 40 22.05	S013202323773	0.01						17.008		16.59		15.604	15.731		
RP1926	05 05 33.48	-66 51 17.98	S01320107742	0		U0225-01577904	0.017	206		16.564	16	17.51		15.792	15.636	16.6	
RP1821	05 05 39.09	-68 43 20.20	S013203039737	0.07	SC13 106982				14.977			14.41	15.02		14.982		
RP1861	05 05 56.94	-68 20 03.23	S013203055506	0.01								14.99					
RP1915	05 06 08.53	-67 01 23.16	S013201331482	0		U0225-01587235	0.01	220		16.001	16.2	15.69		15.563	15.351	16	
RP1882	05 06 26.66	-67 42 58.32	S013201126372	0		U0150-02552100	0.01	337			14.9	14.98				14.6	
RP1822	05 06 38.01	-68 44 41.58	S013203037812	0.01		U0150-02557868	0.009	64		15.762	16.8	15.35		15.38	14.509	15.5	
RP1754	05 06 39.31	-69 01 22.52	S013203018107	0.01						18.002		17.5		16.338	16.384		
RP1879	05 06 50.97	-67 46 53.76								18.763					17.529		
RP1865	05 06 54.00	-68 16 08.94				U0150-02566013	0.019	220		20.146	19.9				17.563	17.8	
RP1847	05 06 59.17	-68 31 56.55	S013203049161	0		U0150-02568818	0.009	125			14.9	14.89		14.592	14.627	15.6	
RP1811	05 07 01.08	-68 46 60.08	S013203035408	0		U0150-02569744	0.014	228		17.901	19.5	16.61		16.017	16.051	17.1	

RP Object	RA J2000	DEC J2000	GSC2.2 Catalog Reference	d mins GSC2.2	OGLE Catalog Reference	USNO Catalog Reference	d mins USNO	PA deg.	B Mag Ogle	B Mag SC	B Mag USNO	V Mag GSC2.2	V Mag OGLE	I Mag SC	I Mag OGLE	R Mag SC	R Mag USNO
RP1837	05 07 11.00	-68 36 31.84	S013203045734	0		U0150-02574919	0.007	118		16.031	17.9	15.46		14.917		14.893	15.9
RP1744	05 07 11.44	-69 10 50.04	S01320308726	0.01						14.615		15.42			15.346	15.08	
RP1914	05 07 11.54	-67 02 23.09	S013201330984	0.01		U0225-01605095	0.005	106		14.877	14.6	14.92		14.784		14.502	15.4
RP1836	05 07 16.78	-68 39 06.64	S013203043527	0						16.763		15.6		15.039		14.954	
RP1262	05 07 26.42	-69 59 41.56	S013202345622	0.02	SC12 163287	U0150-02582713	0.004	262	15.55		16.3	15.25	15.527		15.346	14.376	15
RP1302	05 07 41.85	-69 22 30.31	S01320302287	0.02	SC11 21389				14.886			15.04	14.934		14.814	14.939	
RP1132	05 07 44.47	-71 23 53.67	S010101332560	0		U0150-02592415	0.007	131		16.502	16.5	16.34		15.533		15.748	16.1
RP1862	05 07 47.09	-68 18 59.60	S013203055955	0.01		U0150-02593797	0.017	46			16.5	16.55					16.7
RP1136	05 08 01.19	-71 21 25.87	S010101333852	0		U0150-02600716	0.008	83		15.56	15.6	15.36		14.825		14.988	15.4
RP1171	05 08 07.04	-70 55 15.97	S0132021400	0.01		U0150-02603530	0.006	57		15.896	15.9	15.67		15.043		14.918	15.9
RP1322	05 08 12.63	-68 58 15.08	S013203022170	0.05	SC11 145977				16.387			15.97	16.286		15.987		
RP1459	05 08 13.68	-68 36 12.82								14.516				15.943		16.13	
RP1501	05 08 29.55	-68 21 09.23	S013203055110	0		U0150-02613620	0.022	93		16.501	17.5	16.57		15.342		15.609	16.2
RP1206	05 08 29.91	-70 20 42.62	S013202112913	0.01		U0150-02613698	0.008	36		15.341	15.9	15.47		14.811		14.601	15.7
RP1473	05 08 32.37	-68 28 51.71				U0150-02614748	0.016	1		16.779	17.3	17.04		15.823		15.955	17.1
RP1393	05 08 33.49	-69 04 48.63			SC11 135957				17.737				17.732		17.623		
RP1151	05 08 36.12	-71 11 28.13	S010101238204	0.01						18.552		17.9				17.561	
RP1299	05 08 38.80	-69 25 34.16	S01320301794	0.01	SC11 103743				15.482			15.78	15.592		15.681	16.127	
RP1298	05 08 41.11	-69 24 44.97				U0150-02618204	0.073	276		19.725	21.1			16.197		17.75	17.8
RP1483	05 08 52.73	-68 26 29.41	S013203052475	0.05		U0150-02623498	0.035	266		18.32	18.3	16.73		15.213		15.464	16.3
RP1472	05 09 01.39	-68 32 12.55	S013203049034	0.01		U0150-02627193	0.029	238		15.819	15.9	14.72		15.395		15.231	15.3
RP1133	05 09 06.46	-71 21 10.97	S01010133400	0		U0150-02629404	0.013	246		16.024	16.3	16.29		15.566		15.795	15.9
RP1145	05 09 29.88	-71 15 23.17	S010101336440	0		U0150-02639307	0.007	265		14.659	14.4	14.71		14.399		14.361	14.5
RP1126	05 09 41.93	-71 27 41.54	S010101330832	0		U0150-02644165	0.08	266		13.319	11.1	14.8		14.779		14.225	11.7
RP1531	05 09 44.24	-67 57 50.52	S013201113250	0.01		U0150-02645526	0.011	273		15.495	16.4	15.4		14.887		14.679	15.4
RP1326	05 09 47.58	-69 00 31.59	S013203019488	0.02	SC11 320107				15.696	16.889		15.96	15.86	16.016		15.595	
RP1311	05 09 58.94	-69 10 39.65	S01320309053	0.01	SC11 300974				15.548			15.5	15.63		15.711		
RP1134	05 10 08.37	-71 20 35.51	removed							20.45		15.36				18.401	
RP1471	05 10 12.42	-68 32 31.14	S013203048876	0.05		U0150-02658721	0.012	40		17.128	17.8	17.07		16.35		17.174	17.7
RP1312	05 11 03.97	-69 07 32.65	S01320337993	0.01	SC10 109818				16.337			15.98	16.029		15.334	15.734	
RP1419	05 11 56.00	-68 53 18.67			SC10 275054				19.15				18.657		17.889		
RP1290	05 12 07.66	-69 28 35.07			SC10 225872				16.347				16.34		16.081	15.516	
RP1209	05 12 08.38	-70 28 40.36	S01320218129	0.04		U0150-02712096	0.042	283		13.905	14.1			15.163		13.164	13.5
RP1158	05 12 09.11	-71 06 49.92	S01010124742	0.01		U0150-02712630	0.001	33		14.981	14.9	14.18		13.841		14.003	14.4
RP1316	05 12 20.07	-69 04 49.51	S01320339785	0.01	SC10 260043	U0150-02717762	0.008	24	16.386		18.6	16.06	16.313		16.041	15.518	16
RP1422	05 12 22.83	-68 52 38.19	S013203319485	0	SC10 274142				14.644			14.51	14.534		13.918	14.703	
RP1211	05 12 32.12	-70 29 03.30	S01320217919	0.02		U0150-02723407	0.017	349		15.675	16.7	15.83		15.184		14.9	15
RP1205	05 12 36.18	-70 24 58.65	S013202110184	0.01		U0150-02725347	0.004	193		16.497	17.2	16.66		15.937		15.961	16.9
RP1597	05 12 36.69	-66 38 22.51	S013201340035	0		U0225-01698237	0.014	201		15.279	14.9	14.87		14.516		14.253	15.2
RP1392	05 12 47.90	-69 03 06.42	S013203310954	0.01	SC9 65324				15.875			15.08	15.657		15.079	14.655	
RP1461	05 12 49.60	-68 33 55.66	S013203336221	0.01		U0150-02731588	0.007	74		17.634	17.1	17.46		15.843		16.406	17.2
RP1389	05 13 17.44	-69 19 55.02	S013203146573	0.01	SC9 127600	U0150-02744501	0.023	318	15.891	15.95	17.2	15.9	16.032		16.154	14.659	14.5
RP1348	05 14 13.05	-69 33 24.67	S013203123689	0.01	SC9 198321				14.14			13.93	14.232		14.178	14.262	
RP1350	05 14 14.90	-69 36 08.78	S013203119056	0.05	SC9 193733				17.369				16.977		16.378	15.813	
RP1499	05 14 29.85	-68 20 50.90	S013203346200	0.02						17.988		15.17				16.226	
RP1470	05 14 32.47	-68 32 46.92	S013203360939	0.09		U0150-02778970	0.049	134			12.9	17.98					16.1
RP1574	05 14 43.41	-67 12 25.30	S013201257215	0.01						14.451		15.12		15.22		14.239	
RP1563	05 15 09.95	-67 32 15.37	S013201282937	0.01		U0150-02796061	0.004	51		16.459	16.1			15.99		15.867	17.3
RP1260	05 15 10.00	-70 01 21.60	S013202132262	0.01		U0150-02796107	0.015	151		18.569	19.4	17.82		16.525		16.877	17.6
RP1524	05 15 41.41	-67 58 52.40	S013203269318	0.01		U0150-02809040	0.009	320		13.685	12.3	14.62		14.311		12.963	11.7
RP1582	05 15 45.61	-66 58 42.37								19.508						18.534	
RP1469	05 15 48.74	-68 33 04.01	S013203336767	0.3		U0150-02811982	0.008	239		17.038	18.3	17.43		16.025		16.39	17.2
RP1414	05 16 24.57	-68 55 27.64	S013203316735	0.01	SC8 264446				16.914			16.98	16.905		16.895		
RP1335	05 16 27.14	-69 26 22.60	S013203135789	0.07	SC8 212582				17.5			15.92	17.372		16.95		
RP1529	05 16 31.96	-67 56 50.21	S013203270696	0.01						15.188		15.6		15.148		15.083	
RP1334	05 16 33.24	-69 31 29.28	S013203126607	0.08	SC8 205674				18.499			16.1	18.293		17.742		
RP1423	05 16 39.06	-68 53 20.56	S013203357211	0.01	SC8 268942	U0150-02832201	0.002	74	17.842		20	17.96	17.689		17.657		17.7
RP1386	05 16 39.11	-69 20 47.90	S013203144919	0.02	SC8 225386				17.131			16.71	17.21		17.019		
RP1382	05 16 52.29	-69 33 56.40	S013203122593	0.03	SC8 198896				15.499			15.05	15.512		15.439		

RP Object	RA J2000	DEC J2000	GSC2.2 Catalog Reference	d mins GSC2.2	OGLE Catalog Reference	USNO Catalog Reference	d mins USNO	PA deg.	B Mag Ogle	B Mag SC	B Mag USNO	V Mag GSC2.2	V Mag OGLE	I Mag SC	I Mag OGLE	R Mag SC	R Mag USNO
RP1381	05 17 01.02	-69 34 10.57	S013203121696	0	SC8 291817	U0150-02842280	0.012	69	15.57		20	15.21	15.64				15.9
RP1525	05 17 06.93	-68 00 27.87	S013203267977	0		U0150-02844993	0.009	130		16.88	17	17.68		16.546	15.574	16.591	17.2
RP1526	05 17 07.33	-68 00 18.54	S013203268101	0.01		U0150-02845215	0.013	59		16.376	16.8	16.5		15.502		15.686	16.3
RP1331	05 17 08.13	-69 07 02.17	S013203161741	0.01	SC8 343463				17.164			17.16	17.021		16.886		
RP2054	05 17 08.93	-69 32 21.18	S013203124892	0								13.19					
RP1588	05 17 31.40	-66 43 30.17	S013201275581	0								15.27					
RP1537	05 17 34.45	-67 50 08.79	S013203275596	0.01		U0150-02857306	0.005	84		14.043	14	14.53				14.221	14.1
RP1538	05 17 35.37	-67 46 40.31	S013203278001	0		U0150-02857700	0.003	34		16.17	16.2	16.08		15.17		15.426	16.1
RP1592	05 17 40.69	-66 42 08.87	S013201276255	0.02								12.72					
RP1591	05 17 40.80	-66 42 04.80									11.293			13.375		11.072	
RP1593	05 17 40.96	-66 42 08.74															
RP1478	05 17 46.26	-68 30 03.20	S013203339118	0		U0150-02862624	0.006	148		16.779	16.9	16.61		15.52		15.842	16.5
RP1374	05 17 53.26	-69 11 44.15	S013203156585	0	SC7 86307	U0150-02865761	0.013	113	14.3		20.1	14.46	14.405		14.36	15.413	16.1
RP1373	05 17 57.65	-69 11 10.32	S013203157288	0.01	SC7 86310	U0150-02867663	0.024	79	14.137		20.2	14.11	14.159		13.942		15.6
RP1384	05 17 59.80	-69 30 07.65	S013203128623	0	SC7 47341				15.566			14.9	15.297		14.722	15.515	
RP1383	05 18 02.98	-69 29 49.10	S013203129049	0.01	SC7 47422	U0150-02869905	0.077	13	17.346		25.7	17.22	16.881		16.034	16.048	17.3
RP1448	05 18 08.15	-68 42 39.95	S013203327977	0		U0150-02872068	0.013	86		15.329	15.2	16.04		15.391		15.075	15.5
RP1503	05 18 59.76	-68 14 39.44	S013203349201	0		U0150-02894246	0.011	39		16.745	17.1	16.91		15.827		16.06	16.9
RP1514	05 19 07.79	-68 05 42.02	S0132032100278	0.01		U0150-02897667	0.013	95		13.989	13.9	14.22		13.392		13.572	13.4
RP1517	05 19 07.91	-68 02 57.76	S013203266058	0		U0150-02897663	0.007	10		17.672	18.1	17.77		16.734		16.815	17.4
RP1468	05 19 08.33	-68 34 01.54	S013203335485	0.02						17.659		17.44		16.845		16.625	
RP1339	05 19 11.45	-69 41 55.90	S013203110644	0.01	SC7 255063				16.681			16.6	16.688		16.487	17.04	
RP1437	05 19 12.83	-68 44 04.63	S013203326554	0.04		U0150-02899625	0.036	217		17.287	17.7	17.44		15.788		16.811	16.1
RP1506	05 19 17.99	-68 13 45.02	S013203349570	0.01		U0150-02901912	0.006	312		15.803	16.1	15.8		15.278		15.354	16
RP1479	05 19 25.11	-68 29 36.74	S013203339293	0.01						15.084		15.27		14.53		14.222	
RP1149	05 19 29.28	-71 15 50.72	S01010121311	0.01		U0150-02906586	0.017	191		15.608	15.5	15.45		14.798		15.12	15.3
RP1436	05 19 33.68	-68 45 24.53	S013203358719	0.01		U0150-02908458	0.003	76		18.211	18.8	17.97		16.678		17.084	17.7
RP1370	05 19 34.20	-69 57 50.60	S013202136684	0.01						16.123		15.25		15.684		15.404	
RP1539	05 19 37.30	-67 49 30.51	S0132032122868	0		U0150-02910003	0.008	68		15.412	14.9	15.04		14.692		14.334	15.1
RP1340	05 19 44.00	-69 40 28.35	S013203112354	0	SC7 380031	U0150-02912749	0.008	132	15.72		21.2	15.79	15.791		15.821	16.14	16.7
RP1449	05 20 11.54	-68 37 53.71	S013203331963	0		U0150-02924445	0.007	51		16.308	17.6	17.73		15.935		15.859	17
RP1452	05 20 12.96	-68 38 08.34	S013203331770	0.03		U0150-02925160	0.027	87		14.195	14	14.7		14.619		13.99	15.5
RP1342	05 20 15.34	-69 40 28.99	S013203112114	0.01	SC6 48573	U0150-02926079	0.02	172	15.291		20.5	15.19	15.468		15.696	15.998	16.5
RP1600	05 20 17.83	-66 52 53.59				U0225-01843046	0.045	270		12.385	10.6			14.196		12.883	12.2
RP1265	05 20 34.34	-70 00 33.07	S013202132471	0.01	SC6 5808				17.489			17.04	17.273		16.756	16.53	
RP1356	05 20 39.89	-69 44 59.15	S01320317243	0.01	SC6 155977	U0150-02937513	0.041	119	15.096		20.7	15.06	15.075		14.892	15.967	15.5
RP1586	05 20 40.11	-66 48 49.19	S0132012107706	0.01						14.225		15.5		14.697		14.98	
RP1355	05 20 45.17	-69 58 24.55	S013202164516	0.01	SC6 131604				19.95			17.83	19.224		18.385		
RP1343	05 20 47.86	-69 39 56.26	S013203112973	0.01	SC6 170496	U0150-02940959	0.01	67	16.815		20.8	15.74	16.672		16.227		16.5
RP1238	05 20 49.08	-70 12 40.84	S013202118344	0.02	SC21 85424				16.875				16.664		16.295	15.851	
RP1344	05 20 51.12	-69 38 28.95	S013203114418	0	SC6 170538				15.637			15.55	15.628		15.378	16.01	
RP1173	05 20 54.35	-70 49 42.11	S010101215216	0	SC21 57039	U0150-02943793	0.011	137	15.166		16.1		15.093		14.853	15.645	15.7
RP1535	05 20 57.37	-67 49 21.14	S0132032122838	0.01		U0150-02945105	0.01	81		18.94	12.6	14.77				18.19	13.1
RP1368	05 21 05.22	-69 01 03.36	S013203166749	0.01								17.58				16.224	
RP1156	05 21 15.37	-71 05 29.79								18.041						18.145	
RP1515	05 21 15.85	-68 01 59.79	S013203266326	0		U0150-02953157	0.009	38		14.641	15.4	14.56		14.349		13.874	14.4
RP1551	05 21 16.35	-67 57 01.68	S0132032276	0.02		U0150-02953460	0.028	60		14.739	14.7	14.71		14.231		13.72	13.7
RP1365	05 21 16.97	-69 04 57.86	S013203163113	0.01		U0150-02953636	0.01	12		17.135	16.5	16.22		15.632		15.992	16.4
RP1360	05 21 17.30	-69 19 53.92	S013203145276	0.03	SC6 214298	U0150-02953582	0.04	294	14.923		18.5	14.53	14.97		14.817	15.089	13.5
RP1542	05 21 20.43	-67 47 06.80	S0132032136264	0		U0150-02955143	0.003	3		16.716	16.4	16.92		16.007		15.989	16.4
RP1266	05 21 21.48	-69 59 00.25	S013203132018	0.01	SC6 249718				20.585			15.88	19.856		18.229		
RP1362	05 21 29.45	-69 07 25.43				U0150-02959152	0.014	97		18.631	20.2			16.513		17.747	17.8
RP1494	05 21 31.88	-68 20 59.57	S013203345472	0.02		U0150-02960101	0.017	348		14.859	15	14.84		14.424		14.043	14.9
RP1367	05 21 36.06	-69 02 30.74	S013203165372	0.01		U0150-02962041	0.015	82		15.584	17.5	15.04		15.201		15.235	14.6
RP1481	05 21 36.52	-68 28 55.79	S013203339471	0.01		U0150-02962176	0.008	14		15.867	16.1	15.69		15.112		15.006	15.9
RP1543	05 21 38.09	-67 46 52.11	S0132032136292	0.01		U0150-02962911	0.011	48			12.6	16.22					12.9
RP1480	05 21 38.47	-68 28 21.11	S013203339932	0						17.85		17.84		16.704		16.932	
RP1359	05 21 40.54	-69 26 06.11	S013203134543	0.01	SC6 322365	U0150-02963896	0.015	212	16.448		20.4	15.42	16.555		16.315	16.237	15.6
RP1715	05 21 47.25	-69 52 33.50	S013202142948	0.01	SC6 260753	U0150-02966957	0.019	53	17.018		20.9	16.68	16.605		15.867	16.721	17.1

RP Object	RA J2000	DEC J2000	GSC2.2 Catalog Reference	d mins GSC2.2	OGLE Catalog Reference	USNO Catalog Reference	d mins USNO	PA deg.	B Mag Ogle	B Mag SC	B Mag USNO	V Mag GSC2.2	V Mag OGLE	I Mag SC	I Mag OGLE	R Mag SC	R Mag USNO
RP2173	05 21 54.96	-69 46 35.99	S01320315582	0.03	SC6 273912	U0150-02970166	0.012	355	15.671		20.8	15.42	15.576		15.263	16.07	16.7
RP852	05 22 02.11	-69 02 05.82	S013203165603	0.01						17.39			16.937		15.911		
RP2174	05 22 02.73	-69 46 14.48	S01320315848	0		U0150-02973617	0.007	31		19.393	20.6	15.17		15.57	15.788	16.5	
RP985	05 22 03.16	-67 47 04.28	S0132032136219	0.02		U0150-02973891	0.032	45		17.785	11.1	17.08			16.28	11.5	
RP606	05 22 07.95	-70 17 01.10	S010101233265	0.02		U0150-02975873	0.011	16		16.942	18.8	15.63		15.094	15.404	16.3	
RP718	05 22 10.51	-69 49 43.17	S01320313308	0.05	SC6 384268	U0150-02977015	0.05	155	16.712		21.1	15.44	16.787		16.781	15.99	16.2
RP1059	05 22 10.82	-67 34 50.59	S0132032138256	0						14.933		16.19		15.427	14.953		
RP813	05 22 14.14	-69 19 30.62	S013203145154	0	SC6 448194				16.836			16.42	16.876		16.702	16.36	
RP854	05 22 17.44	-69 03 04.86	S013203164675	0.04		U0150-02979844	0.018	214		16.478	19.1	15.71		14.917	15.315	15.4	
RP716	05 22 17.90	-69 50 49.09	S01320312663	0.01	SC6 384140	U0150-02979990	0.02	272	15.842		19.4	16.02	15.786		15.491	15.878	16.2
RP925	05 22 22.88	-68 41 00.85	S013203328716	0.01		U0150-02982252	0.026	17		16.497	17.4	17.47		15.585	15.692	15.9	
RP853	05 22 28.54	-69 00 43.20	S013203166806	0.01		U0150-02984565	0.009	21		15.213	16.2	14.71		14.562	14.364	14.8	
RP600	05 22 30.03	-70 23 53.60	S010101230117	0.02	SC21 171353	U0150-02985154	0.011	322	14.416		15.3	14.27	14.361		14.228	14.365	14.5
RP978	05 22 39.72	-67 55 24.75	S013203270557	0.01		U0150-02989134	0.004	141		16.289	14.8	16.64		15.767	15.478	16.4	
RP948	05 22 48.19	-68 32 41.73	S013203335987	0.03						14.48		15.17		14.925	14.427		
RP924	05 22 54.11	-68 41 42.73	S013203327953	0.04						15.527		15.93		15.461	15.119		
RP871	05 22 54.20	-69 40 09.63	S013203180941	0.01	SC5 58478				17.329			17.33	17.312		17.111	17.363	
RP901	05 22 58.45	-68 45 34.58	S013203175078	0.08		U0150-02996851	0.057	274		17.336	18.3	17.13		16.501	16.405	17.1	
RP752	05 22 58.47	-69 44 01.53			SC5 51095				19.39				18.946		18.212		
RP984	05 22 59.58	-68 04 07.97	S0132032119529	0.01								14.32					
RP962	05 23 00.14	-68 11 21.29	S013203298277	0		U0150-02997846	0.006	347		16.529	15.8	16.23		15.154	15.366	15.5	
RP814	05 23 05.25	-69 16 12.10	S013203149822	0.01	SC5 112858				15.134			14.66	15.16		14.947	14.837	
RP1054	05 23 07.93	-67 38 14.11	S0132032125862	0.01		U0150-03001218	0.008	347		15.926	16.4	16.34		15.458	15.683	16.2	
RP420	05 23 12.37	-70 47 51.08								18.807					17.967		
RP761	05 23 17.39	-69 40 53.51	S013203110893	0.01	SC5 177908	U0150-03005238	0.003	208	16.408		20.8	16.18	16.555	17.008	16.664	16.911	16.7
RP870	05 23 17.43	-69 38 50.42	S013203113442	0.01	SC5 177730				16.955			15.49	16.248		14.044	16.573	
RP982	05 23 17.73	-67 59 38.97	S0132032119870	0.01								17.39					
RP922	05 23 21.91	-68 39 53.94	S013203329551	0.01						13.748		14.99		14.747	14.101		
RP762	05 23 22.81	-69 41 15.32	S013203110589	0.01	SC5 169541				15.108			15.06	15.329		15.526	15.621	
RP1010	05 23 24.32	-70 39 08.00	S010101241139	0								14.545		13.732	13.654		
RP552	05 23 26.98	-70 41 26.91	S010101220158	0.02		U0150-03009243	0.012	258		15.439	16.1	15.26		15.049	14.899	15.6	
RP1094	05 23 30.46	-66 41 53.46	S013201242884	0.01		U0225-01908742	0.007	177		15.9	15.6	15.87		15.389	15.256	16.3	
RP983	05 23 31.90	-68 01 00.92	S013203266543	0.01						13.775		14.9		15.251	13.948		
RP1062	05 23 33.30	-67 24 10.22	S0132032139806	0.01		U0225-01909733	0.039	181		12.985	10.8	14.88		14.225	12.464	14.6	
RP961	05 23 40.48	-68 05 28.85	S013203299979	0		U0150-03015069	0.011	33		15.81	15.8	15.8		15.146	14.879	15.5	
RP966	05 23 47.74	-67 56 32.42	S0132032120443	0.01		U0150-03018199	0.013	101		16.391	16.1	16.9		15.976	15.856	16.3	
RP964	05 23 49.64	-67 57 26.35	S0132032120266	0.01						16.034	17	15.751		15.751	15.505		
RP899	05 24 03.12	-68 56 21.41	S013203169747	0.01		U0150-03025393	0.072	107		15.192	16.3	15.48		14.915	14.246	12.9	
RP928	05 24 06.36	-68 41 59.26	S013203176069	0.01						14.769		14.57		14.047	14.118		
RP898	05 24 09.71	-68 57 04.01	S013203169181	0		U0150-03027958	0.009	159		17.055	18.1	16.89		16.276	16.21	17	
RP804	05 24 11.91	-69 21 17.80	S013203141719	0.08	SC5 328219				18.16			17.65	18.092		17.878	17.055	
RP1061	05 24 12.33	-67 26 37.74	S013203243584	0.02						13.92		16.56		15.324	13.017		
RP1060	05 24 12.47	-67 26 32.58	S0132032129072	0						13.92		16.43		15.324	13.017		
RP847	05 24 12.49	-69 13 20.54	S013203153262	0						16.205		15.22		15.189	15.393		
RP778	05 24 14.14	-69 27 40.38	S013203130687	0.01	SC5 315475				14.272			13.52	14.391		14.477	14.499	
RP601	05 24 17.73	-71 31 50.28	S010103090792	0.01		U0150-03031463	0.001	0		15.601	13	13.27		13.156	12.722	11.7	
RP873	05 24 23.07	-69 39 08.90	S013203112703	0.01	SC5 292195				16.487			15.29	16.595		16.501	15.918	
RP874	05 24 23.70	-69 38 53.60	S013203113188	0.02	SC5 292390	U0150-03033969	0.02	297	17.109		20.8	15.64	17.055		16.847	17.123	16.4
RP1073	05 24 27.98	-67 09 10.43	S013201298143	0		U0225-01928397	0.005	216		13.143	11.9	14.74		14.337	14.453	11.7	
RP817	05 24 37.95	-69 15 36.79			SC5 456570	U0150-03040201	0.019	195	19.802		20.7		19.411		18.786	18.285	17.8
RP1055	05 24 46.26	-67 38 11.12	S0132032137588	0		U0150-03043726	0.01	8		14.924	15	14.59		14.143	13.89	14.6	
RP1109	05 24 57.81	-67 24 58.21	S0132032139573	0		U0225-01938335	0.025	63		14.707	14.1	14.62		13.331	13.156	16.3	
RP2147	05 24 58.51	-69 03 04.55	S013203164014	0						16.343		15.63		15.213	15.299		
RP944	05 25 00.39	-68 19 30.46	S013203345810	0.01		U0150-03049480	0.013	315		13.716	12.2	15.16		14.425	13.117	12.4	
RP567	05 25 01.95	-70 37 09.52	S010101222557	0.02		U0150-03050235	0.026	46		15.061	17.4	14.4		13.992	14.499	14.5	
RP2155	05 25 05.75	-69 06 56.48	S013203160353	0.01						16.826		16		13.919	14.538		
RP943	05 25 10.22	-68 25 16.41	S013203341727	0		U0150-03053584	0.015	38		15.052	14.8	15.42		14.859	14.146	14.9	
RP800	05 25 10.89	-69 20 37.12	S013203142276	0.01	SC4 119963							16.23			16.189	15.376	
RP707	05 25 12.29	-69 55 26.91	S0132031767	0	SC4 36261				15.32			15.81	15.431		15.373	16.742	



RP Object	RA J2000	DEC J2000	GSC2.2 Catalog Reference	d mins GSC2.2	OGLE Catalog Reference	USNO Catalog Reference	d mins USNO	PA deg.	B Mag Ogle	B Mag SC	B Mag USNO	V Mag GSC2.2	V Mag OGLE	I Mag SC	I Mag OGLE	R Mag SC	R Mag USNO
RP s2149	05 25 20.02	-69 20 24.34	S013203142564	0		U0150-03057554	0.007	87		16.931	18.6	14.88		14.289		14.722	14.9
RP s869	05 25 25.72	-69 12 55.70	S013203153169	0.01		U0150-03059808	0.016	179		15.61	17.6	15.24		15.238		14.827	14.9
RP s724	05 25 29.68	-69 50 30.40	S0132031501	0.02	SC4 53506				15.33			12.46	15.081		14.715	15.118	
RP s725	05 25 39.77	-69 50 59.75	S013203178612	0.02	SC4 176812				17.564			17.52	17.545		17.518	17.35	
RP s942	05 25 40.09	-68 30 46.16	S013203337006	0.01						14.978		14.87		13.521		13.911	
RP s727	05 25 44.66	-69 53 20.57	S01320311372	0	SC4 168200				16.558			16.37	16.691	16.404	16.777	17.224	
RP s2166	05 25 46.00	-69 14 02.37	S013203151726	0.01		U0150-03068130	0.059	33		16.525	19.4	16.28		15.5		15.128	17.3
RP s2146	05 25 50.55	-69 05 29.47	S013203161376	0		U0150-03069827	0.002	353		17.685	18.8	16.37		14.597		15.294	15.9
RP s779	05 25 50.62	-69 27 33.16	S013203129921	0	SC4 227136				15.743			14.84	15.732		15.524	14.549	
RP s672	05 25 56.58	-70 15 06.66	S010103273114	0.01						17.205		16.19			15.653	16.14	
RP s592	05 25 58.15	-70 28 42.46	S010103245998	0.02		U0150-03072773	0.044	6		15.113	17.4	14.54		14.421		14.634	14.8
RP s886	05 26 00.41	-69 53 26.99	S01320311186	0.01	SC4 167932	U0150-03073596	0.012	315	15.43		20.6	15.11	15.11		13.904	15.633	15.1
RP s988	05 26 05.58	-68 36 26.40	S013203177237	0.02		U0150-03075655	0.012	67		13.678	11.1	14.83		14.672		12.98	13.7
RP s989	05 26 07.35	-68 36 35.93	S013203177238	0.01						14.26		15.84		15.112		13.508	
RP s2162	05 26 11.28	-69 19 21.57	S013203143764	0						15.307		14.96		15.206		14.228	
RP s798	05 26 13.74	-69 25 45.16	S013203186338	0.01	SC4 234440	U0150-03078721	0.022	67	17.598	18.851	19.4	17.69	17.679		17.644	17.824	17.7
RP s2160	05 26 22.19	-69 18 07.45	S013203145785	0.02						14.719		13.73		13.747		13.474	
RP s1110	05 26 30.57	-67 40 36.50	S0132032137044	0.01						15.515		15.74		14.614		13.48	
RP s878	05 26 34.51	-69 06 32.29	S013203160225	0.01		U0150-03086154	0.006	57		16.617	17.6	15.77		15.374		15.393	16.1
RP s818	05 26 44.77	-69 14 55.77	S013203150054	0.02						17.106		16.54		15.719		15.961	
RP s845	05 26 46.73	-69 11 58.34	S013203153775	0.01		U0150-03090646	0.007	32		17.427	19.1	17.26		16.496		16.815	17.6
RP s941	05 26 49.05	-68 25 45.54	S013203341011	0.01		U0150-03091528	0.055	11		13.191	11.1	14.32		14.37		12.587	12.7
RP s859	05 26 51.89	-69 00 30.43	S013203165783	0.02						16.711		17.7		16.864		16.54	
RP s858	05 26 52.67	-69 00 49.35	S013203165575	0.08		U0150-03092932	0.019	52		19.064	19.7			17.303		17.48	17.8
RP s542	05 26 53.39	-71 22 08.18	S0101033146050	0.01		U0150-03093142	0.003	39		18.565	15.3	16.12		14.662		13.668	13.7
RP s1011	05 27 00.26	-71 18 54.48	S0101033148216	0		U0150-03095818	0.008	107		17.718	17.8	18		16.029		16.436	17.2
RP s730	05 27 02.49	-69 52 17.26	S013200296144	0	SC4 408905	U0150-03096674	0.017	138	15.768		21.1	16.06	15.881		15.745	17.178	17.3
RP s731	05 27 02.99	-69 46 00.70	SC4 427114						18.436	20.297			16.754	14.33	13.928	15.425	
RP s797	05 27 03.26	-69 24 26.77	SC4 474303			U0150-03096948	0.005	129	16.514		19.4		16.567		16.428	16.12	16.9
RP s599	05 27 07.19	-70 20 02.12	S010103263838	0		U0150-03098415	0.007	216		16.427	17.1	15.42		15.337		15.681	15.9
RP s820	05 27 11.02	-69 15 55.13	S0132002115870	0.01		U0150-03099966	0.015	78		15.793	16.7	14.18		14.344		14.813	15.1
RP s1108	05 27 12.29	-67 23 47.95	S0132032139620	0.01		U0225-01983059	0.012	23		14.228	13.5	13.99		12.813		12.878	14.8
RP s765	05 27 13.11	-69 42 12.31	S013200299415	0.02	SC4 436093				15.279				15.43		15.397		
RP s2157	05 27 15.26	-69 14 36.82	S0132002116794	0						15.294		13.6		13.986		14.015	
RP s536	05 27 20.01	-71 14 01.82	S0101033151527	0.01		U0150-03103156	0.009	288		15.635	15.6	14.85		14.464		14.715	14.8
RP s821	05 27 42.74	-69 14 11.96	S013200228223	0						16.029		15.47		15.39		15.394	
RP s1107	05 27 43.16	-67 25 47.77	S0132032114013	0.02		U0225-01994367	0.021	176			10.9	14.63					15.6
RP s861	05 27 43.63	-69 03 21.59	S0132002160125	0.01		U0150-03111731	0.02	337		18.018	18.8	17.94				16.61	17.2
RP s842	05 27 44.38	-69 08 32.22	S0132002121181	0.01						16.36		15.01		15.046		15.139	
RP s843	05 27 47.62	-69 09 27.65	S0132002120018	0.03								14.77					
RP s605	05 27 49.37	-71 31 19.83	S0101030141793	0.01		U0150-03113887	0.01	345		16.621	16.2	16.3		15.453		15.578	16.2
RP s1057	05 28 02.72	-67 31 16.51	S0132032138471	0		U0150-03118691	0.014	314		14.671	13	14.49		13.562		13.371	14.5
RP s840	05 28 03.99	-69 09 57.19	S0132002119622	0.01						17.052		15.97		15.322		15.528	
RP s2185	05 28 04.23	-69 05 26.84	S013200239082	0						15.86		14.63		14.493		13.703	
RP s823	05 28 04.41	-69 13 33.06	S013200229367	0.02		U0150-03119362	0.019	39		17.904	18.9	17.14		15.965		16.674	17.1
RP s822	05 28 07.61	-69 14 28.47	S013200228705	0.01						15.733		14.82		14.306		14.144	
RP s841	05 28 08.09	-69 10 22.61								19.085						18.048	
RP s702	05 28 14.06	-69 54 37.88	S010100115217	0.03	SC3 162119				14.629			14.14	14.283		13.412	15.144	
RP s879	05 28 20.08	-68 59 10.39	S0132002127477	0								15.16					
RP s512	05 28 20.82	-70 59 22.38	S0101032156647	0.02		U0150-03125209	0.005	22		14.399	13.6	13.71		13.669		13.685	14
RP s2186	05 28 27.04	-69 05 37.54	S013200238728	0.01						15.716		14.94		14.433		14.191	
RP s510	05 28 28.87	-71 00 48.55	S0101032156358	0		U0150-03128178	0.018	81		17.4	18.3	17.76		16.578		16.697	17.4
RP s796	05 28 32.24	-69 19 56.84	S013200222913	0	SC3 226218	U0150-03129266	0.011	19			19	17.97			17.546	17.242	17.7
RP s472	05 28 36.50	-70 56 21.47	S0101032157252	0		U0150-03130734	0.006	67		15.483	16.3	15.69		14.936		14.785	16.5
RP s436	05 28 36.57	-70 48 25.96	S010103220240	0.01		U0150-03130728	0.003	192		15.188	15.9			14.379		14.756	15.3
RP s839	05 28 38.27	-69 11 07.61	S013200233133	0.01						17.74		14.25		13.938		14.561	
RP s688	05 28 40.90	-70 01 38.12	S0101032190566	0.01	SC3 146260				15.708			15.87	15.706		15.442	15.746	
RP s2179	05 28 45.59	-68 59 23.76	S0132002127585	0								14					
RP s2181	05 28 48.85	-69 01 19.63	S0132002125603	0.01		U0150-03135172	0.025	25		16.001	16	15.68		14.814		14.192	15.8

RP Object	RA J2000	DEC J2000	GSC2.2 Catalog Reference	d mins GSC2.2	OGLE Catalog Reference	USNO Catalog Reference	d mins USNO	PA deg.	B Mag Ogle	B Mag SC	B Mag USNO	V Mag GSC2.2	V Mag OGLE	I Mag SC	I Mag OGLE	R Mag SC	R Mag USNO
RP874	05 28 53.10	-69 24 51.39	S0132002149010	0	SC3 328853	U0150-03136671	0.006	252	16.894		19.1	17.32	17.026		16.978	16.063	17.3
RP873	05 28 57.69	-69 25 09.57	S0132002148868	0	SC3 328843	U0150-03138364	0.008	81	17.055		19.4	17.3	17.177		17.094	17.594	17.7
RP2182	05 28 58.82	-69 03 55.04	S0132002123411	0		U0150-03138765	0.001	0		15.75	15	15.94		15.287		14.172	15.8
RP8794	05 29 01.97	-69 22 50.66	S0132002149891	0.01	SC3 333494	U0150-03139883	0.02	187	14.074		16.8	14.01	14.139		13.924	14.779	14.8
RP2183	05 29 02.92	-69 04 29.12	S0132002181	0		U0150-03140235	0.011	342		18.514	12.5	12.94		14.883		15.492	10.9
RP880	05 29 07.24	-69 04 51.31				U0150-03141879	0.023	27		18.577	18.1			16.952		16.942	16.8
RP8838	05 29 21.10	-69 11 17.82	S0132002155627	0.01						18.592		17.98		16.978		17.433	
RP887	05 29 22.39	-69 00 11.87															
RP8836	05 29 22.71	-69 10 13.79	S0132002156183	0						15.106		14.24		14.028		14.467	
RP8995	05 29 28.71	-68 28 29.96	S013200295451	0.02						14.704		16.57		15.689		13.429	
RP81056	05 29 41.19	-67 35 48.25	S0132001246828	0		U0150-03155306	0.01	324		15.259	15.4	15.22		14.4		14.37	15
RP8864	05 29 41.40	-69 06 53.47	S013200238423	0						15.318		14.91		14.382		14.236	
RP8835	05 29 50.72	-69 10 32.02	S0132002155932	0.01		U0150-03159078	0.009	217		16.097	19	17.38		15.931		15.836	17.1
RP2177	05 29 51.32	-68 59 15.56	S0132002161878	0						15.765		14.87		14.42		14.243	
RP8785	05 29 55.03	-69 26 53.32	S0132002147930	0	SC3 439582	U0150-03160776	0.009	239	17.117		19.4	17.46	17.166		16.904	16.717	17.3
RP2210	05 29 56.15	-68 38 50.13	S0132002139404	0.01		U0150-03161288	0.018	54		15.064	12.9	14.22				12.565	16.6
RP8974	05 30 00.60	-67 57 30.12	S0132001244841	0		U0150-03163080	0.023	35		16.929	17.2	17.65		16.437		16.581	17.4
RP8786	05 30 01.22	-69 28 09.55	S0132002147342	0.01	SC2 103618	U0150-03163263	0.024	192	15.569	16.421	19.1	14.9	15.776		15.537	14.827	15.6
RP8740	05 30 01.79	-69 40 46.64	S0132002173423	0.01	SC3 415377				17.34				17.394		17.193		
RP81083	05 30 14.61	-66 49 12.69	S0112002140324	0.01		U0225-02055412	0.001	0		15.143	15.2	15.3		15.204		13.952	15.7
RP8546	05 30 19.08	-71 20 04.66	S0101033146668	0.01		U0150-03170913	0.025	77		16.282	17	16.8		15.361		15.258	16.1
RP81077	05 30 24.32	-67 14 54.67	S0132001237840	0.02		U0225-02059428	0.007	7		15.138	15.7	15.29		14.36		13.731	14.8
RP8667	05 30 26.08	-70 15 07.20	S0101032142643	0.01	SC2 6916	U0150-03173722	0.028	341	17.737	17.613	20	15.54	16.297		13.946	15.885	16.5
RP8867	05 30 26.65	-69 05 35.80	S0132002158437	0		U0150-03174069	0.012	57		17.942	18.3	17.12		16.031		16.559	17.3
RP81079	05 30 33.33	-66 57 41.90	S0132001193065			U0225-02063052	0.021	270		18.66	18.5			16.147		18.006	17.6
RP8788	05 30 39.18	-69 25 43.85	S0132002107818	0.01	SC2 213961	U0150-03179326	0.002	138	16.724		18	16.28	16.035		15.253	15.816	16.2
RP8930	05 30 39.36	-68 34 03.60	S0132002172460	0.01		U0150-03179418	0.013	166		15.523	16	15.74		15.073		13.838	15.8
RP82203	05 30 39.43	-68 35 28.52	S013200289724	0		U0150-03179463	0.015	26		16.149	16.4	16.75		15.206		15.592	16.6
RP8787	05 30 40.67	-69 25 31.17	S0132002148407	0.01	SC2 213896	U0150-03179891	0.019	230	14.469		17.2	14.39	14.58		14.462	14.839	15
RP8834	05 30 41.64	-69 11 34.61	S0132002242	0.01		U0150-03180443	0.013	82		13.862	13	11.93		11.664		12.784	12
RP8587	05 30 43.25	-70 25 57.89	S010103257948	0.01						15.86		17.24		15.721		15.565	
RP8556	05 30 55.02	-70 45 28.25	S0101032160728	0		U0150-03186062	0.003	44		14.58	14.4	14.49		13.899		14.26	14.9
RP81075	05 31 04.25	-67 08 22.32	S0132001240405	0.01		U0225-02075923	0.012	195		16.432	16.9	16.09		15.993		15.169	15.9
RP8881	05 31 10.07	-69 05 25.01	S013200215838	0.01		U0150-03192469	0.009	317		15.209	15.2	15.03		14.407		13.895	14.4
RP8824	05 31 10.86	-69 14 16.93	S0132002153803	0						18.046		17.97		16.791		17.068	
RP8444	05 31 15.62	-70 53 48.44	S010103216359	0.01						14.153		13.7		13.614		13.63	
RP82209	05 31 16.89	-68 40 05.94	S0132002171204	0.02		U0150-03195492	0.027	348			13.5	14.12					15.1
RP8443	05 31 18.75	-70 54 07.70	S0101032113553			U0150-03196278	0.056	345		15.404	16.8			14.848		14.963	15.6
RP8992	05 31 21.06	-68 31 34.37	S0132002172642	0.01		U0150-03197684	0.064	85		13.501	11.9	15.03		15.473		15.644	11.7
RP8915	05 31 22.11	-68 36 42.03	S0132002172022	0		U0150-03197966	0.024	124		13.584	11.4	14.17		13.994		12.356	11.7
RP82208	05 31 24.25	-68 41 33.65	S0132002170752	0		U0150-03198862	0.013	87		14.276	14.1	12.74		12.502		12.851	12
RP8832	05 31 30.75	-69 11 52.06	S0132002154933	0.01						15.484		15.19		14.673		14.472	
RP8432	05 31 33.11	-70 46 17.91	S0101032160217	0		U0150-03202769	0.01	33		15.813	16.4	15.58		15.073		15.394	16.2
RP8507	05 31 36.20	-71 10 42.96	S010103341468	0						19.771				16.389		17.962	
RP8825	05 31 36.24	-69 18 45.66	S0132002151300	0.01						17.238		16.11		15.617		15.888	
RP8938	05 31 40.51	-68 22 44.10	S013200324507	0		U0150-03205851	0.004	258		16.387	16.3	16.29		15.662		15.226	16.4
RP8453	05 31 45.97	-70 51 22.98	S0101032158316	0		U0150-03208195	0.007	95		16.399	17.1	16.28		15.304		15.401	16.6
RP82207	05 31 46.25	-68 33 59.94	S0132002140403	0								15.32					
RP8831	05 31 46.26	-69 09 57.19	S0132002155810	0.01		U0150-03208276	0.011	12		15.896	16.5	15.38		15.083		15.225	15.8
RP8868	05 31 57.78	-69 06 10.87	S0132002157753	0.01		U0150-03213293	0.015	70		15.952	17.2	14.94		13.988		14.41	15.4
RP8953	05 32 02.67	-68 11 59.54	S0132003164943	0.02						18.625				17.236		17.958	
RP8937	05 32 05.19	-68 12 46.40	S0132003186467	0.01		U0150-03216331	0.016	44		17.785	17.6	17.96		16.345		16.674	17.4
RP8830	05 32 13.66	-69 13 39.62	S0132002153897	0.01		U0150-03219771	0.011	319		15.068	16.9	14.84		14.164		14.227	14.6
RP8975	05 32 14.81	-68 10 25.64	S0132003187360	0.02		U0150-03220310	0.007	4		18.005	17.8	17.96		16.36		16.673	17.2
RP8912	05 32 15.68	-68 40 14.55	S0132002138390	0.01		U0150-03220723	0.016	74		16.455	16.5	16.85		15.682		15.537	17.1
RP8448	05 32 17.29	-70 47 33.98								16.793				16.033		16.078	
RP8935	05 32 18.75	-68 17 30.96	S0132003184683	0		U0150-03221939	0.006	344		16.849	17.5	17.04		15.885		15.93	16.8
RP8914	05 32 18.77	-68 41 59.26	S013200279876	0						14.729		13.88		14.933		14.103	
RP8936	05 32 22.20	-68 17 33.87	S013200336431	0.02		U0150-03223325	0.014	318		17.97	18	17.44		16.593		16.751	17.7

RP Object	RA J2000	DEC J2000	GSC2.2 Catalog Reference	d mins GSC2.2	OGLE Catalog Reference	USNO Catalog Reference	d mins USNO	PA deg.	B Mag Ogle	B Mag SC	B Mag USNO	V Mag GSC2.2	V Mag OGLE	I Mag SC	I Mag OGLE	R Mag SC	R Mag USNO
RP911	05 32 26.47	-68 39 03.91	S013200285951	0.01							17.57	18.79		16.469		16.621	
RP1014	05 32 26.98	-70 47 44.35	S0101032159496	0		U0150-03225440	0.014	93		18.045	18.1	17.98		16.846		17.051	17.8
RP447	05 32 27.03	-70 47 44.05	S0101032159496	0.01		U0150-03225440	0.012	120		18.045	18.1	17.98		16.846		17.051	17.8
RP449	05 32 28.35	-70 47 28.58								17.737				16.48		17.222	
RP532	05 32 30.10	-71 13 30.24	S0101033150569	0.02		U0150-03226663	0.012	292		15.85	15.3	16.7		15.322		15.132	15.8
RP790	05 32 33.61	-69 24 56.01															
RP502	05 32 34.68	-71 06 49.83	S0101033154884	0.01		U0150-03228696	0.01	62		15.698	16.5	15.53		14.642		14.994	14.4
RP682	05 32 41.08	-70 09 51.65	S010103294073	0.02		U0150-03231537	0.008	77			19.9	18.68					17.6
RP773	05 32 50.20	-69 35 35.58	S010100155397	0.01		U0150-03235543	0.032	340		16.276	17.8	17.71		16.849		15.9	17.4
RP826	05 33 02.38	-69 16 55.89	S0132002151887	0						14.931		14.42		13.587		14.133	
RP744	05 33 05.02	-69 38 47.30	S010100151529	0.03	SC1 90124	U0150-03242717	0.011	142	15.697		18.2	15.41	15.818		15.684	14.915	14.8
RP1102	05 33 05.55	-67 37 15.59	S0132001225698	0						14.076		13.4		12.515		12.822	
RP1101	05 33 06.23	-67 36 49.19	S0132001225883	0.01		U0150-03243298	0.008	51			15.8	14.9					15.3
RP827	05 33 07.23	-69 15 27.72	S0132002152665	0.01		U0150-03243768	0.007	43		17.074	16.5	16.17		15.602		15.934	16.9
RP1001	05 33 07.49	-68 47 55.08	S0132002167580			U0150-03243832	0.013	324		17.668	18.6	17.91		16.499		16.318	17.5
RP1098	05 33 07.61	-67 18 05.48	S0132001235563	0.01		U0225-02122575	0.008	207		15.475	15.5	14.83		14.563		13.96	16.2
RP791	05 33 07.62	-69 29 46.15				U0150-03243605	0.06	284				20.6					16.7
RP1100	05 33 22.24	-67 38 48.57	S0132001225082	0.01		U0150-03251351	0.013	80		16.829	17.2	17.04		15.838		15.599	16.7
RP908	05 33 23.24	-68 39 34.85	S0132002171079	0.03		U0150-03251834	0.011	95		16.707	16.3	17.37		16.29		15.935	16.7
RP529	05 33 24.93	-71 11 38.88	S0101033151576	0.01		U0150-03252579	0.002	265		17.668	17.8	17.24		16.583		16.917	17.3
RP829	05 33 25.56	-69 13 11.76	S0132002153829	0.01		U0150-03252829	0.018	254		16.299	17.7	16.17		15.202		15.119	16.2
RP697	05 33 29.21	-69 52 33.06	S0101001141665	0.01	SC1 158224				17.263			17.2	17.175		16.934	16.643	
RP698	05 33 29.89	-69 52 28.79	S010100128465	0.01	SC1 158227	U0150-03255253	0.014	81	16.616	16.04	19	15.64	16.61		16.474	16.15	15.9
RP1106	05 33 33.12	-67 24 54.05	S0132001206852	0.01		U0225-02131628	0.02	294				10.4					15.7
RP1105	05 33 37.50	-67 25 39.32	S0132001206429	0		U0225-02133176	0.013	243				11.3	13.7	13.899		15.303	13.7
RP828	05 33 40.24	-69 12 50.65	S0132002153948	0.01		U0150-03260558	0.017	73				17.1	16.65				16.7
RP909	05 33 44.06	-68 40 15.22	S0132002170818	0.01						14.647		14.07		13.476		13.687	
RP574	05 33 44.39	-70 33 21.24	S0101032166788	0	SC1 94850	U0150-03262731	0.015	86	15.891	16.255	16.9	15.97	15.97		15.825	15.47	16.6
RP495	05 34 26.46	-71 16 31.19	S0101033147898	0.02		U0150-03284978	0.01	12		17.461	17.7	17.58		16.426		16.338	17.2
RP934	05 34 39.65	-68 21 55.77	S0132003182517	0						15.127		15.88		15.595		14.028	
RP500	05 34 47.82	-71 05 48.91	S0101033154904	0.01		U0150-03296375	0.008	107		15.56	17	15.66		15.24		15.272	15.9
RP419	05 34 52.63	-70 45 45.82	S0101033165225	0		U0150-03298983	0.024	59		15.447	15.5	15.42		15.124		14.738	14.8
RP471	05 35 05.47	-70 51 14.81	S010103376510	0		U0150-03305683	0.008	82		15.972	17.3	16.67		15.677		15.439	16.3
RP696	05 35 13.68	-69 49 46.90	S0101001143559	0.02	SC16 62137	U0150-03310013	0.025	348	15.62		14.9	15.27	15.511		15.108	14.519	13.1
RP362	05 35 29.44	-66 50 33.84								20.348				16.935		18.211	
RP326	05 35 30.21	-67 38 05.94	S0132001106691	0		U0150-03318863	0.009	231				15.4					16.6
RP304	05 35 35.23	-67 40 22.13	S0132001103204	0.01		U0150-03321531	0.019	302		15.209	14.7			13.887		13.642	14.5
RP364	05 35 49.19	-66 51 26.06	S0112002138861	0.01		U0225-02179737	0.07	32		15.686	17.9	16.44		15.319		16.474	17.7
RP365	05 35 53.94	-66 52 32.37								18.907				18.415		18.475	
RP368	05 35 55.73	-66 51 08.67	S0112002138912	0.01						15.274		15.51		15.087		14.263	
RP369	05 35 57.84	-66 50 53.75	S0112002138960	0		U0225-02182717	0.002	140		16.319	16.8	16.24		15.904		15.439	16.3
RP1033	05 36 04.27	-67 55 37.06	S0132003191683	0		U0150-03337033	0.013	303		14.928	15.7	15.05		14.603		13.394	16.4
RP487	05 36 04.46	-70 51 01.47	S010103377689	0.01		U0150-03337222	0.002	66		15.125	16.4			14.256		14.429	14.5
RP684	05 36 09.68	-70 06 07.98	S0101001130880	0.01	SC16 115376	U0150-03340052	0.008	13	17.595		20.1	17.11	17.054		16.74	16.576	17.3
RP1005	05 36 16.32	-70 26 21.89	S0101032170811	0.02	SC16 85520	U0150-03343653	0.012	116	16.498		18.5	15.99	16.396		16.055	15.969	15.9
RP531	05 36 16.96	-71 09 41.93	S0101033151968	0		U0150-03343962	0.005	54		17.91	18.5	17.4		16.293		16.485	17.4
RP348	05 36 28.63	-66 53 02.58	S0112002133460	0.01		U0225-02194151	0.006	132		15.752	16.5	15.33		15.216		15.342	15.6
RP370	05 36 33.18	-66 51 18.61	S0112002138783	0.01		U0225-02195731	0.012	252		17.499	17.8	17.53		16.637		16.683	17.1
RP639	05 36 37.12	-69 22 09.43	S010100171266	0.01								15.27					
RP557	05 36 39.75	-70 44 37.44	S0101033165322	0.02		U0150-03356202	0.017	33		18.386	18.1	17.64		16.407		16.704	17.5
RP258	05 36 43.71	-69 36 44.62	S0101001152792	0.01		U0150-03358332	0.009	205				18.2	14.89				14.5
RP259	05 36 48.63	-69 26 44.67	S0101001158575	0.01								17.12					
RP231	05 36 49.38	-69 23 55.20	S010100170174	0.01		U0150-03361422	0.008	168				19.5		16.93			17.7
RP2163	05 36 54.13	-66 30 04.10	S0112002119673	0.02						15.188		15.01		14.962		14.157	
RP330	05 36 57.68	-67 34 02.68	S0132001226147	0.02						13.866		16.18		14.881		16.094	
RP284	05 37 12.85	-68 37 11.79	S01320033915	0		U0150-03374341	0.008	26		17.003	17.1	16.75		15.831		16.039	16.8
RP353	05 37 14.27	-66 26 59.25														14.807	
RP352	05 37 14.60	-66 26 52.61	S011200283937	0.02								15.88				14.807	
RP27	05 37 25.41	-70 30 47.89			SC16 214851				17.742				17.754		17.657		

RP Object	RA J2000	DEC J2000	GSC2.2 Catalog Reference	d mins GSC2.2	OGLE Catalog Reference	USNO Catalog Reference	d mins USNO	PA deg.	B Mag Ogle	B Mag SC	B Mag USNO	V Mag GSC2.2	V Mag OGLE	I Mag SC	I Mag OGLE	R Mag SC	R Mag USNO
RP298	05 37 28.44	-68 12 34.72	S0132003185437	0.02		U0150-03382920	0.015	95		17.026	17.1	16.98		16.041		16.342	16.7
RP257	05 37 35.37	-69 34 59.56	S0101001153570	0.01		U0150-03386570	0.007	4		16.633	18	16.48		15.297		15.591	15.7
RP29	05 37 38.98	-70 32 46.34	S0101033169023	0.01	SC16 211454	U0150-03388603	0.009	84	17.395		17.8	17.74	17.148		16.938	16.782	16.9
RP1043	05 37 40.59	-67 31 37.14	S0132001226952	0.01		U0150-03389408	0.009	312		15.412	15.5	15.56		14.785		16.118	15.6
RP283	05 37 48.30	-68 39 54.66	S0132002170098	0.01		U0150-03393904	0.012	174			16	16.58					16.2
RP372	05 37 50.31	-66 55 40.25	S0112002137919	0.01		U0225-02223619	0.024	160		16.345	16.6	16.68		15.833		15.728	15.9
RP285	05 37 58.73	-68 33 39.28	S0132003176545	0		U0150-03400127	0.008	32		15.429	15.8	15.02		15.024		14.659	14.8
RP226	05 38 03.07	-69 31 58.98	S0101001155176	0.02		U0150-03402588	0.017	247		15.19	16.9	14.81		15.07		13.926	16.2
RP81	05 38 03.78	-70 50 28.37	S010103380091	0.01		U0150-03403052	0.006	283		16.183	17	16.21		15.785		15.263	15.5
RP634	05 38 04.67	-69 59 18.48			SC17 56064				18.588				18.368		18.012	18.05	
RP2198	05 38 07.83	-70 01 37.80	S0101001132450	0	SC17 117727	U0150-03405545	0.008	50	19.87	19.186	19.4	17.81	18.301	14.902	14.246	16.979	17.3
RP338	05 38 12.92	-67 18 27.78	S0132001233560	0.02		U0225-02232093	0.009	357		17.343	17.7	17.9		17.359		16.896	17.8
RP337	05 38 15.55	-67 15 49.24	S0132001235119	0		U0225-02233063	0.003	214		16.383	17.1	16.09		15.717		15.665	16
RP224	05 38 17.32	-69 32 05.07	S0101001155028	0.02		U0150-03411003	0.009	7		16.14	18.1	15.32		15.064		14.354	13.8
RP335	05 38 17.82	-67 34 39.81	S0132001225536	0.01		U0150-03411254	0.011	216		16.275	16.7	15.85		15.741		15.67	15.8
RP301	05 38 19.82	-67 45 01.54	S0132003194083	0.02		U0150-03412390	0.018	231		14.648	14.2	15.75		14.255		14.17	14.1
RP1952	05 38 22.79	-71 15 13.55	S0101033115164	0						17.57		17.97		16.926		17.161	
RP91	05 38 22.87	-70 18 01.51	S0101032176883	0.01	SC17 99368				18.207			18.04	18.143		17.954	17.644	
RP146	05 38 26.35	-70 10 50.00			SC17 107879	U0150-03416162	0.032	300	19.701		19.3		19.019		18.087		17.8
RP290	05 38 40.83	-68 24 00.70	S0132003180554	0.01						20.605		16.85				19.199	
RP311	05 38 44.16	-68 43 53.98	S0132002168062	0.02		U0150-03427123	0.019	127		16.154	15.1	15.22		15.573		13.436	14.6
RP325	05 38 49.92	-67 32 04.57	S0132001226438	0.01		U0150-03430369	0.018	330		17.521	17.9	17.6		16.689		16.657	17
RP256	05 38 51.35	-69 44 51.17	S0101001145885	0								16.26		15.901		14.817	
RP248	05 38 51.39	-69 21 42.55	S0101001160306	0.01		U0150-03431273	0.005	257		18.408	18.7	17.57		16.863		17.141	17.8
RP339	05 38 55.12	-67 19 31.69	S0132001232673	0.01		U0225-02247665	0.005	205		17.343	17.8	17.48		16.586		16.376	17.6
RP104	05 39 03.10	-70 23 43.89	S0101032127853	0	SC17 154001				16.644				16.574		16.288	16.477	
RP1034	05 39 12.67	-67 42 49.92	S0132003194425	0.01		U0150-03443816	0.013	360		17.277	16.8	17.47		16.545		16.927	17
RP66	05 39 14.02	-70 45 03.78	S0101033164488	0		U0150-03444617	0.004	356			19.4	17.87		16.91		17.16	17.6
RP340	05 39 16.59	-67 23 42.93	S0132001230272	0		U0225-02255396	0.001	0		14.385	14.4	14.39		13.784		15.437	13.4
RP391	05 39 19.80	-67 08 55.76								17.287				15.989		16.331	
RP286	05 39 25.87	-68 33 16.19	S0132003176360	0.02						17.388		17.53		16.416		16.16	
RP390	05 39 36.81	-67 08 33.66	S0132001165739	0		U0225-02262700	0.014	103			17.5						17.2
RP92	05 39 37.63	-70 15 43.91	S0101032178491	0.01	SC17 214830	U0150-03457915	0.005	263	16.142		17.9	15.77	15.725		14.957	15.053	15.4
RP141	05 39 40.03	-70 10 16.77	S010103210324	0.04	SC17 218115	U0150-03459087	0.037	311	18.273		17.9		18.139		17.835	18.662	17.4
RP632	05 39 44.61	-70 01 00.95	S0101001132285	0.01		U0150-03461897	0.008	141		18.058	18.6	17.98		17.266		17.352	17.5
RP341	05 39 48.49	-67 23 23.57	S0132001230235	0.01		U0225-02266870	0.008	8		15.439	15.8	16.36		15		15.888	16.4
RP83	05 40 04.53	-70 39 44.92	S0101033166448	0.01	SC17 191780	U0150-03473049	0.009	20	14.801		15.5	14.73	14.694		14.575	13.639	14.1
RP138	05 40 10.00	-70 09 20.14	S010100112949	0	SC18 41480	U0150-03475984	0.01	15	17.084		17.6	16.7	16.956		16.811	15.632	16.8
RP139	05 40 12.00	-70 09 15.16				U0150-03476854	0.044	303			17.5		20.531		19.786		15.5
RP625	05 40 15.33	-70 46 13.20	S010103386817	0.01	SC18 3151	U0150-03478837	0.011	277	17.219		17.9	17.21	16.914		16.468	16.427	16.9
RP288	05 40 19.60	-68 29 19.94	S0132003177685	0.02		U0150-03481321	0.008	120		17.589	16.5	17.4		16.918		16.972	17.5
RP21	05 40 19.65	-70 13 47.30	S0101032179885	0.01		U0150-03481348	0.02	163		16.105	18.4	16.55		15.48		15.259	15.9
RP160	05 40 24.80	-69 57 15.56			SC18 53340	U0150-03484121	0.025	198	15.254	14.485	16.3	15.23	15.237	14.712	15.247	12.943	12.3
RP387	05 40 25.58	-67 07 55.64	S0132001238328	0.01						16.349		16.13		15.881		15.501	
RP2197	05 40 26.74	-70 07 18.49	S0101001129838	0.01	SC18 41387	U0150-03485347	0.014	151	18.737	17.84	18.8	17.38	16.699	14.692	14.335	14.929	16.1
RP1029	05 40 26.95	-68 09 40.34	S0132003185822	0.01		U0150-03485381	0.006	298			18.3	17.91					17.5
RP629	05 40 37.20	-70 09 09.80	S0101001129469	0.03	SC18 96356	U0150-03491122	0.022	329	15.554		17.1	15.44	15.605		15.657	15.35	14.9
RP239	05 40 39.38	-69 15 29.86	S0101001162156	0.01						13.828		14.11		13.475		12.84	
RP1032	05 40 49.76	-67 57 22.57	S013200376874	0		U0150-03498231	0.015	205		15.083	15.9	15.02		16.055		16.054	15.3
RP236	05 40 50.29	-69 21 26.30	S0101001159947	0.06		U0150-03498246	0.061	304			17.6	16.19					15.5
RP115	05 40 50.99	-70 36 37.94	S010103396533	0.01		U0150-03498836	0.02	263		16.074	16.5			15.439		15.194	15.5
RP306	05 40 51.97	-68 55 09.93	S0132002160969	0.02		U0150-03499468	0.01	295		15.793	16.1	16.11		16.113		15.387	16.3
RP240	05 40 55.46	-69 14 09.92	S0101001162473	0.01		U0150-03501438	0.008	309			19.7	17.89					17.6
RP238	05 40 55.93	-69 16 14.57	S0101001161863	0.01		U0150-03501760	0.006	8		15.059	16.2	14.46		14.482		13.328	14.7
RP237	05 41 00.76	-69 22 05.10	S0101001159576	0.01		U0150-03504585	0.017	86		17.707	18.3	16.74		15.996		16.668	17.2
RP96	05 41 04.59	-70 19 58.41	S0101033138668	0.01	SC18 85335	U0150-03506820	0.025	142	17.467		17.7	16.86	17.399		17.15	16.065	16.8
RP113	05 41 05.19	-70 32 30.99	S0101033136132	0.01		U0150-03507037	0.007	226		13.54	14.8			14.475		15.463	12.9
RP56	05 41 10.12	-70 53 38.73	S0101033159770	0.02		U0150-03509774	0.024	207		12.877	12.6	13.67		14.171		12.634	12.2
RP95	05 41 13.73	-70 23 24.73	S0101033104838	0.04		U0150-03511700	0.034	234			17.1	17.88					16.6

RP Object	RA J2000	DEC J2000	GSC2.2 Catalog Reference	d mins GSC2.2	OGLE Catalog Reference	USNO Catalog Reference	d mins USNO	PA deg.	B Mag Ogle	B Mag SC	B Mag USNO	V Mag GSC2.2	V Mag OGLE	I Mag SC	I Mag OGLE	R Mag SC	R Mag USNO
RP159	05 41 15.29	-69 58 10.34			SC18 107209				15.565				15.685		15.791	13.784	
RP159	05 41 15.29	-69 58 10.34															
RP343	05 41 20.97	-67 22 02.98	S013200123035	0.01		U0225-02299544	0.007	199		17.787	17.6	17.44	15.685	16.799		16.566	17.3
RP1022	05 41 22.94	-68 36 24.99	S0132003175066	0		U0150-03517086	0.003	339		15.671	17.1	16.44		16.367		15.831	15.9
RP1036	05 41 30.41	-68 53 44.06	S0132002161489	0		U0150-03521288	0.012	339		15.661	16.3	14.78		14.5		14.109	14.7
RP20	05 41 31.63	-70 15 31.42	S0101032177542	0		U0150-03521919	0.014	295		16.35	17.3	16.81			15.895	15.872	16.7
RP260	05 41 34.57	-68 56 02.77	S0132002160239	0.01		U0150-03523676	0.007	30		17.164	18.2	17.63		17.003		17.006	16.9
RP355	05 41 36.91	-66 41 57.37	S011200260834	0		U0225-02305156	0.005	212		16.614	16.3			15.959		15.618	15.8
RP63	05 41 40.07	-70 43 55.48	S010103390057	0	SC18 116493	U0150-03526806	0.003	310	18.227			17.94	17.675		16.879	16.508	17
RP1963	05 41 42.41	-71 21 18.57	S0101033142649	0								14.23					
RP1027	05 41 43.34	-68 14 48.76	S0132003183617	0		U0150-03528821	0.016	43		16.701	16.8	16.85		16.632		16.268	16.1
RP300	05 41 45.26	-67 43 41.21	S0132003193854	0.01		U0150-03529837	0.014	355		16.386	16.3	15.39		15.368		15.359	15.4
RP282	05 41 45.42	-68 42 30.39	S01320031421	0.01		U0150-03529846	0.015	274		15.514	16.2	15.49		15.4		14.842	15.4
RP1023	05 41 45.82	-68 34 32.03	S0132003175491	0.01		U0150-03530261	0.015	47		17.643	16.5	17.28		16.329		16.865	17.1
RP377	05 41 49.44	-66 58 20.14				U0225-02309549	0.012	221		19.874	19.2			16.853		17.787	17.8
RP276	05 41 57.35	-68 47 46.85	S0132002164860	0.01		U0150-03536761	0.019	302		17.632	17.8	17.36		16.629		16.608	16.8
RP354	05 41 58.11	-67 30 39.02	S0132003196262	0.02		U0150-03537308	0.01	185		14.784	15.5	15.43		14.55		14.425	14.4
RP124	05 42 03.05	-70 44 21.90	S0101033164091	0.01	SC18 168877	U0150-03540250	0.004	156	15.347			17.4	15.426		15.187	15.147	15.4
RP280	05 42 08.95	-68 41 50.82	S01320032576	0.02		U0150-03543477	0.015	287		15.33	16.1	15.36		15.385		14.729	15.5
RP386	05 42 15.04	-67 07 25.97	S0112002129203	0.01						15.04		16.01		14.538		14.488	
RP1020	05 42 18.08	-68 37 51.41	S0132003174642	0		U0150-03548799	0.014	285		16.439	17.3	15.93		16.146		15.84	15.4
RP1112	05 42 19.59	-67 18 58.04	S0132001231659	0.01						13.92		16.56		15.324		13.017	
RP385	05 42 25.60	-67 08 42.03	S01120022149	0.01		U0225-02321639	0.019	214		16.59	16.8			15.52		15.41	16.9
RP293	05 42 27.21	-68 17 46.07	S0132003182230	0		U0150-03554279	0.002	34		16.592	16.8	16.31		15.878		15.733	15.5
RP1949	05 42 28.75	-68 16 48.23												17.992		17.649	
RP11	05 42 47.38	-70 28 48.91	S0101031146656	0.01	SC19 28805	U0150-03566085	0.012	50	16.343		17.4	16.34	16.217		15.862	15.67	15.6
RP1026	05 42 47.40	-68 32 57.39	S0132003175744	0.01		U0150-03566037	0.018	359		17.614	17	17.68		16.855		16.879	17.2
RP249	05 42 57.60	-69 16 32.91	S0101001161360	0.01		U0150-03571635	0.02	246		14.472	14.7	15.6		15.359		13.213	13.7
RP307	05 43 12.41	-67 50 53.39	S0132003169093	0.01		U0150-03579596	0.032	257			11.5	15.68					17.3
RP161	05 43 14.37	-69 59 10.45				U0150-03580732	0.025	334		16.237	13.5	16.47		16.479		15.938	15.2
RP309	05 43 20.77	-67 49 44.59	S0132003169349	0.02								15.02					
RP204	05 43 51.09	-69 05 54.96	S010100357576	0.01								17.6		16.941		16.804	
RP287	05 44 12.00	-68 27 27.10	S0132000188398	0.01		U0150-03610579	0.01	250		16.041	16.4	15.65		15.385		14.953	15.5
RP322	05 44 14.25	-67 29 59.96	S0132003101252	0.02		U0150-03611957	0.075	148			14	16.17					13.4
RP321	05 44 20.90	-67 25 33.83	S0132003103306	0.01		U0225-02357949	0.016	248		15.2	14.1			15.159		15.983	15.6
RP274	05 44 41.56	-68 51 29.37	S0101003104200	0		U0150-03625293	0.021	268		14.859	16.1	15.47		15.511		14.467	15.3
RP344	05 44 47.54	-67 19 33.83	S0132000244905	0						15.598				15.27		16.068	
RP131	05 44 49.65	-70 08 26.17	S010100283771	0.01	SC19 192239	U0150-03629373	0.002	270	17.659		18.3	17.86	17.718		17.741	17.285	17.7
RP383	05 45 08.11	-67 05 58.12	S0112003916	0.01		U0225-02372832	0.007	202		16.474	17.4			15.813		15.469	16.2
RP244	05 45 19.02	-69 48 02.46	S010100398203	0.02		U0150-03643299	0.026	340		15.834	15.3	16.94		15.886		15.628	16.2
RP174	05 45 24.39	-69 50 09.80				U0150-03645972	0.012	10		16.809	16.8			15.549		16.322	16.6
RP255	05 45 29.40	-69 22 37.38	S0101003101378	0.01		U0150-03648334	0.002	133		14.839	14.3	14.43		14.518		13.929	14.4
RP294	05 45 29.63	-68 11 45.82	S013200016793	0.02		U0150-03648345	0.019	283		14.45	14.8			13.161		13.051	13.1
RP262	05 45 44.23	-69 14 05.13	S010100393765	0.01		U0150-03655287	0.015	355		18.497	17.3			17.347		17.073	17.6
RP636	05 45 48.11	-69 38 32.63	S010100399497	0.01		U0150-03657145	0.004	24		18.122	18	17.34		16.418		16.771	16.7
RP261	05 45 58.15	-69 08 57.52	S0101003102807	0.01		U0150-03661590	0.021	229			15.1	15.8					15.1
RP305	05 46 01.62	-67 35 54.95	S0132000152221	0.01		U0150-03663178	0.05	324		14.004	13.8			14.17		13.285	13.6
RP1948	05 46 04.82	-68 27 41.11	S01320005698	0.01		U0150-03664710	0.006	2		16.539	16.2			16.442		15.471	16
RP1017	05 46 27.15	-68 43 15.97	S010100011724	0.01		U0150-03674406	0.02	273		15.72	15.3	15.17		15.024		15.135	14.8
RP1041	05 47 19.53	-70 04 31.39	S010100284193	0.01		U0150-03697134	0.007	98		16.619	17	16.31		16.477		15.897	16
RP1947	05 47 29.74	-68 39 46.00	S010100017874	0.01		U0150-03701537	0.003	123		15.53	15.8			15.618		15.279	15.3
RP1950	05 48 32.75	-68 13 10.85	S013200016354	0		U0150-03729278	0.003	26		17.539	17.3			16.529		16.405	16.7
RP211	05 48 40.08	-69 12 00.84	S010100350774	0.01		U0150-03732356	0.012	298		16.76	16.5			16.141		15.993	15.8
RP1035	05 48 43.48	-67 36 10.62	S013200067154	0		U0150-03733940	0.002	81		16.077	16.3			14.047		14.618	14.1
RP210	05 49 10.14	-69 11 03.97	S01010035295	0.01		U0150-03744464	0.016	318		16.459	16			16.046		15.64	15.7
RP633	05 49 41.16	-70 01 36.29	S010100227484	0.01		U0150-03755767	0.003	32		15.624	16.1	15.06		15.542		14.959	15.9
RP17	05 50 08.52	-70 09 49.47				U0150-03765643	0.016	58		18.165	16.8			15.96		16.608	17.2

This paper has been typeset from a  $\text{T}_\text{E}\text{X}$ / $\text{L}^{\text{A}}\text{T}_\text{E}\text{X}$  file prepared by the author.